UNIVERSITÄT ZU LÜBECK

From the Research Center Borstel

Leibniz Lung Center

Priority Research Area Infections

Director: Prof. Dr. Stefan Niemann

Research Group Host Determinants in Lung Infection

Dr. Bianca Schneider

The impact of biological sex on the interaction of *Mycobacterium tuberculosis* with human macrophages

Dissertation

for Fulfillment of Requirements

for the Doctoral Degree

of the University of Lübeck

from the Department of Natural Sciences

Submitted by

Lara Buer

from Paris, France

Lübeck 2025

First referee:

PD Dr. Norbert Reiling

Second referee:

Prof. Dr. Denis Nurjadi

Date of oral examination: Lübeck, 01.04.2026

Approved for printing: Lübeck, 15.04.2026

Table of content

List of figures and tables

List of tables

Abbreviations and symbols

°C	Degree Celsius
AB	Antibiotics
ADCC	Antibody-dependent cell-mediated cytotoxicity
AECs	Airway epithelial cells
AF	Alexa Fluor
AIDS	Acquired immunodeficiency syndrome
AMs	Alveolar macrophages
APC	Antigen presenting cells
APC	Allophycocyanine
APCs	Antigen-presenting cells
AR	Androgen receptor
ARE	Androgen responsive element
AUC	Area under the curve
BCG	*Mycobacterium bovis Bacillus Calmette-Guérin*
BNITM	Bernhard-Nocht Institute for Tropical Medicine
BPaLM	Bedaquiline, Pretomanid, Linezolid and Moxifloxacin
BSA	Bovine serum albumin
BUV	Brilliant Ultraviolet
BV	Brilliant violet
cAMP	Cyclic AMP
CASP	Caspase
CCL	CC-Chemokine ligand
CCR	CC-Chemokine receptor
CD	Cluster of differentiation
CLR	C-type lectin receptor

CNS	Central nervous system
CS	Complement system
CXCL	CXC Motif Chemokine Ligand
CXCR	CXC motif chemokine receptor
CYBB	Cytochrome b-245 heavy chain
DAPI	4,6-Diamidin-2-phenylindol
DCs	Dendritic cells
ddH_2O	Double-distilled water
DEGs	Differentially expressed genes
DHEA	Hydroxyepiandrosterone
DHT	5-α-Dihydrotestosterone
DIC	Different interference contrast
dLN	Draining lymph node
DMSO	Dimethyl sulfoxide
DNA	Deoxyribonucleic acid
DNA2	ATP-dependent helicase/nuclease DNA2
DR-TB	Drug-resistant tuberculosis
DS	Drug sensitive
E2	17-β-Estradiol
e.g.	Exempli grate (lat.: for example)
EMB	Ethambutol
ERα	Estrogen receptor alpha
ERβ	Estrogen receptor beta
ERE	Estrogen response element
FACS	Fluorescence activated cell sorting
FC	Fold change
FcR	Fc receptors
FCS	Foetal calf serum
Figure	Figure
FITC	Fluorescein isothiocyanate
FM	Foamy macrophages
FSC	Forward scatter

FSH	Follicle-stimulating hormone
g	Gram
GAHT	Gender-affirming hormone therapy
GFPT2	Glutamine-fructose-6-phosphatase transaminase 2
GM-CSF	Granulocyte-macrophage colony stimulating factor
GnRH	Gonadotropin-releasing hormone
GO	Gene ortholog
GR	Glucocorticoid receptor
h/hrs	Hour/hours
HCS	High content screening
HIF-1a	Hypoxia-inducible factor 1α
HIV	Human immunodeficiency virus
HLA-DR	Human leucocyte antigen - HL subtype
hMdMs	Human monocyte-derived macrophages
HPG	Hypothalamic-pituitary-gonadal
Hpi.	Hours post infection
HRE	Hormone response elements
IFN	Heat shock proteins
Ig	Interferon
IL	Immunoglobulin
ILC	Interleukin
IMID	Innate lymphoid cells
IM	Immune-mediated inflammatory disorders
INH	Interstitial macrophages
iNOS	Isoniazid
IRAK-1	Inducible nitric oxide synthetase
IRF	Interleukin 1 receptor associated kinase 1
ISG	Interferon regulatory factor
KEAP1	Interferon stimulated gene
LH	Kelch-like ECH-associated protein 1

LOS	Lipooligosaccharide
LPS	Lipopolysaccharides
LTBI	Latent TB infection
m	Milli
M	Molar
M-CSF	Macrophage colony-stimulating factor
MACS	Magnetic activated cell sorting
MAPK	Mitogen-activated protein kinase
MARCO	Macrophage receptor with collagenous structure
MDR	Multidrug-resistant
MFI	Median fluorescence intensity
MHC	Major histocompatibility complex
Min	Minute(s)
MIP	Macrophage inflammatory protein
miRNA	MicroRNAs
MOI	Multiplicity of infection
MR	Mannose receptor
MRC1	Macrophage mannose receptor 1
MRS	Macrophage scavenger receptor
Ms	Millisecond
mTEC	Medullary thymic epithelial cells
MTB	*Mycobacterium tuberculosis*
MyD88	Myeloid differentiation primary response protein 88
n	Sample size
NAAT	Nucleic acid amplification tests
NCF2	Neutrophil cytosolic factor
NETs	Neutrophil extracellular traps
Nf-kB	Nuclear factor kappa-light-chain-enhancer of activated B cells
NGS	Next Generation Sequencing

NK	Natural killer
NLRs	NOD-like receptors
NO	Nitrogen oxide
NOD	Nucleotide-binding oligomerization domain
NOTCH1	Neurogenic locus notch homolog protein 1
NOX	NADPH oxidase
on	Overnight
PAMPs	Pathogen associated molecular patterns
PAR	Pseudo-autosomal regions
PBMCs	Peripheral blood mononuclear cells
PBS	Phosphate buffers saline
PC	Principal Component
PCA	Principal Component Analysis
PDIM	Phthiocerol dimycocerosate
PE	Phycoerythrin
Per-CP	Peridinin-Chlorophyll-protein
PFA	Paraformaldehyde
PMNs	Polymorphonuclear neutrophils
PPARα	Peroxisome proliferator–activated receptor alpha
PRRs	Pattern recognition receptors
PZA	Pyrazinamide
QFT	QuantiFERON-TB Gold
RIF	Rifampicin
RLPs	RIG-1-like receptors
RNA	Ribonucleic acid
RNI	Reactive nitrogen species
RNS	Reactive nitrogen species
ROS	Reactive oxygen species
rpm	Rounds per minute
RPMI	Roswell Park Memorial Institute
RR	Rifampicin-resistant

RT	Room temperature
Spp	Species
SRs	Scavenger receptors
SSH	Sex steroid hormones
SSC	Sideward scatter
StAR	Steroidogenic acute regulatory protein
T	Testosterone
Tab	Table
Taq	Thermus aquaticus
TB	Tuberculosis
TGF	Transforming growth factor
TH	T-helper cells
TLRs	Toll-like receptors
TNF	Tumour necrosis factor
Treg	Regulatory T-cells
TST	Tuberculin skin test
U	Unit
WHO	World Health Organization
XCI	X chromosomal inactivation
XDR-TB	Extensively drug-resistant TB
Xie	X-inactivation centre
Xist	X-inactive specific transcript
µ	Micro

Summary

Tuberculosis (TB) is a global health threat disproportionally affecting males compared to females, yet the biological mechanisms driving this sex disparity remain largely elusive. This doctoral thesis aims to elucidate sex-specific differences in human monocyte-derived macrophages (hMdMs) infected with *M. tuberculosis*, a cell type of crucial importance in the host immune response to TB. An in vitro infection model was employed to examine the interaction of *M. tuberculosis* with male and female hMdMs, integrating high-content confocal imaging for bacterial quantification and cell polarization analysis, alongside cytokine profiling and transcriptomic analysis, with and without the sex hormones dihydrotestosterone (DHT) and estradiol (E2). Bacterial uptake and intracellular replication did not differ significantly between male- and female-derived hMdMs. Infection induced polarization towards M2-like phenotype, irrespective of donor sex, suggesting a preferential expansion of *M. tuberculosis* within anti-inflammatory macrophage subsets. Cytokine profiling indicated that male hMdMs produced higher levels of the pro-inflammatory cytokine TNF-α, a finding that was confirmed by qPCR, while female hMdMs secreted greater amounts of IL-17A and IL-23. Hormone treatment, especially DHT, promoted M2-polarization and slightly increased the number of infected cells, while the effects on cytokine production were minimal and varied greatly between donors.

Comprehensive unbiased transcriptome-wide analyses revealed infection as the primary driver of transcriptomic changes. Nevertheless, a subset of differentially expressed genes were unique to each sex. Male hMdMs exhibited enrichment of innate responses including NF-κB signalling and type II IFNs, while female hMdMs showed upregulation of antiviral and adaptive immune pathways alongside negative regulatory pathways, indicative of a more balanced response. Interestingly, DHT had no effect at the transcriptomic level in naïve hMdMs, in contrast to E2, which already induced transcriptomic changes in naïve cells.

Overall, these findings suggest sex- and hormone-specific immune responses of hMdMs to *M. tuberculosis* and highlight the need for further mechanistic research to better understand the underlying pathways and their potential implications for susceptibility to *M. tuberculosis* infection and the development of novel therapies.

Zusammenfassung

Tuberkulose (TB) ist eine bedeutende Ursache globaler Morbidität und Mortalität, wobei Männer stärker betroffen sind als Frauen. Die biologischen Mechanismen dieser geschlechtsspezifischen Unterschiede sind jedoch weitgehend ungeklärt. Diese Dissertation untersucht geschlechtsspezifische Unterschiede in humanen Monozyten-abgeleiteten Makrophagen (hMdMs), die mit *Mycobacterium tuberculosis* infiziert sind, einem Zelltyp, der eine Schlüsselrolle in der Wirtsimmunantwort auf TB spielt. Ein In-vitro-Infektionsmodell wurde verwendet, um die Interaktion von *M. tuberculosis* mit männlichen und weiblichen hMdMs zu analysieren. Hochauflösende konfokale Bildgebung, Zytokin-Profiling und Transkriptomanalysen – jeweils mit und ohne die Sexualhormone Dihydrotestosteron (DHT) und Östradiol (E2) – wurden kombiniert. Die Aufnahme der Bakterien und die intrazelluläre Replikation unterschieden sich nicht signifikant zwischen den Geschlechtern. Die Infektion induzierte eine Polarisierung hin zum M2-ähnlichen Phänotyp, unabhängig vom Geschlecht, was auf eine bevorzugte Expansion von *M. tuberculosis* in dieser anti-entzündlichen Subpopulation hindeutet. Zytokinmessungen zeigten, dass männliche hMdMs höhere TNF-α-Konzentrationen produzierten, während weibliche hMdMs größere Mengen an IL-17A und IL-23 sekretierten. Hormonbehandlung, insbesondere mit DHT, förderte die M2-Polarisierung und erhöhte leicht die Anzahl infizierter Zellen, hatte jedoch minimale Effekte auf die Zytokinproduktion, die zwischen den Spendern stark schwankte. Die umfassende, nicht zielgerichtete Transkriptomanalyse identifizierte die Infektion als Haupttreiber transkriptomischer Veränderungen. Dennoch wies jede Geschlechtsgruppe eine charakteristische Gruppe unterschiedlich exprimierter Gene auf: Männliche hMdMs zeigten eine Anreicherung angeborener Signalwege, insbesondere NF-κB und Typ-II-Interferon, während weibliche hMdMs neben negativen Regulationswegen antivirale und adaptive Immunwege hochregulierten, was auf eine ausgewogenere Immunantwort hinweist. Interessanterweise hatte DHT in naiven hMdMs kaum transkriptomischen Effekte, während E2 bereits in naiven Zellen signifikante Veränderungen induzierte. Insgesamt deuten diese Ergebnisse auf geschlechts- und hormonspezifische Immunantworten von hMdMs auf *M. tuberculosis* hin und unterstreichen die Notwendigkeit weiterer mechanistischer Untersuchungen, um die zugrunde liegenden Signalwege und deren Einfluss auf Infektionsanfälligkeit und therapeutische Strategien besser zu verstehen.

1 Introduction

Sex matters in tuberculosis- yet it's often overlooked. While men account for the majority of TB cases globally and consistently show higher incidence rates, women face distinct health risks, particularly during reproductive age and pregnancy. Despite these known differences, most studies on TB do not consider biological sex or hormonal influences as variables in experimental design or data interpretation. Emerging evidence suggests that sex hormones such as testosterone and estrogen significantly influence the immune response to *Mycobacterium tuberculosis*. Understanding how sex and hormones shape the immune response to TB is, therefore, essential.

1.1 TB: A global health challenge persists

Tuberculosis (TB) remains the leading cause of death from a single infectious agent globally, with an estimated one-quarter of the world's population infected by *Mycobacterium tuberculosis (M. tuberculosis)*, according to the World Health Organization (WHO) (2). Of those infected, approximately 5–10 % will develop symptoms and progress to active TB disease. Despite the preventability and curability of TB, 10.8 million new cases were diagnosed in 2023, resulting in 1.25 million deaths (including 161 000 among people with HIV) (2). The WHO recommends a 4–6-month treatment regimen for drug-susceptible TB that cures approximately 85 % of cases; without treatment, TB mortality is around 50 % (3, 4). Of all global TB deaths 87 % occurred in the African and South-East Asian regions. India alone accounted for 26 % of these deaths. Among all cases, 6.3 % of individuals were co-infected with HIV, a proportion that has been declining steadily over recent years (4, 5).

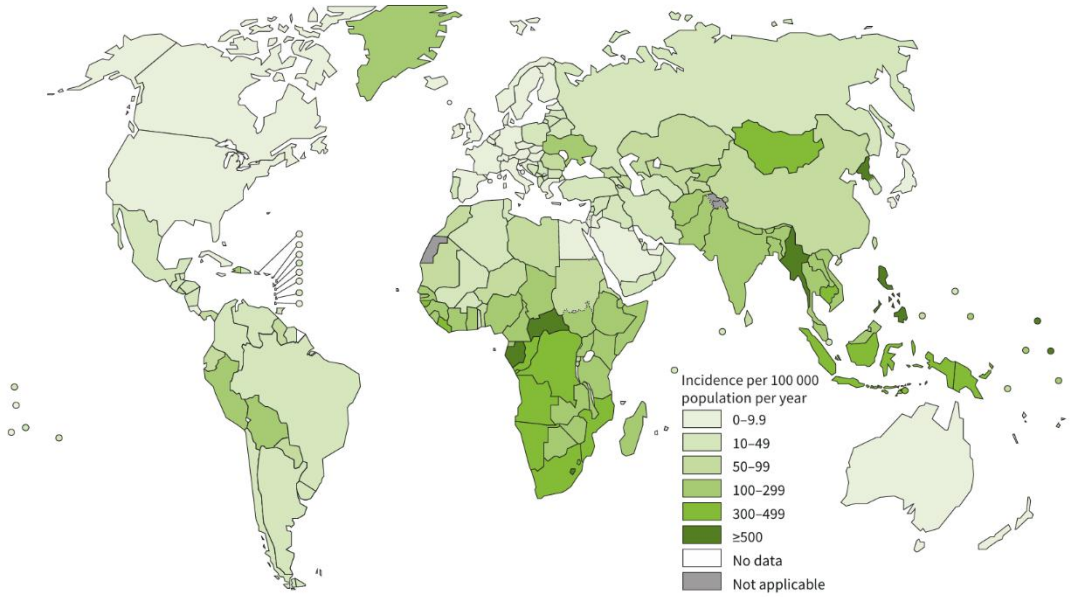

Figure 1 **Global Distribution of Estimated TB Incidence Rates, 2023 (2)**

TB is caused by the bacterium *Mycobacterium tuberculosis,* a non-motile, obligate aerobic bacterium. It's genus, *Mycobacterium*, is thought to have originated more than 150 million years ago and has caused infections since ancient times (6, 7). In the 18th century, TB was widespread and known as the 'white plague'. In 1882, Robert Koch, a pioneering German physician and microbiologist, successfully isolated the tubercle bacillus. After fulfilling Koch's postulates, which require that a microorganism is found in diseased individuals, isolated in pure culture, reproduces the disease in a healthy host, and is re-isolated from

that host, *M. tuberculosis* was confirmed as the causative agent of TB (8). Over the past century, discoveries such as Piquet and Mantoux's tuberculin skin test, Albert Calmette and Camille Guérin's Bacillus Calmette-Guérin (BCG) vaccine, and Selman Waksman's anti-TB drug streptomycin have advanced, but never won, the battle against this global killer (7, 9). The BCG vaccine, still the only licensed vaccine against TB, shows variable efficacy in adults but provides protection against severe forms of TB in children, such as TB meningitis and disseminated TB. It remains an important tool in reducing TB-related illness and death in children and is routinely administered to newborns in high-prevalence areas and to at-risk children elsewhere (10-12).

Culturing the bacteria from patient samples, such as sputum, remains the gold standard for TB diagnosis, as it allows for definitive identification and drug susceptibility testing. However, due to the slow-growing nature of *M. tuberculosis*, culture results can take several weeks. Alternatively, molecular tests like the GeneXpert detect mycobacterial DNA rapidly and provide results much faster. In addition, immune-based tests and chest X-rays are often used to support the diagnosis, especially when bacterial detection is difficult (2, 13-16).

The global TB epidemic is challenged by drug resistance, underdiagnosis, underreporting, and social stigma, which hinder care and treatment adherence. Limited diagnostic and treatment access, especially in resource poor settings, along with conflicts and political instability, disrupt control programs. These complex biomedical, social, and political factors impede progress toward WHO End TB Strategy goals, necessitating a comprehensive, multisectoral response. Understanding the pathogenesis of *M. tuberculosis* infection is crucial for advancing disease control by new therapeutic measures and intervention development.

1.2 From infection to disease: The TB pathogenesis cascade

TB is an airborne infectious disease that even though *M. tuberculosis* is primarily a pulmonary pathogen can still cause disease in almost all parts of the body. Bones, joints, kidneys but particularly the central nervous system (CNS) can get infected by those bacilli who escaped the first site of infection and have entered the blood stream (17, 18). This non-pulmonary TB mainly occurs in young children. In these cases, inadequate nutrition shifts the balance toward the survival of the bacteria rather than the host, increasing the risk and severity of the disease (18). TB exists on a dynamic spectrum, ranging from silent, asymptomatic infection to severe, life-threatening disease. An individual can move along this spectrum over time, progressing to more serious stages or, in some cases, returning to a milder or latent form, depending on factors like immune status and treatment. The overall infection process can be divided into three distinct stages. The primary infection, latent TB infection and active TB disease (2).

Following aerosol transmission via droplets containing the pathogen, *M. tuberculosis* will enter the lungs and reside in tissue-resident alveolar macrophages (AMs), and dendritic cells (DCs), causing mild inflammation. A significant proportion of individuals exposed to *M. tuberculosis* clear the infection without progressing to active disease, a phenomenon attributed to effective innate immune responses (19). Should *M. tuberculosis* evade the bactericidal effects of macrophages and continue to multiply, resulting in the destruction of the cells, blood monocytes and neutrophils will be attracted to the site of infection(20). The aggregation of DCs, neutrophils, monocyte-derived macrophages (MdMs) and natural killer cells (NK) mark the initial stages of granuloma formation. The granuloma environment induces macrophage differentiation into various specialized forms. In addition to fully developed macrophages, this microenvironment gives rise to several distinct macrophage subtypes including multi-nucleated giant cells and foamy macrophages, characterized by their accumulation of lipid bodies, and epithelioid macrophages (21, 22). Epithelioid macrophages tightly interdigitate and aggregate with their neighbouring cells using their zipper like arrays integrated into their cell membranes that link to adjacent cells (23, 24). Each of these macrophage variants plays a unique role in the granulomatous response, contributing to the complex cellular landscape within the granuloma structure (25). The activation of the adaptive immune system in the lung draining lymph node (dLN), resulting

in T and B cell activation and migration, causes the formation of early stage granulomas with an organized structure (26-29). Effective containment of the pathogen at the site of the primary lesion leads to latent TB infection (LTBI). It is notable that over 90 % of infected individuals remain asymptomatic. However, 5-10 % of patients will develop active TB disease, either soon after the initial infection (primary disease) or later in life as a result of reactivation of latent infection. Both primary progression and reactivation are closely linked to changes or deficiencies in the host's immune system, particularly in the ability to develop and maintain immune responses that are crucial for keeping the bacteria under control (25). Such changes could be caused as the result of HIV coinfection(30), stress and/or advanced age, as well as the use of certain immunosuppressive therapies, diabetes, smoking, only to mention a few (28, 31).

Granulomas can be classified into different types based on their histological characteristics, including necrotic, fibrotic, suppurative, and calcified forms, as well as non-necrotic granulomas (32, 33). The diversity of granuloma types reflects the complex interplay between the host immune response and the pathogen, with each form potentially representing different stages or outcomes of the infection process. While organized, non-necrotic granulomas can successfully contain *M. tuberculosis*, necrotic granulomas represent failed containment and instead provide a permissive niche for bacterial persistence and replication (32, 34). The ongoing influx of immune cells helps clear debris but also increases the number of infected cells within the granuloma, contributing to the chronic nature of TB infection (24). This complex interplay between host defence and bacterial survival mechanisms contributes to the chronic nature of TB infections. When a granuloma ruptures, bacteria can be released into the airways, enabling transmission of *M. tuberculosis* to new hosts through coughing or sneezing.

1.3 Role of macrophage in pathogenesis

Macrophages, as phagocytic cells, are part of the first line of defence of the innate immune system against pathogens. They can either be of embryonic origin, localised in specific tissues in utero where they are maintained by *in situ* proliferation (e.g. tissue resident macrophages) or of haematopoietic origin, derived from monocytes recruited from the BM during inflammation (35). The first cells that get infected with *M. tuberculosis* are tissue resident AMs, which arise during embryogenesis (Figure 3). These cells populate the lung

early in development and maintain their population independently of circulating monocytes under steady-state conditions through self-renewal (36, 37). Under steady state conditions, AMs display a predominantly M2-like, anti-inflammatory phenotype, which helps maintain lung homeostasis but may also facilitate persistence of pathogens like *M. tuberculosis* (38).

Infected AMs migrate into the lung interstitium which depends on the ESX-1 secretion system of *M. tuberculosis* and the production of host IL-1β (35). *M. tuberculosis* exploits AMs as host cells, gaining access to essential nutrients such as iron and fatty acids. By modulating the host cell environment to minimize oxidative and nitrosative stress, *M. tuberculosis* creates favourable conditions for its survival and replication (35, 39). This strategic manipulation of AMs allows the pathogen to maintain high replication rates within these primary host cells. As a result, AMs are considered a permissive niche that facilitates the establishment of the infection (35). Nevertheless, after 3 weeks of infection, AMs can exhibit a pro-inflammatory response as shown by Lee et al.(40). Subsequently, *M. tuberculosis* diversifies its niche, infecting polymorphonuclear neutrophils (PMNs) and alternative tissue-resident and recruited macrophage populations (35, 41, 42). PMNs can eliminate a broad range of pathogens through the production of ROS and the release of neutrophil extracellular traps (NETs). However, *M. tuberculosis* exhibits a high degree of resistance to both ROS-mediated and NET-mediated killing (43). Instead, following *M. tuberculosis* infection, PMNs undergo necrosis, creating a vicious cycle in which macrophages phagocytose the dying PMNs, become infected themselves, and subsequently recruit additional PMNs. As a result, neutrophils contribute more to immunopathology than to effective protection during TB (44).

Current research indicates that the recognition of *M. tuberculosis* by the immune system is not governed by a single receptor, but rather involves a combination of pattern recognition receptors acting together. The exact mechanisms by which these different receptors coordinate to detect and respond to *M. tuberculosis* are not yet fully understood, highlighting the complexity and ongoing mystery of host-pathogen interactions. Phagocytes such as macrophages use specific cell surface receptors to recognize and internalize *M. tuberculosis*, whether opsonized or not (45, 46). They express a variety of PRRs including TLRs, NOD-like receptors (NLRs), and SRs, which enable them to recognize

and engulf *M. tuberculosis* and orchestrate downstream immune responses (47, 48). TLR2, TLR4 and TLR9 recognize different mycobacterial components and trigger pro-inflammatory cytokine production (49-52). Interestingly, *M. tuberculosis* itself modulates macrophage responses through pattern recognition receptors. TLR2 interaction enhances bacterial uptake but suppresses MHC class II expression and antigen presentation, while TLR9 recognition of bacterial DNA triggers pro-inflammatory cytokine production (53, 54) (50). These opposing signals may allow the pathogen to balance immune evasion with creating a suitable survival niche. Within the host cytosol *M. tuberculosis* can be detected via sensing of *M. tuberculosis* DNA via the STING/TBK1/IRF3 pathway or RNA via RIG-I and MDA5 leading to interferon type I production (55). The complement system promotes opsonization and phagocytosis of *M. tuberculosis*, facilitating bacterial uptake by macrophages, although the pathogen can also exploit complement components for survival (56, 57).

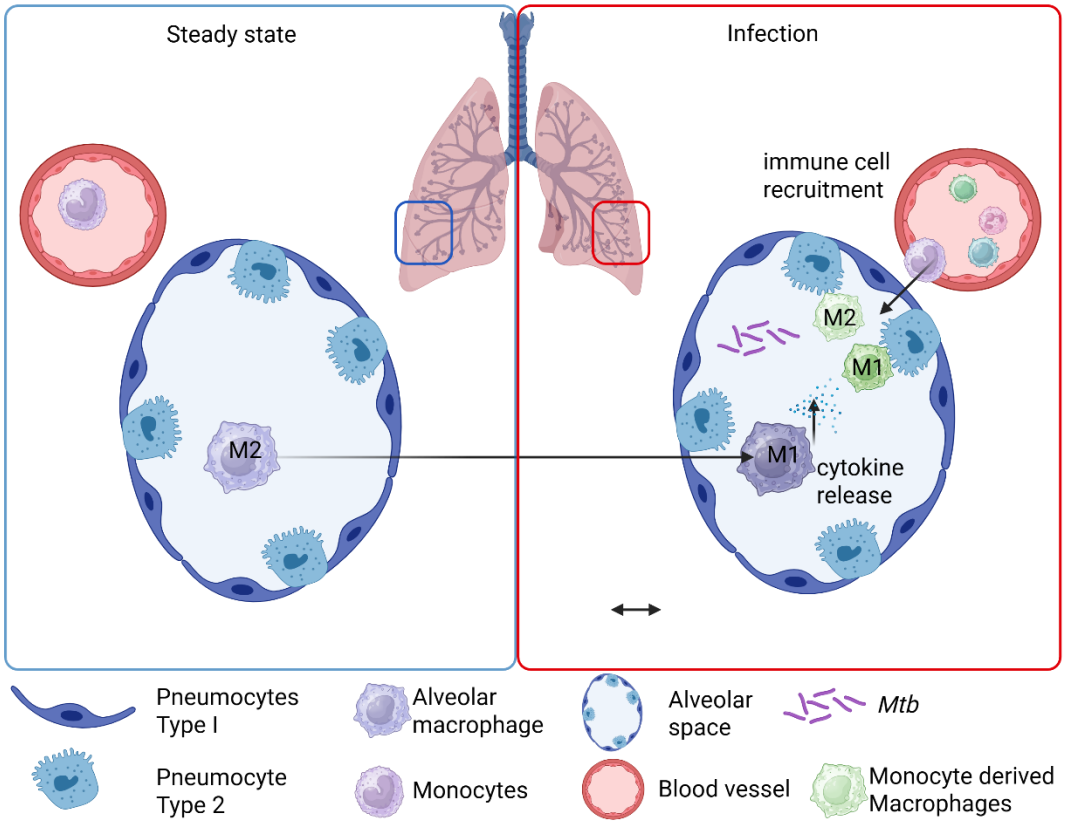

Figure 2 **Steady sate and infection status in the lung (adapted from Kulle et al.(1))**

Macrophages play a key role in presenting antigens via MHC class II to activate $CD4^+$ T cells, which in turn help control *M. tuberculosis* by secreting cytokines like IFNγ to boost

macrophage function. CD8+ T cells, on the other hand, directly kill infected cells. Macrophages produce a wide range of cytokines, including pro-inflammatory (IL-1, IL-6, IL-12, TNF-α) and inhibitory (IL-10, TGF-β) types, after exposure to microbial antigens to regulate both T cell and innate immune responses (58). The timing and balance of these cytokines are critical in orchestrating granuloma formation and maintenance. In the following weeks, infected monocyte-derived DCs migrate to the draining lymph nodes, where they present antigens to naïve T cells and initiate their priming. Upon migration to the lung, *M. tuberculosis*-specific T cells modulate myeloid cell function by promoting antimicrobial subsets, such as IFNγ-activated macrophages, that limit bacterial growth through reactive oxygen/nitrogen species. In contrast, other myeloid populations, such as IL-10-producing macrophages foster an immunosuppressive niche favouring pathogen persistence (59).

M. tuberculosis has several bacterial immune evasion strategies. It successfully delays T cell priming by impairing DC maturation caused by efficient interfering of antigen presentation, requiring 2-8 weeks before TB-specific T cell responses can be detected in humans.(60). In addition, *M. tuberculosis* impairs DCs ability to prime CD4+ T cells by exporting antigens out of the cell, inhibiting antigen possessing mediated by EsxH or antigen degradation. T cell responses can be directly impaired by lipoglycan exported by *M. tuberculosis* (61). Finally, *M. tuberculosis* prevents antigen presentation in infected macrophages to preventing its recognition (50). Paradoxically, macrophages also provide a favourable environment for *M. tuberculosis* survival and replication. The bacteria have evolved mechanisms to inhibit phagosome-lysosome fusion and resist killing by macrophages, creating an intracellular niche where they can evade other immune defences. *M. tuberculosis* manipulates phagosome maturation, preventing phagosome-lysosome fusion and acidification, and thereby create a niche that supports their survival and replication (62, 63). Additionally, *M. tuberculosis* neutralizes ROS and interferes with host immune signalling pathways, further enhancing its persistence within macrophages (64-66). *M. tuberculosis* has developed strategies to interfere with both MHC class II and class I presentation, thereby preventing effective activation of CD4+ and CD8+ T cells (88). Inhibition of phagosomal maturation not only allows the bacteria to survive and replicate within macrophages but also impairs the processing and loading of antigens onto MHC molecules. Some *M. tuberculosis* proteins

may directly interact with MHC molecules or antigen processing machinery, further modulating antigen presentation. Infected macrophages can also spread the infection to other parts of the body, and *M. tuberculosis* can manipulate macrophage responses to create an environment more favourable for its survival.

Understanding the dual role of macrophages in TB has important implications for disease management and treatment strategies. Host-directed therapies that modulate macrophage function could be a potential avenue for TB treatment, particularly in drug-resistant cases. Enhancing the protective functions of macrophages while limiting their permissive role could improve treatment and vaccine efficacy.

1.4 Drivers of TB infection

The risk of TB infection is governed by a complex interplay of host, environmental, and social determinants, each influencing susceptibility, transmission dynamics, and disease outcomes. Transmission risk correlates with the intensity and duration of exposure to *M. tuberculosis* bacilli, with smear-positive individuals being significantly more infectious; an untreated, sputum-positive patient can transmit TB to approximately 10 new individuals per year. Close contacts of infectious TB cases including household contacts, care givers and health care workers are at a higher risk of becoming infected. Host-related factors, including age, sex, immune status, malnutrition, and comorbidities like diabetes or HIV coinfection, modulate risk across the spectrum from exposure to disease progression. According to recent WHO data, adult men (>15 years) bear the highest burden (6.0 million cases in 2023), followed by adult women (3.6 million) and children/adolescents aged 0–14 years (1.3 million). Both paediatric and elderly populations are particularly susceptible to TB infection and disease progression. Socioeconomic status is a well-established determinant of TB risk, with poverty serving as a primary driver of both TB incidence and disease progression. Individuals living in low socioeconomic conditions face multiple interconnected risk factors that increase their vulnerability to TB. These include overcrowded and poorly ventilated housing, limited access to healthcare services, malnutrition, and higher rates of HIV infection. Despite the downward trend in recent years, HIV coinfection remains a significant risk factor for developing active TB disease. In 2023, 6.1 % of all incident TB cases were in people coinfected with HIV, with the WHO African Region particularly affected (2). Limited access to healthcare often leads to delayed diagnosis and treatment, further exacerbating the spread of TB within communities. Additionally, poverty is associated with higher rates of smoking, alcohol abuse, and occupational exposures that can increase TB risk.

TB disproportionately affects men, with nearly twice as many cases reported in men as in women (male-to-female ratio ~1.9:1) (2). This well-documented disparity has traditionally been attributed to gender-related factors such as socially constructed roles, behaviours, and identities that societies assign to individuals. Gender encompasses both gender identity (one's internal sense of self) and gender expression (outward presentation), and is distinct from biological sex, which refers to physiological and genetic differences; both

gender and sex exist on spectrums and are non-binary (67, 68). While behaviours such as smoking and alcohol consumption, which are more prevalent among men in many high-burden countries, do increase risk, they alone do not sufficiently explain the consistent global male bias in TB incidence (69-71). For example, a 2016 national TB prevalence survey in the Philippines identified male biological sex itself as a significant independent risk factor for TB, even when accounting for smoking status (71, 72). Occupational exposures, social behaviours, and differential access to healthcare and health-seeking patterns contribute to increased risk and delayed diagnosis among men in certain settings (71, 73, 74).Even though the prevalence is higher in men, TB remains a major health threat for women and ranks among the top five causes of female mortality worldwide (75). Some studies indicate that disease progression and mortality are higher among women during their reproductive years, with pregnancy further increasing the risk of TB progression (71, 76-78). Despite this vulnerability, global TB mortality rates are consistently higher in males than females across all age groups aged 15 and older (2, 71). However, these sociocultural risk factors vary widely across cultures highlighting the need to move beyond gender-related explanations and incorporate a deeper understanding of biological sex differences in TB susceptibility.

1.5 Sex as a key variable in immune system regulation

In contrast to gender, sex refers to biological characteristics, such as chromosomes, reproductive anatomy, and hormone profiles, that typically define males, females, and intersex individuals. While commonly assigned at birth, biological sex exists on a spectrum and is not strictly binary. Sex bias in disease prevalence, severity, and outcomes is a widespread phenomenon observed across many infectious and non-infectious conditions. Women generally exhibit a more robust immune response compared to men when it comes to fighting infections, responding to vaccinations, and combating certain types of cancer. However, this same heightened immune responsiveness also has a downside. Women are more susceptible to inflammatory conditions and autoimmune diseases such as systemic lupus erythematous, autoimmune hepatitis, primary biliary cholangitis but also inflammatory disease of the central nervous system (79-81). The innate immune response in women is characterised by enhanced phagocytic activity, elevated expression of PRR pathways (e.g. TLRs), and more efficient antigen presentation (82, 83).Sex differences in the incidence and clinical presentation of infectious diseases show a more varied picture. Females generally demonstrate more robust immune responses, producing higher levels of immunoglobulins and mounting stronger antibody responses to both viral infections and vaccinations. Male individuals show increased susceptibility to respiratory tract infections, gastrointestinal infections, and systemic bloodstream infections while female individuals demonstrate higher rates of urinary tract infections, certain vector-borne diseases, and specific sexually transmitted bacterial infections (73, 84-94).

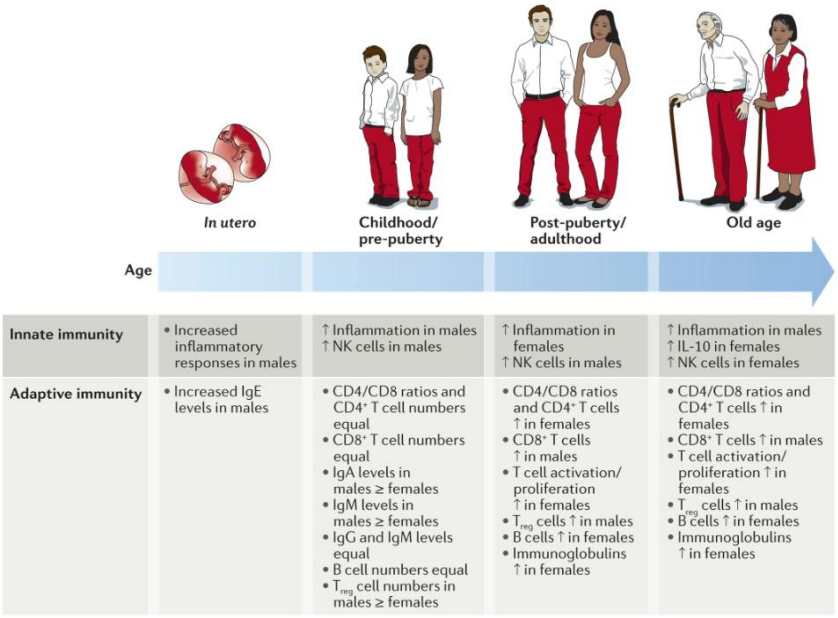

Innate immunity	• Increased inflammatory responses in males	↑ Inflammation in males ↑ NK cells in males	↑ Inflammation in females ↑ NK cells in males	↑ Inflammation in males ↑ IL-10 in females ↑ NK cells in females
Adaptive immunity	• Increased IgE levels in males	• CD4/CD8 ratios and $CD4^+$ T cell numbers equal • $CD8^+$ T cell numbers equal • IgA levels in males ≥ females • IgM levels in males ≥ females • IgG and IgM levels equal • B cell numbers equal • T_{reg} cell numbers in males ≥ females	• CD4/CD8 ratios and $CD4^+$ T cells ↑ in females • $CD8^+$ T cells ↑ in males • T cell activation/ proliferation ↑ in females • T_{reg} cells ↑ in males • B cells ↑ in females • Immunoglobulins ↑ in females	• CD4/CD8 ratios and $CD4^+$ T cells ↑ in females • $CD8^+$ T cells ↑ in males • T cell activation/ proliferation ↑ in females • T_{reg} cells ↑ in males • B cells ↑ in females • Immunoglobulins ↑ in females

Figure 3 **The impact of sex and age on the human immune system (95)**

Sex differences in immune responses arise partly from variations in immune cell composition. Females exhibit higher CD4+ T cell numbers (linked to enhanced thymic activity), elevated CD19+ B cells, plasma cells, regulatory T cells, naïve CD8+ T cells, and mucosa-associated invariant T cells compared to males (96-99). Additionally, females demonstrate stronger humoral immunity, with increased IgM antibody production (99, 100). Conversely, females show reduced proportions of classical (CD14+) and non-classical (CD16+) monocytes, fewer myeloid cells, and lower NK cell counts(101).

In summary, understanding the interplay between sex and gender, alongside their biological and social influences on immunity, is essential for advancing precision medicine and improving prevention, diagnosis, and treatment strategies for both infectious and non-infectious diseases.

1.5.1 Genetic determinants of host defence mechanisms

X-linked gene expression differs substantially between males and females. While males carry only one X chromosome inherited from their mother and one paternal Y chromosome, females carry two copies of the X chromosome, resulting in a potentially toxic double dose of X-linked genes. To balance gene dosage between sexes, females undergo X chromosome inactivation (XCI), a process where one of the two X chromosomes in each somatic cell is randomly silenced early in development (102-104). This process

results in a mosaic pattern of X-linked gene expression in females. This genetic mosaicism provides females with a significant advantage: in the presence of a mutation on one X chromosome, the second, functional X chromosome can compensate in many cells, reducing the severity of potential diseases. In contrast, males, with only one X chromosome, are more susceptible to X-linked disorders. Thus, XCI contributes to the resilience of females against certain genetic conditions. Importantly, approximately 15–23% of X-linked genes in humans escape XCI, leading to their expression from both X chromosomes in females. Notably, the X chromosome harbours a substantial number of genes integral to immune functions, encompassing roles in differentiation, proliferation, cellular activation, metabolism, immune cell trafficking, and signalling. Thus, this biallelic expression in females can enhance immune responses by increasing the production of certain gene products that escape inactivation, such as FoxP3, TLR7, TLR8, CXCR3 or CD40L (81, 99, 105, 106). The escape from XCI is not uniform; some genes consistently escape, while others do so variably across different tissues and individuals. The enhanced expression of immune-related genes in females, due to XCI escape, can provide females with a more robust immune system, potentially offering better protection against infections. However, it may also contribute to the increased prevalence of autoimmune diseases observed in females, as the heightened immune activity can lead to the development of autoimmunity.

Although the Y chromosome is significantly smaller and was once considered a 'genetic wasteland,' recent research has shifted this view, revealing its crucial roles in male biology beyond sex determination. The discovery that loss of the Y chromosome (LOY) in some cells is linked to increased disease risk has highlighted its unexpected importance in maintaining male health. Approximately half of the single-copy genes on the Y chromosome have corresponding functional copies on the X chromosome due to their shared evolutionary origin, although these Y-linked and X-linked gene pairs often exhibit functional divergence. Moreover, when gene functions were ranked, immune system-related genes represented the second most prominent category on the Y chromosome (107).

In summary, the X chromosome's involvement in immune regulation underscores its significance beyond sex determination, highlighting its role in maintaining immune system balance and influencing disease susceptibility. The human Y chromosome has a distinct

evolutionary trajectory and is increasingly recognized for its contribution to sex differences in health and disease, acting through both direct genetic effects and indirect regulatory mechanisms(108).

1.5.2 Hormonal determinants of host defence mechanisms

Sex steroid hormones (SSH) are known to regulate sexual differentiation, secondary sex characteristics, sexual behaviours and reproduction. SSHs include androgens (e.g. testosterone (T), dihydrotestosterone (DHT), androstenedione, androstenediol and hydroxyepiandrosterone (DHEA)), estrogens (e.g. estrone, estradiol (E2), estriol and estrerol), and progesterone (e.g. progesterone itself). Sex hormones are produced primarily in the gonads under the regulation of the hypothalamic-pituitary-gonadal (HPG) axis. The hypothalamus releases GnRH, stimulating the pituitary to secrete LH and FSH, which promote the synthesis of testosterone, estradiol, and progesterone from cholesterol through enzymatic pathways. In certain androgen-responsive tissues, T can be converted to DHT by the enzyme 5α-reductase. DHT is a more potent androgen than T, amplifying the androgenic effects in these tissues (109). E2, the most potent form of estrogen, is mainly produced by aromatization of testosterone (or androstenedione) via the enzyme aromatase. It is primarily produced in the reproductive organs, particularly the ovaries in women. However, it is also synthesized in smaller amounts in the testes, adrenal glands, and adipose tissue (110). In postmenopausal female and men, most of the E2 is produced through peripheral aromatization of androgens in tissues such as adipose and skin, rather than in glandular tissues (111).

The predominant hypothesis for sex-based immunological differences is that SSHs influence the functioning of immune cells (95). SSHs signal through androgen receptors (AR) and estrogen receptors (ERα/ERβ) via classical and non-classical pathways. Classical receptors are cytoplasmic, bound to heat shock proteins until ligand binding triggers nuclear translocation. Hormone response elements (HREs), such as androgen (AREs) and estrogen response elements (EREs) have been identified in the promoter regions of numerous innate immunity genes, directly linking sex hormones to gene transcription (110, 112, 113) (114) and immune function regulation (115-117) . In addition, non-classical G

protein-coupled receptors, typically located in the plasma membrane, trigger rapid responses via ion channels and second messenger pathways, leading to gene transcription at lesser extent compared to other signalling mechanism (118, 119).

SSHs exert profound and diverse effects on both innate and adaptive immune responses, as highlighted in the comprehensive review by Klein and Flanagan (95). Focussing on the innate immunity first, androgens and estrogens differentially regulate the function of innate immune cells such as macrophages, DCs, and NK cells. Monocytes and macrophages express both AR and ERs, enabling them to directly sense and respond to fluctuations in circulating sex steroids (95, 110). T acts as an immunosuppressive agent in macrophages, reducing pro-inflammatory mediators like TNF and iNOS while promoting anti-inflammatory cytokines such as IL-10 and TGF-β. In contrast, E2 exerts dose-dependent effects on macrophage function (120, 121) (122). Low concentrations enhance pro-inflammatory cytokine production and iNOS expression, while high concentrations suppress NF-κB activity and increase IL-10 production (123, 124). This dual effect allows E to fine-tune the balance between pathogen clearance and inflammation-induced tissue damage.

In regard to the adaptive immune system, androgens enhance thymic self-tolerance by upregulating the autoimmune regulator (Aire), a transcription factor that promotes expression of self-antigens in the thymus to eliminate self-reactive T cells and prevent autoimmunity. Additionally, androgens induce T cell apoptosis, inhibit B cell development, and promote T cell exhaustion (125-127). E2 exhibits dose-dependent effects: low doses enhance Th1/IFNγ responses, high doses promote Th2/humoral immunity and expand Tregs while suppressing Th17.(128). Moreover, Estrogen enhances B cell hypermutation and class-switching (129).

Gender-affirming hormone therapy (GAHT), involving estrogen and anti-androgens for transgender women and testosterone for transgender men, can significantly influence immune system regulation. Studies have shown that T therapy in transgender men can suppress type I interferon responses and enhance inflammatory pathways, while E2 therapy in transgender women alters inflammatory related immune characteristics (125). GAHT induces changes in immune cell composition, gene expression, and epigenetic regulation, with effects observed on regulatory T cells, monocytes, NK cells, and cytokine

signalling pathways. Understanding these effects is important for optimizing healthcare in transgender individuals (130). Hormones also play a crucial role in treating hormone-sensitive cancers (131, 132). The female survival advantage in infectious disease mortality declines after the fifth decade of life, aligning temporally with menopause and reduced estradiol (E2) and progesterone (P4) levels, suggesting a potential role for these hormones in modulating immune responses. Brundin et al purposed: As the levels of hormones shift, so might the immune response, affecting the temporal severity of autoimmune and infectious diseases (133).

The intricate relationship between sex hormones and immune regulation provides a compelling framework for understanding sex-based disparities in TB. While androgens may drive immunosuppressive pathways that favour *M. tuberculosis* persistence in males, estrogens dual roles in inflammation and immune activation could underlie protective effects in females during reproductive years.

1.5.3 Exploring the impact of biological sex on TB

For many years, research and public health strategies focused primarily on gender-related determinants, often overlooking the potential impact of biological sex on TB susceptibility and progression. However, recognizing and disentangling the effects of both sex and gender is essential for developing targeted, equitable TB control strategies that address the specific needs of all populations (2, 74). Animal models are particularly well-suited for studying the role of biological sex, as they allow controlled experiments free from many human-specific confounding factors such as environment, lifestyle, and social influences.

Early 1940s studies demonstrated that castration of male and female guinea pigs enhanced TB survival and reduced caseation, suggesting sex hormone involvement in TB susceptibility (134). Recent studies confirmed male bias in mycobacterial infections, with male mice showing increased susceptibility to *M. intracellulare*, *M. marinum*, and *M. tuberculosis*, exhibiting higher bacterial burdens and accelerated mortality that can be prevented by castration (135) (136) (137).

Inherent functional differences between male and female innate immune cells during the early host-pathogen interactions likely contribute to sex-specific outcomes in *M. tuberculosis* infection. Cells of the innate immune system like macrophages express sex

hormone receptors and are the first line of defence against *M. tuberculosis*. Female macrophages exhibit enhanced phagocytic and antimicrobial activity against *M. tuberculosis* compared to males, with estrogen signalling through ERs increasing intracellular NO production and iNOS activity(66). In murine models, female and castrated male mice show significantly higher iNOS expression and enhanced pro-inflammatory responses (TNF-α, IFN-γ, IL-12, IL-17) compared to intact males during early TB infection, correlating with better bacterial control. Conversely, T appears to suppress optimal immune responses through multiple mechanism. Males demonstrate T mediated suppression of NO production and anti-inflammatory cytokines, leading to dysregulated immune responses and increased TB susceptibility (137). T impairs macrophage activation and reduces pro-inflammatory cytokine production, potentially contributing to inadequate bacterial control and TB disease progression. Additionally, estrogen influences macrophage lipid metabolism by restricting foamy macrophage formation through downregulation of scavenger receptors and promotion of cholesterol efflux (138).

E2 enhances Th1-mediated IFN-γ production and macrophage activation, promoting the expression of key antimycobacterial cytokines including TNF-α, IL-1β, and IL-12. In contrast, testosterone generally suppresses these pro-inflammatory cytokine responses. The resulting hormonally-regulated cytokine profiles may contribute to sex-specific TB immunopathology, with enhanced female IFN-γ/IL-12 responses theoretically conferring protective immunity against mycobacterial infection (73, 95). PRR expression also differs between sexes, influenced by both sex hormone signalling and X-chromosome gene dosage effects. TLR8 variants associate with pulmonary TB susceptibility specifically in men, while TLR4 shows higher baseline expression in male macrophages (122) (139).

CD4+ T cells play a crucial role in protective immunity against *M. tuberculosis* (140). Female CD4+ T cells demonstrate a more robust Th1 response compared to their male counterparts. This enhanced Th1 profile in females is characterized by increased production of key cytokines such as IFNγ and TNFα, which are critical for controlling *M. tuberculosis* infection (141). In experimental models using the H37Rv strain, *M. tuberculosis* levels remain consistently higher in male lungs throughout infection, even after adaptive immunity activation. Importantly, this pattern is not universal as infection with the HN878 strain shows minimal sex differences in bacterial loads until very late in infection, when

CFU counts finally diverge between sexes. The Schneider laboratory demonstrated that increased male susceptibility to H37Rv infection is associated with reduced B cell follicle formation in the lungs (142, 143). Rather than indicating defective bacterial control per se, these findings suggest that sex differences in early innate immune responses primarily influence granuloma architecture and organization, particularly B cell follicle formation (71).

While previous research has established that early events in *M. tuberculosis* infection, particularly the activation state of initially infected cells, play a critical role in determining clinical outcomes, the specific contribution of sex-based differences to these early interactions remains poorly understood. Mounting evidence demonstrates that innate immune responses differ substantially between sexes, particularly in macrophage activation patterns and cytokine production profiles. However, whether these sex-based differences in innate immunity directly influence the early determinative events of TB infection is unknown. Understanding these mechanisms requires direct investigation of how sex hormones modulate host-pathogen interactions during TB infection. But do sex and sex hormones actually influence how macrophages respond to *M. tuberculosis* infection and can we study these interactions *in vitro*?

2 Research aims and questions

This PhD thesis aims to investigate the impact of biological sex on the interaction between *M. tuberculosis* and human macrophages, its primary host cells. Despite advances in diagnosis and treatment, TB remains a significant global health challenge, with adult males generally more affected than females in most populations worldwide. The study aims to elucidate the immunological, cellular, and transcriptional differences between male and female macrophages in response to *M. tuberculosis* infection. Additionally, it explores the influence of sex steroid hormones on macrophage phenotype and *M. tuberculosis* infection outcomes. The research focuses on two main areas:

1. Investigation of sex differences in an *in vitro* infection assay using *H37Rv M. tuberculosis* and primary human monocyte-derived macrophages:
    - Establishment and utilization of a high content screening confocal microscope and automated customized image data analysis software to quantify cell count, infection rate, and bacterial load in female and male monocyte-derived human macrophages.
    - Morphology- and phenotype-based analysis of macrophage polarization upon *M. tuberculosis* infection.
    - Bead-based immunological analysis of secreted cytokines from monocytes and macrophages.
    - Transcriptional analysis of *M. tuberculosis* infected female and male-derived macrophages using RT-qPCR and RNA bulk-sequencing.
2. Analysis of *M. tuberculosis* infected primary human monocyte-derived macrophages differentiated and infected under constant treatment with sex hormones. This analysis employs the same methods and techniques as in 1, but with an additional focus on the influence of sex hormones.

The aim of these analyses was to elucidate the comprehensive interplay between macrophage from male and female donors with *M. tuberculosis*, in the presence and absence of sex hormones, with the potential to uncover molecular mechanisms that underlie sex-based differences in TB susceptibility and progression.

3 Material and Methods

3.1 Material

3.1.1 Chemical, Reagents and Sera

Table 1 Chemicals, reagents and sera

Chemicals	Company
7H9 Agar	BD
7H11 Agar	BD
Albumin bovine fraction V, protease-free (BSA)	SERVA Electrophoresis GmbH
Aqua destilled	
Aqua nuclease free	Carl Roth GmbH & Co.
BioColl separation solution	Bio-sell
Bovine Serum, heat inactivated	BIOWEST SAS
Charcoal, dextran coated	Sigma-Aldrich
Chloroform	Carl Roth GmbH & Co. KG
Dimethylsulfate (DMSO)	Carl Roth GmbH & Co. KG
Dulbecco´s Phosphate Buffered Saline (DPBS) w/o Calcium & Magnesium	PAN$_{TM}$-Biotech GmbH
Entellan	MERCK
Ethanol (EtOH)	Merck KGaA
Ethylenediaminetetraacetic acid (EDTA)	Carl Roth GmbH & Co. KG
Fetal calf serum (FCS), heat inactivated	BIOWEST SAS

Glycerol	Carl Roth GmbH & Co. KG
Recombinant human M-CSF (carrier-free)	BioLegend, Inc.
L-Glutamine (200 mM)	PANTM-Biotech GmbH
Methylenblue (Löfflers)	Carl Roth GmbH & Co.
Mouse Serum	PANTM-Biotech GmbH
OADC (oleic acid, albumin, dextrose, catalase)	BD Biosciences
Paraformaldehyde (PFA)	Carl Roth GmbH & Co. KG
Potassium Hydrogencarbonate (KHCO3)	Carl Roth GmbH & Co. KG
2-Propanol	Carl Roth GmbH & Co. KG
Roswell Park Memorial institute Medium (RPMI) 1640, w/o:L-Glutamin, w/o: Phenol red, w:2.0 g/L $NaHCO_3$	PAN Biotech
Sealing Tape, optical clear (for 96-well plates)	Sarstedt AG & Co. KG
Sodium azide (NaN3)	Carl Roth GmbH & Co. KG
Sodium carbonate (Na2CO3)	Carl Roth GmbH & Co. KG
Sodium Hydrogencarbonate (NaHCO3)	Carl Roth GmbH & Co. KG
Sodium pyruvate (100 mM)	PANTM-Biotech GmbH
Sulfuric acid 95-98 % (H2SO4)	Carl Roth GmbH & Co. KG
TMB substrate solution	BioLegend, Inc.

TRI Reagent® RNA/DNA/Protein isolation rea-gent	Zymo Research Corporation
Triton X-100	Carl Roth GmbH & Co. KG
Trypan blue, 10 g	Carl Roth GmbH & Co. KG
Tween20	Carl Roth GmbH & Co. KG
Tween80	Carl Roth GmbH & Co.
water (BioScience-grade, nuclease-free, DEPC-treated)	Carl Roth GmbH & Co. KG
Xylol	Carl Roth GmbH & Co. KG
Ziehl-Neelson carbolfuchsin	Carl Roth GmbH & Co. KG

3.1.2 Consumables

Table 2: Consumables

Consumable	Company
1 ml luer	BD
6 well cell culture plate	Sarstedt AG & Co. KG
12 well cell culture plate	Sarstedt AG & Co. KG
96 well LightCycler Plate	Sarstedt AG & Co. KG
96 well cell culture plate, flat bottom	Sarstedt AG & Co. KG
96 well cell culture plate, round bottom	Sarstedt AG & Co. KG
96 well cell culture plate, V-bottom	Sarstedt AG & Co. KG
96 well PhenoPlate, black, optically clear flat-bottom, tissue-culture treated, lids	Revvity

BD BBL™MGIT™	BD
Biosphere® Safe Seal Tube 1.5 ml	Sarstedt AG & Co. KG
Biosphere® plus DNA-, DNase, Rnase-free fil-ter tips (200 µL, 20 L, 10 µL)	Sarstedt AG & Co. KG
Blunt syringe 0.4x25 mm 27 G x 1	BRAUN
CD14 Microbeads, human	Miltenyi Biotec
Cell Strainer (70 µm)	Corning Inc.
Cell Strainer (70 µm)	Miltenyi Biotek
Costar® 96-well Cell Culture Plates (flat bottom, round bottom)	Corning Inc.
Costar® 24-well Cell Culture Plates	Corning Inc.
Costar® 12-well Cell Culture Plates	Corning Inc.
Costar® 6-well Cell Culture Plates	Corning Inc.
Combitips advanced® 0.5 ml	Eppendorf
Combitips advanced® 5 ml	Eppendorf
Combitips advanced® 10 ml	Eppendorf
Deep Well MegaBlock®, 2.2 ml, PP	Sarstedt AG & Co. KG
Filter tip 100-1.000 µL, DNA-, Dnase, Rnase-free	nerbe plus GmbH & Co. KG
Micro-touch blue nitril gloves M	Ansell
Multiply® -µStrip 0.2 ml chain	Sarstedt AG & Co. KG
Multiply®-Pro cup 0.2 ml	Sarstedt AG & Co. KG
Parafilm®	Bemis Company, Inc.

Petri dish, 92 x 16 mm, transparent, with cams	Sarstedt AG & Co. KG
Pipette tips (10 µL, 200 µL, 1000 µL)	Sarstedt AG & Co. KG
Pipette tips, filter tips (10 µL, 200 µL, 1000 µL)	Sarstedt AG & Co. KG
Rotilabo® glass rods	Carl Roth GmbH & Co. KG
Rubber policeman, 7×25 mm	Glaswarenfabrik Karl Hecht GmbH & Co. KG
Rubber policeman, 35×25×32 mm	Glaswarenfabrik Karl Hecht GmbH & Co. KG
Reaction tube, 1.5 ml & 2 ml, PP	Sarstedt AG & Co. KG
Rnase-ExitusPlus™	ITW Reagents, S.R.L.
Sarstedt Screw cab tube, 15 ml, PP with conical base, sterile	Sarstedt AG & Co. KG
Sarstedt Screw cab tube, 50 ml, PP with conical base, sterile	Sarstedt AG & Co. KG
SepMate™ tubes-50 (IVD)	Stemcell
Schülke mikrozid®	Schülke & Mayr GmbH
Sealing Tape, optical clear (for 96-well plates)	Sarstedt AG & Co. KG
Stericup Quick Release 500 ml	Merck KgaA
StripetteTM Serological Pipets 1 ml, 5 ml, 10 ml, 25 ml	Corning Inc.
Syringe filter, Filtropur S plus, pore size 0.2 µm	Sarstedt AG & Co. KG
Tissue culture dish, 100 x 20 mm	Sarstedt AG & Co. KG

3.1.3 Technical devices

Table 3: Devices

Equipment	Company
- 20 °C freezer S2	Liebherr-Hausgeräte GmbH
- 80 °C freezer S2	PHC Europe
4 °C fridge S2	Robert Bosch GmbH
Autoclave Systec DX-150	Systec GmbH, Germany
BioTek Synergy HTX multimode reader	Biotek
Cell Counting Chamber Neubauer improved, depth 0.1 mm, 0.0025 mm2	Hecht
Eppendorf Multipette Stream	Eppendorf
FACSDiscover™ S8 Cell Sorter	BD
Finnpipette™ (20 µL, 100 µL, 200 µL, 1000 µL)	Starlab
Heraeus Multifuge X1R Centrifuge	Thermo Fisher Scientific Inc
Heraeus Pico 17 Centrifuge	Thermo Fisher Scientific Inc
Incubator Heratherm	Thermo Fisher Scientific Inc
Incubator BD 53	BD
Incubator S2	Binder
Infinite M200 PRO® Plate Reader	
labcycler Basic thermocycler	
MACSQuant® Analyzer 10	Miltenyi Biotek
MACSQuant® Analyzer 16	Miltenyi Biotek
Multi-channel Transferpette® S -8 (20-200 µL)	Starlab

Multi-channel Transferpette® S -12 (20-200 µL)	Starlab
NanoDropTM 1000	ThermoFischer
Nikon Eclipse TS100 Microscope	Nikon
Nikon Eclipse Ti Microscope	Nikon
Opera Phenix Plus	PerkinElmar, Revity
Pipetus	Hirschmann
Grant bio PMS 1000 microplate shaker	Keison Products
Sterile Working Bench Herasafe Safe 2020	Heraeus instruments
Rotilab glass rods	Carl Roth GmbH & Co. KG
Techne Dri-Block DB-2D heater	
Vortexer IKA MS 3 basic	
Water Bath sub Aqua 18 Plus	Grant

3.1.4 Overview of commercial kits applied

Table 4: Kits applied

Kit Name	Provider	Product Code
Human IL-8 ELISA MAXTM Deluxe Set	BioLegend, Inc.	B391392
Human TNFα ELISA MAXTM Deluxe Set	BioLegend, Inc.	430204
Ilumina NextSeq 100, P3 reagent kit for NextSeq 2000	Ilumina	

LightCycler® 480 SYBR Green I Master	Roche Deutschland Holding GmbH	
Maxima First Strand cDNA Synthesis Kit for RT-qPCR	Thermo Fisher Scientific Inc	K1642, LOT 258429
RNA Clean & Concentrator-5 (200 Preps.)	Zymo Research	R1016
W270224-LB-FB Costum Biolegend Legendplex	BioLegend, Inc.	H-101335-116-L.Buer
Zymo-Seq RiboFree ® Total RNA Library Kit	Zymo Research	R3000

3.1.5 Antibodies used for Flow Cytometry

Table 5 Antibodies

Antigen	Clone	Fluorophore	Isotype	Dilution	Company (order nr.)
CD45 mouse anti-human	HI30	BV421	Mouse IgG1, κ	5 µl for 1x10^6 cells	BD (563879)
CD14 mouse anti-human	MoP9	BV510	BALB/c IgG2b, κ	5 µl for 1x10^6 cells	BD (563079)

3.1.6 Culture media, buffers and Solutions

Table 6: Culture media, buffers and solutions

Name	Composition
1% PFA solution	1% PFA (w/v) in DPBS
2% PFA solution	2% PFA (w/v) in DPBS
4% PFA solution	4% PFA (w/v) in DPBS
7H9 agar medium for use	4.7g 7H9 base per 1L broth, 0.2% glycerol v/v, and 0.05% Tween 80 v/v, 10% v/v OADC in H_2O
7H11 agar for use	1.9% (w/v) 7H11 agar, 0.5% (v/v) glycerol, 10% (v/v) bovine serum in dH_2O
Red blood cell lysis buffer	0.5% (v/v) Triton X-100 in ddH2O, sterile
Charcoal stripped FCS (csFCS)	FCS supplemented with 5 % charcoal, centrifuged and sterile filtrated
ELISA wash buffer	PBS + 0.05% Tween-20
ELISA stop solution	2N H_2 SO_4
EDTA solution	0.02 mol/L in H20, sterile
Erylysis buffer	155 mM NH4Cl, 10 mM KHCO3, 0,1 mM EDTA in ddH2O, sterile
Fluorescence assisted cell sorting (FACS) buffer	3% (v/v) Fetal calf serum (charcoal filtered, heat-inactivated), 0.1% (w/v) NaN3, 2 mM EDTA in 1x PBS
csRPMI cell culture medium	5% L-Glutamin, 10% csFCS
MACS buffer	0.05% BSA, 0.2 mM EDTA, in DPBS
Trypan blue working solution	0.05% (w/v) in DPBS
WTA buffer	1% (w/v) BSA, 1% (v/v) Tween80 in ddH2O, sterile

3.1.7 Hormone stimulation for *in-vitro* treatment

Table 7: Hormones

Name	Company	Cas No
5α-Dihydrotestosterone (DHT)-Solution	MERCK	521-18-6
17β-Estradiol-Solution	MERCK	50-28-2

3.1.8 Mycobacterium strains used for infection assays

Table 8: Mycobacteria strains

Latin name	short	Provided by
Mycobacterium Bovis Bacillus Calmette-Guérin	*BCG*	Reiling group
Mycobacterium Bovis Bacillus Calmette-Guérin expressing GFP	*BCG-GFP*	Reiling group
Mycobacterium tuberculosis H37Rv 2010	*MTB H37Rv*	Niemann group
Mycobacterium tuberculosis H37Rv expressing dsRED 2010	*MTB H37Rv dsRED*	Schaible group

3.1.9 Human samples

Ethical approval

Blood donation (ranging from 100-350 ml) of healthy donors were collected at the internal blood donation service from the research center borstel free of charge. Samples were directly processed in downstream experiments. Donor's year of birth and sex were provided. Ethical approval from the University of Lübeck was granted under the reference number 2025-364.

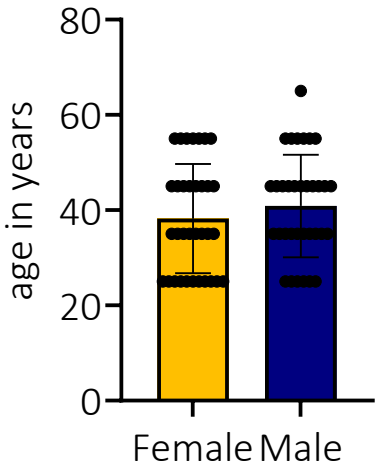

Figure 4 **Age distribution of blood donors from all experiments**

Age distribution blood donors separated by sex and grouped in 20-30, 30-40, 40-50, 60-70 years. The data include mean +/- SEM of 34 individuals/sex.

3.1.10 Software and Databases

Table 9: Software and databases

Software / Databases	Application
BioRender.com	Figure composition
EndNote X9.3.3	Literature library and citation manager
FCS Express	Flow analysis, evaluation of LEGENDplex data
GraphPad Prism10, version 10.0.1	Graphical illustration and statistical analysis of data
Harmony software (v 4.6, Perkin Elmer)	Automated image analysis of confocal, immunofluorescent pictures
Harmony software (v 5.2, Perkin Elmer)	Automated image analysis of confocal, immunofluorescent pictures
legendplex.qognit.com	Evaluation of LEGENDplex data

LightCycler® 480 SW 1.5	qPCR analysis
Perplexity, Deepl, googleAI, claude, Pubmed-NCBI	Writing/ spelling/ phrasing/ Literature research// coding
TeamViewer	Remote access
rStudio and R4.2.2	Data analysis

3.2 Methods

3.2.1 Cell biological methods

All cell culture work was performed in laboratories under biosafety 2 and 3 condition according to the guidelines.

3.2.1.1 Cultivation of Mycobacterium strain and stock generation

In this study the *Mycobacterium tuberculosis (MTB) H37Rv* strain and genetically modified variants (GMOs) based on this strain were provided by Prof. Dr. Ulrich Schaible from the working group cellular microbiology at the Research Center Borstel, by PD Dr. Norbert Reiling from the working microbial interface biology and by Prof. Dr. Stefan Niemann from the working group molecular and experimental mycobacteriology at the Research Center Borstel. In addition to that *Mycobacterium bovis Bacillus Calmette-Guérin* (*BCG*) was provided by PD Dr. Norbert Reiling. Stocks are stored at - 80 °C under BSL2 and BSL3 conditions. All steps related to *M. tuberculosis* were performed in accordance with BSL3 guidelines.

3.2.1.2 Stock generation of *M. tuberculosis* H37Rv

For the stock generation of *Mycobacterium* strain*s* a preculture was generated first. Therefor 1 millilitre (ml) of frozen stock were thawed and transferred in 10 ml *MTB/BCG* growth medium in a 30 ml culture medium bottle incubated at 37 degrees Celsius (°C) on a rolling unit with 0.8-1 rounds per minute (rpm). Samples were incubated until reaching an optical density of optical density (OD) OD600 = 0.1-0.150. Therefor 1 ml of the sample were transferred into a cuvette and measured with a photometer. The tightness of the culture flask was checked by incubating 50 ml of the growth medium for 24 h at 0.8-1 rpm 24 hours (h) before transferring the preculture. Next the remaining preculture was transferred to the main culture. The main crop was grown to an OD600 of 0.8. The stocks were aliquoted in 2 ml screw-top vials, 1 ml culture in each vial and stored at - 80 °C.

3.2.1.3 Sterility control during the main culture

To ensure sterility of the newly generated stocks, 50 microliters (µl) of the main culture is inoculated in brain heart infusion (BHI) medium, a nutrient-rich growth medium commonly used in microbiology for cultivating a wide variety of microorganisms, including fastidious

bacteria and Luria-Bertani (LB) medium another widely used bacterial culture medium. Uninoculated medium is considered as a negative control. Samples are incubated at 37 °C for 5 days (d). Furthermore, 50 µl of the main culture is plated on blood agar plates and incubated at 37 °C for 2 d.

3.2.1.4 Ziehl-Neelsen staining of *M. tuberculosis*

The Ziehl-Neelsen (ZN) stain is a bacteriological staining method that is employed for the identification of acid-fast bacteria, particularly members of the Mycobacterium genus. The cell walls of acid-fast bacteria contain mycolic acid, which confers resistance to decolorization by acid. A 10 µl droplet of the bacteria solution is added to a microscope slide and dispersed using a second slide. Following a 20-minute (min) drying period under a fume hood, the slide is transferred into a 40 ml solution of 5 % phenol and 70 % ethanol, where it is fixed for a further 10 min. Subsequent staining procedures were conducted in a BSL2 facility. The samples were initially incubated in the clearing agent xylol for a period of five minutes on each of three occasions. Next, the samples were incubated for 1 min in a solution of xylol and ethanol (1:2), followed by three times 5 min incubation steps with ethanol (100 %). Subsequently, the samples were expeditiously transferred into 96 % ethanol, 70 % ethanol, and 40 % ethanol, and finally into distilled water for a period of five minutes. The samples were then incubated with carbolfuchsin, which has a strong affinity for mycolic acids found in mycobacterial cell walls, before being heated over a flame without boiling. Once the remaining staining solution had cooled, it was discarded, and the samples were washed with distilled water. Decolourisation was then performed using 0.5 % hydrochloride (HCL) in 70 % ethanol. The samples were stained with methylene blue and washed in distilled water. This was followed by washing steps using ethanol 96 % and isopropanol. Finally, another xylol clearing was performed, after which the slides were covered with cover slips. The acid-fast bacteria were coloured red, while the cell nuclei were coloured blue.

3.2.1.5 Determination of stock concentration by colony forming units (CFU)

In order to determine the number of bacteria per ml a colony-forming unit (CFU) assay was performed. CFU is a measure to determine the number of viable bacteria. Samples were tested in triplicates and the mean was calculated for further analysis. Therefor veils of

frozen stocks were thawn at room temperature (RT) and the bacteria were dissociated using a blunt 27 G syringe and 1 ml luer by drawing up the syringe 10 times (table 1). Afterwards a serial dilution of 1:10 (from 10^{-1} to 10^{-8}) was performed using a deep-well plate (900 µl medium + 100 µl stock). From each of these dilutions, 50 µl was plated on half of an agar plate supplemented with calf serum (FCS), sealed with parafilm and incubated at 37 °C for 21 d. In order to ensure the reliability of the results, triplicates are needed for each veil tested, with three veils being the minimum number required. After 21 d, the number of colonies for each dilution is counted. This allows the calculation of the number of bacteria per 1 ml of the original sample, as follows:

$$\frac{Bacteria}{ml} = (mean\ of\ counted\ number\ of\ colonies)\ x\ 20\ x\ dilution\ factor$$

3.2.1.6 Determination of cell count

In order to determine the cell count of isolated cells with the help of the Neubauer counting chamber (depth=0.1 mm, area=0.0025 m²), cells were diluted in 0.004 % trypan blue. Trypan blue indicates the intactness of cells, staining apoptotic cells blue by passing the perforated membrane. Cells which did not turn blue were counted in all four squares, and the cell count was calculated using the following equation:

$$C = n * D * 10.000$$

$$C = concentration\ of\ cells\ \left(\frac{cells}{mL}\right)$$

$$n = mean\ number\ of\ viable\ cells\ per\ square$$

$$D = dilution\ factor\ of\ cell\ solution$$

$$10.000 = correction\ factor\ of\ Neubauer\ counting\ chamber\ used$$

3.2.1.7 Isolation of human peripheral blood mononuclear cells

For the isolation of human peripheral monocular cells (PBMCs) heparinized peripheral blood from healthy donors was used. Blood from male and female blood donors were used in parallel. One day before the PBMCs isolation, SepMate™ PBMC isolation tubes (50 ml, StemCell) were supplemented with 15 ml density gradient medium BioColl carefully pipetted through the central hole of the inserts and stored at RT. The day of PBMC isolation

blood was diluted 1:1 with warm DPBS. Pipette 30 ml diluted blood down the side of the tube onto the insert for low layering of the blood on the density gradient medium. Always keep the tubes vertical. Centrifuge samples at 1200 x g for 10 min at RT, with the brake on. For samples older than 24 h the company recommends 20 min centrifugation. Pour off the top layer, which contains the enriched monocular cells (MNCs) into a new tube. Avoid holding the SepMate^{TM} in a vertical position for more than 2 seconds (sec). Wash enriched MNCs with 10 ml 1X DPBS. To avoid platelets contamination, the next centrifugation step is performed at 120 x g without break. The pellet is resuspended in 10 ml 1 X DPBS again and centrifuged at 300 x g for 10 min. Afterwards the pellets belonging to one donor are pooled in one 50 ml falcon and again centrifuged at 300 x g for 8 min.

Before monocyte purification, red blood cells were lysed using erylysis buffer without facing a harmful effect on the remaining leukocytes. Therefor the cell pellet containing the PBMCs was resuspended in 5 ml lysis buffer and incubated for 5 min at RT. The incubation process was stopped after 5 min by adding 10 ml 1X DPBS and the cells were centrifuged at 600 x g for 5 min at 4 °C. The supernatant was discarded, and the cell pellet was checked for a clear phase. If so, the cells were washed with 10 ml 1 X DPBS at 600 x g for 5 min at 4 °C. In case the pellet remained red, a second red blood cell lysis was performed. To avoid cell clumps the PBMC solution was filtered through a 0.70 µm cell strainer and finally resuspended in 5 or 10 ml 1X DPBS to determine the cell number by using a Neubauer Chamber (as described in 3.2.1.6) for further applications.

3.2.1.8 Isolation of CD14+ monocytes using MACS MicroBeads by Miltenyi Biotek

Approximately 10% of PBMCs in human peripheral blood are CD14+ monocytes. The isolation of CD14+ monocytes from PBMCs was performed by using the magnetic-activated cell sorting (MACS) MicroBeads system by Miltenyi Biotek. This system enables a gentle cell isolation technique with minimum labelling with non-toxic nano-sized magnetic beads using a high magnetic gradient in the MACS Columns. All reagents and the magnet should be ice cold. The isolation was performed according to the manufacturer's instructions on ice. For washing the PBMCs an excess volume of 1X MACS buffer (40 µl per 1 x 10^7 cells) at 300 x g for 10 min at 4 °C was used. The cell pellet was resuspended in 20 µl of anti-human CD14+ particles per 10^7 total cells and mixed thoroughly. After 15 min incubation at 4 °C, the cell-beads solution was diluted with 1X MACS buffer (1-2 ml per 1 x10^7 cells). The

suspension was centrifuged at 300 x g for 10 min at 4 °C. Up to 10^8 cells can be resuspended in 500 µl 1X MACS buffer. Follow the protocol for magnetic separation with MS and LS columns.

3.2.1.9 Magnetic isolation of CD14+ monocytes using MS or LS Columns

Magnetic isolation of CD14+ monocytes was performed according to manufacturer's instructions. Place the columns in the precooled magnet suitable for MS or LS columns. Columns were placed correctly into the magnet provided. The columns were prepared by rinsing either 3x3 ml for the LS column or 3x500 µl for the MS column. Next the cell suspension was allied onto the column and the unlabelled cells that pass through were collected. The columns were washed with the appropriate amount of buffer (LS: 3x3 ml, MS: 3x500 µl) and the flow through was collected. New buffer was only added when the column reservoir was empty. CD14+ cells were collected by removing the column from the magnet separator and placing it on a suitable collection tube. Either 5 ml MACS buffer for the LS or 1 ml for the MS column were added and the magnetically labelled cells were immediately flushed out by firmly pushing the plunger into the column. Positive cell fraction was resuspended in 2 ml csRPMI per 10^7 cells at 300 x g for 10 min. Lastly, cells were resuspended in 1 ml warm medium and counted using a 1:10 dilution and the Neubauer Chamber (as described in 3.2.1.6).

3.2.1.10 Generation of human monocyte-derived macrophages *in vitro*

After the purification of the CD14+ monocytes, cells were cultured in complete and charcoal stripped FCS supplemented RPMI (csRPMI) medium containing RPMI 1640 (without phenol red) supplemented with 10 % inactivated FCS stripped with charcoal (csFCS), L-Glutamine (2 mM). For the inactivation of the foetal bovine serum, FCS was incubated at 56 °C for 30 min. In order to remove non-polar materials including certain growth factors, hormones and cytokines 50 ml FCS were incubated with 1 g activated charcoal, gently shaking at 4 °C over night. The csFCS was then centrifuged at 2000 rpm for 15 min at 4 °C to remove the activated carbon and filtrated sterile using a 0.2 µM sterile filter.

For the induction of monocytes differentiation into macrophages, monocytes were cultured in the presence of human macrophage colony stimulating factor (M-CSF) (10

ng/ml). For the high-content screening assays, the cells were initially incubated in a CellCarrier ™-96 ultra-microplate with an optically clear cyclic olefin foil bottom (PerkinElmer, Revvity) at a cell concentration of 1.0 x 10^6 cells/ml (1.0 x 10^5 cells/well in 200 µl csRPMI supplemented with 10 ng/ml M-CSF) at 37 °C and 5 % CO_2 for 10 d. On day 4 and 6, half of the medium was exchanged, on day 8 a complete medium change was performed. After successful differentiation of monocytes into human monocyte-derived macrophages (hMdMs), cells were used for further analysis.

Table 10: Cell seeding formats

Plate type	**Number of cells and medium per well**	**Application**
6-well plate	1x10^6 cells in 5 ml	Staining for flow cytometry
12-well plate	5x10^5 cells in 2 ml	RNA isolation
96-well plate	1x10^5 cells in 200 µl	CFU analysis of *MTB* strains
96-well plate	2x10^5 cells in 200 µl	Legendplex analysis of Monocytes
96-well plate	4x10^5 cells in 200 µl	Legendplex analysis of hMdMs
96-well Phenoplates	1x10^5 cells in 200 µl	Confocal high content screening assays

3.2.1.11 Assessing cell concentration with the Neubauer haemocytometer

The Neubauer haemocytometer is used to quantify the cell number per ml in a suspension. Depending on the type and concentration of the sample, a dilution with a suitable concentration should be prepared for cell counting. As a vital stain, trypan blue is used. Intact cells do not take up the dye and are therefore not stained. Dead or damaged cells take up the dye and appear blue under the microscope. Trypan blue itself is cytotoxic causing cell death after 10-15 min. Due to this, samples should be analysed within 5 min after staining. Normally a 1:10 or 1:100 dilution was used for staining and 10 µl were then transferred into the Neubauer chamber itself. Cells within the four corner squares of the

haemocytometer were counted and the mean was calculated. The cell count per ml was calculated as followed:

$$\frac{cells}{ml} = mean\ cellcount\ of\ corner\ squared\ x\ dilution\ factor\ x\ 10^4$$

3.2.1.12 *In-vitro* treatment of macrophages with steroid hormones

The objective of this study was to investigate the influence of steroid hormones on monocyte to macrophage differentiation and *M. tuberculosis* infection. To this end, cells were subjected to constant treatment with various hormone concentrations throughout the differentiation and infection periods. To prevent additional stress on the cells, hormone treatment was conducted concurrently with medium replacement using preheated supplemented csRPMI without phenol red with 10 ng/ml M-CSF on days 4, 6, and 8. On the day of infection, cells were treated before and additionally at 4 hpi for assays lasting longer than 24 hours. For Legendplex and RNA generation assays, cells were further incubated within the infection medium in accordance with the procedures outlined in chapter 3.2.1.13. For hormonal treatment, 5α-Dihydrotestosterone (DHT) and 17β-Estradiol solutions (E2) were employed in concentrations ranging from 10 nM to 20 µM.

3.2.1.13 Infection of monocyte-derived macrophages with *M. tuberculosis*

Human MDMs were infected with *M. tuberculosis H37Rv wild-type* and GMOs and *Mycobacterium Bovis (BCG) GFP* for various experimental set-ups. All experiments including *M. tuberculosis* strains were performed under BSL3 conditions, *BCG-GFP* under BSL2 conditions. Therefor veils of frozen stocks were thawn at RT and the bacteria were dissociated using a blunt 27 G syringe and 1 ml luer by drawing up the syringe 10 times (table 1). Cells were infected either using a MOI of 0.1 – 2 for *M. tuberculosis* or MOI=1 - 10 for *BCG*. Multiplicity of Infection (MOI) is a quantitative parameter commonly employed in virology and microbiology to characterize the concentration of infectious agents, such as viruses or microorganisms, in relation to the number of susceptible host cells within a given experimental system. After the incubation of 4 h at 5 % CO_2 and 37 °C, cells were either fixed with 2 % PFA for 4 hours post infection (hpi) time point, or medium was removed, and an adequate volume of csRPMI + 10 ng/ml M-CSF was added and further incubated at 5 % CO_2 and 37 °C for 5 d for 5 dpi time point. For Legendplex analysis infection medium was

not removed and supernatants were harvested 24 hpi. RNA harvesting was performed 6 hpi and 20 hpi without medium change after 4 hpi.

Table 11: Infections of MdMs

Plate type	Strain used for infection	MOI	Application	Time point
6-well plate	*BCG-GFP* *MTB H37Rv dsRED*	1-5 0.5-1	For flow cytometry	4 hpi
12-well plate	*MTB H37Rv*	2	RNA isolation	6 hpi and 20 hpi
96-well plate	*MTB H37Rv*	2	Legendplex analysis of Monocytes, hMdMs	24 hpi
96-well plate	*MTB H37Rv* *MTB H37Rv dsRED*	0.5	CFU, LDH	4 hpi, 5 dpi
96-well Phenoplates	*BCG-GFP* *MTB H37Rv dsRED*	0.5-10 0.1-2, mainly 0.5	Confocal high content screening	4 hpi, 5 dpi

3.2.1.14 Cell viability and cytotoxicity assay via Lactate Dehydrogenase

The Lactate Dehydrogenase (LDH) assay was employed to evaluate cell viability and cytotoxicity in hMdMs under various experimental conditions. This included assessing the effects of different concentrations of DHT and E2, as well as the impact of *MTB* infection on hMdMs. The LDH assay functions by detecting the release of LDH, an intracellular enzyme ubiquitous in all cell types, into the culture medium when cell membranes are compromised, or cells undergo lysis. The assay's principle is based on LDH's enzymatic activity, which catalyses the conversion of lactate to pyruvate while simultaneously reducing NAD+ to NADH. The resulting NADH can be quantified, providing a measurable indicator of cell damage or death. Therefor monocytes were differentiated into hMdMs (as

described in 3.2.1.10) and treated with different DHT and E hormone concentrations (as described in 3.2.1.12) before being infected with *MTB* at an MOI=0.5 (as described in 3.2.1.13). The CyQuant Cytotoxicity Assay (Thermofisher) was used according to the manufacturer's guidelines. This assay was conducted at three critical time points: before infection to evaluate cytotoxicity during the differentiation period, 4 hours post-infection (hpi), and 5 days post-infection (dpi) to measure cytotoxicity following *MTB* infection. All measurements were performed in triplicate wells and the mean was calculated for further analysis. Several controls were included: spontaneous LDH activity (using 1:10 sterile water in total cell culture medium), maximum LDH activity (using 1:10 of 10X Lysis Buffer in total cell culture medium), cell culture medium alone, and untreated cells. The procedure involved incubating samples for 45 minutes at 37°C and 5% CO2, followed by transferring 50 µl of cell culture supernatant from each sample to a 96-well flat-bottom plate in triplicate. An LDH positive control was included by transferring 50 µl of the 1X LDH positive control in triplicate wells. Subsequently, 50 µl of the Reaction Mixture was added to each sample, gently mixed, and incubated for 30 minutes protected from light. After the incubation period, 50 µl of Stop Solution was added to each well and mixed gently. Absorbance was measured at 490 nm and 680 nm using a BioTek Synergy HTX multimode reader. The background absorbance (680 nm) was subtracted from the main absorbance (490 nm). Cytotoxicity was then calculated according to a specific formula

$$\%\, Cytotoxicity = \left(\frac{Compound\ treated\ LDH - \ Sponatnous\ LDH\ activity}{Maximum\ LDH\ activity - Sponatnous\ LDH\ activity}\right) x\ 100$$

3.2.1.15 Cell viability assay (MTT)

The MTT assay (3-(4,5-dimethylthiazol-2-yl)-2,5-diphenyltetrazolium bromide) is a nonradioactive method used to determine cell proliferation, viability and cytotoxicity. The number of viable cells is determined by the cleavage of tetrazolium salts by enzymes of the endoplasmic reticulum added to the culture medium. This bio reduction occurs exclusively in viable cells and is linked to NAD(P)H production via glycolysis. Consequently, the amount of formazan dye produced is directly related to the number of metabolically active cells present in the culture. For the experimental set up f testing the cytotoxicity of the steroid hormones DHT and E2 on hMdMs during differentiation of monocytes to hMdMs and upon

MTB infection in duplicates or triplicates. Therefor 1x10^5 monocytes were differentiated into hMdMs (as described in 3.2.1.10) upon steroid hormone treatment (as described in 3.2.1.12) in a 96 well microplate. Untreated uninfected cells, untreated infected, medium only and lysed cells were used as controls. MTT assay was performed for uninfected cells treated with steroid hormones, cells that were infected for 4 hours and treated with steroid hormones, cells that were infected for 5 days treated with steroid hormones. According to the manufactures protocol 10 % MTBB (final concentration 0.5 mg/ml) labelling were added each well. The microplate was incubated in a humidified atmosphere at 37 °C 5 % CO2 for 4 h before 100 µl solubilization solution was added to each well. The microplate was incubated overnight in a humidified atmosphere at 37 °C 5 % CO2. After checking for complete solubilization of the purple formazan crystals the absorbance was measured using a BioTek Synergy HTX multimode reader at 570 nm and 680 nm. For the corrected absorbance the culture medium background (680 nm) was subtracted from the assay reading (570 nm).

$$\%\, Viable\ cells = \left(\frac{mean\ OD\ treatment}{mean\ OD\ control}\right) x\ 100$$

3.2.1.16 Colony forming unit assay (CFU) in monocyte-derived macrophages

The colony-forming unit (CFU) is a measurement used to estimate the number of viable bacteria within a sample. This is based on the ability of the bacteria to form colonies on agar plates after culturing (as described in 3.2.1.10). Samples were analysed in triplicates, and the mean was calculated for further analysis. Furthermore, this method can be employed to examine the uptake and replication of bacteria in an *in-vitro* cell culture setting. hMdMs were infected in accordance with the methodology outlined in section 3.2.1.13 with *MTB H37Rv dsRED* and wild type at varying multiplicity of infection (MOI) levels between 0.05 and 2. Following a four-hour (4 hpi) and five-day period post-infection (5 dpi), the entire medium was removed, and the cells were rinsed once with csRPMI in a manner that was as careful as possible. Subsequently, 100 µl of ice-cold cell lysis buffer (see 3.1.6) were added to each well, and the cells were detached by pipetting up and down. Following a 10 min incubation period at 4 °C, 100 µl of the cell suspension were transferred into a deep-well plate, which was previously supplemented with 900 µl WTA buffer/well

for serial dilution (1:10). Subsequently, 50 µl of each serial dilution was plated on one half agar plate supplemented with calf serum (KS) using glass bars. The plates were then sealed with parafilm and aluminium foil and incubated for 24 d at 37 °C. After 24 d, the number of colonies was counted and the colony-forming unit per millilitre (CFU/ml) was determined (see 3.2.1.5).

3.2.1.17 Incubation of macrophages with phagocytosis beads

In addition to *M. tuberculosis* infected cells, a phagocytosis control was required for the RNA bulk sequencing approach. Therefor hMdMs were incubated with carboxylate-modified polystyrene latex beads. Beads suspension was diluted in the volume of csRPMI + 10 ng/ml M-CSF required for the number and size of wells. Cells were incubated for either 6 h or 20 h at 5 % CO_2 and 37 °C.

The number of particles per ml in the stock solution was calculated using following equation:

$$N = \frac{(6 * 10^{10}) * S * P_L}{\pi * P_S * d^3}$$

$$N = Number\ of\ particles\ per\ millilitre$$

$$S = \%\ solids\ (\frac{w}{w})$$

$$P_L = = density\ of\ latex\ \left(\frac{g}{mL}\right)$$

$$P_S = density\ of\ bulk\ polymer\ (\frac{g}{mL})$$

$$d = diameter\ of\ particles\ (\mu m)$$

This allowed the calculation of the concentration of 5.712x10^9 particles/ml.

3.2.1.18 Sterility testing of *M. tuberculosis H37Rv* infected monocyte-derived macrophages after fixation

Testing of sample material for the elimination of live *M. tuberculosis* and other bacteria from the MTB complex was performed according to World Health Organization (WHO) standards. This process is crucial for ensuring the sterility of samples before they are discharged from the Biosafety Level 3 (BSL3) area for further use. The standardized testing procedure evaluates the effectiveness of paraformaldehyde (PFA) in killing pathogens of

the *M. tuberculosis* H37Rv strain and genetically modified organisms (GMOs) derived from it. The experiments were designed with samples in triplicate, using three different detection methods: two solid media (Löwenstein-Jensen and Stonebrink agar) and one liquid medium (Mycobacterium Growth Indicator Tube, MGIT) **(Meta-analysis of BACTEC MGIT 960 and BACTEC 460 TB, with or without solid media, for detection of mycobacteria)** . Löwenstein-Jensen medium, developed in the early 20th century, is specifically designed for *M. tuberculosis* growth, featuring a low pH and high lipid content. Stonebrink medium, originally developed for marine bacteria, is also used for M. tuberculosis detection due to its complex nutrient composition and high buffering capacity. The MGIT system, a specialized culture method for detecting mycobacteria, uses a liquid medium with growth factors and a fluorescent indicator. Mycobacterial growth is detected through oxygen consumption, which causes fluorescence monitored by an automated instrument. For the planned experimental setups, the sterility of infected hMdMs (at Multiplicity of Infection, MOI=1 and MOI=10, equivalent to $1x10^5$ and $1x10^6$ bacteria used/well) fixed in 96-well PhenoPlates was tested. Cells were fixed with 2 % and 4 % PFA for either 1 hour or 20 hours. Positive controls (*M. tuberculosis* stock), uninfected cell controls, fixed cells without infection, and *M. tuberculosis* survival in csRPMI medium were also tested. After infection of the previously differentiated hMdMs (described in 3.2.1.10 and 3.2.1.13), the cells were incubated for 4 h at 37 °C 5% CO_2. Subsequently, the hMdMs were washed with csRPMI (100 µl/well) and incubated at 200 µl /well for 5 days in the incubator at 37 °C 5 % CO_2. After the incubation period, the supernatant was removed and the wells were washed twice with DPBS (100 µl/well). For subsequent fixation, 2 or 4 % PFA (100 µl/well) was added for 1 or 20 h. Plates were stored at 4 °C in the refrigerator during fixation. The fixation solution was removed and the cells were washed again with H_20 for 2 times. For lysis of the cells, 100 µl H_20/well was added and the hMdMs were placed on ice for at least 15 min. Afterwards, the hMdMs were carefully removed from the 96 well plate using a pipette tip and pipetting up and down. These 100 µl were pipetted directly onto the solid agar media. For the liquid medium, an additional 400 µl of DPBS were added to the MGIT tubes to meet the total volume. For the positive control, 500 µ of a 1:500 pre-dilution in DPBS was transferred to the MGIT tube at an optical density of the *M. tuberculosis* liquid culture between 0.08 and 0.1. Solid media samples were incubated at 37°C for 54 days and regularly checked for colonies. MGIT samples were monitored in a

BACTEC900 device for 54 days to identify sterile and non-sterile samples. This comprehensive testing protocol ensures the safe handling and processing of potentially infectious materials, adhering to stringent biosafety standards in tuberculosis research.

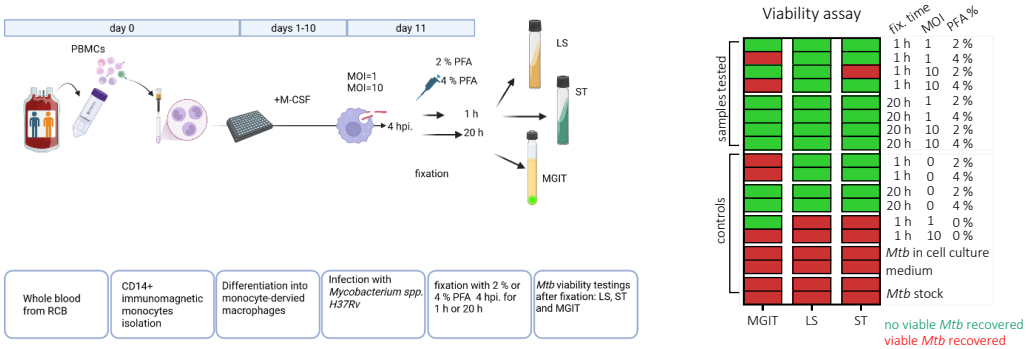

Figure 5 **Workflow (left) and outcomes (right) of sterility testing**

3.2.1.19 Sterile fixation of infected human macrophages in 96 well plate

Following the successful sterility testing of PFA-fixed *M. tuberculosis* infected hMDMs, the hMDMs were subsequently treated with 2 % PFA for 20 h at 4 °C as part of the preparation for all subsequent experiments. For 96 well plates cells were washed once with warm DPBS (100 µl/well) following by 200 µl 2 % PFA for 20 h at 4 °C. The next day the PFA solution was removed and cells were washed again twice with DPBS (100 µl/well) and stored in 200 µl DPBS/well at 4 °C. To safely remove the cells from the S3 containment, the plates were sealed with Parafilm, gently wiped with OptiSept, packed in a clean plastic bag and transferred out of the S3 through the material airlock.

3.2.1.20 Immunofluorescent staining for Flowcytometric analysis

Flow cytometry is a laboratory technique used to detect and visualise individual cells or particles suspended in a fluid stream. This allows the simultaneous analysis of multiple physical and chemical properties of cells, including cell size, shape, count, and the fluorescence intensity of labelled antibodies, refracted light (forward scatter), or elastic scattering (side scatter). Fluorescent staining is employed for the purpose of labelling antibody-specific surface or intracellular markers. It was used to control PBMCs and CD14+ cell purity after isolation (as described in 3.2.1.7 and 3.2.1.9). A minimum of $2x10^5$ cells were required for each sample. All centrifugation steps were performed at 1,000 rpm for

five minutes at 4 °C, and the supernatants were discarded. To prevent unspecific antibody binding, cells were blocked with the corresponding serum (1:100 dilution in DPBS) for 30 min prior to staining. Subsequently, 180 µl of FACS buffer was added to each sample and the mixture was subjected to centrifugation. For intracellular staining, cells were resuspended in 100 µl Perm-Wash Buffer (Biolegend) and incubated for 30 min on ice. Following centrifugation, the cells were incubated with monoclonal antibodies conjugated with a specific fluorescent conjugate, using 5 µl for $1x10^6$ cells diluted in Perm-Wash Buffer to a final volume of 50 µl/sample. All subsequent steps were conducted in the absence of light. Following a 30 min incubation period, the cells were washed twice in FACS buffer prior to commencing the intracellular staining procedure. Subsequently, the cells were incubated with monoclonal antibodies for extracellular markers, using 5 µl for $1x10^6$ cells diluted in FACS buffer to a final volume of 50 µl/sample, for a period of 30 min on ice. Following two washes, 100 µl of fixation buffer was added to each sample and incubated for 20 minutes at RT. The samples were then washed twice again to remove any remaining fixation solution, before being resuspended in 400 µl FACS buffer for measurement. Unstained controls were incubated in FACS buffer only, rather than antibody solution. For the acquisition of the panel, single stains of each antibody were performed. Samples were measured using the MacsQuant16 and data were analysed using FCS Express.

Table 12 Flow panels

Panel used for	Cell type	Antibodies used
PBMCs and monocyte purification testing	PBMCs Monocytes	CD14 (BV421 Mouse ant-human 573879 BD), CD45 (BV510 MoP9 BD 563079)

3.2.2 Molecular methods

3.2.2.1 RNA isolation from macrophages

To prevent cross-contamination, all stages of the RNA isolation process were conducted within a fume hood and in accordance with RNAse-free protocols. For the generation of RNA samples, primary monocytes were differentiated in hMdMS with and without hormone treatment. hMdMs were either infected with *M. tuberculosis* H37Rv or incubated

with phagocytosis beads for a period of either 6- or 20 h. The entire csRPMI medium was removed using a 200 µl pipette in order to prevent the dilution of TRIzol® reagent. The cells were harvested using 500 µl to 1 ml of TRIzol®, depending on the number of wells that were pooled for a given condition. This was done by pipetting up and down. The samples were frozen in 1.5-ml Safe-Lock tubes at - 80°C for a minimum of 24 h prior to their transfer from the BSL3 facility to the BSL2 facility for the RNA isolation procedure. The samples were thawed on ice before RNA purification from the aqueous phase, which was performed by adding 200 µl of chloroform/ml of TRIzol, incubating for 2-3 minutes, and centrifuging for 15 min at 12000 x g at 4 °C. The RNA Clean and Concentrator 5 kit (Zymo Research) was employed for RNA isolation, following the manufacturer's instructions. All procedures were conducted at RT and centrifugation was performed at 10000-16000 x g for 30 sec unless otherwise specified. The aqueous phase containing the RNA was transferred into a new veil and RNA binding buffer was then added to each sample in two equal volumes. Subsequently, an equal volume of 100 % ethanol was added and mixed. The samples were transferred into the Zymo-Spin IC Column in a collection tube and subjected to centrifugation. The flow-through was discarded and the procedure was repeated until the entire sample had been utilised. Next, 400 µl of preparation buffer was added to each column, after which the samples were subjected to centrifugation and the flow-through was discarded. Following two washes with RNA washing buffer at 400 µl and 700 µl, the samples were centrifuged for 1 min to ensure the complete removal of the washing buffer. The column was then carefully transferred into a RNAse-free tube, and 17 µl of DNAse/RNAse-free water was added directly to the column matrix, before being centrifuged again. The RNA yield and quality were determined by nanodrop (NanoDropTM 1000) and samples were immediately diluted 1:10 (1 µl in 9 µl) in RNAse- free water and stored at - 80 °C.

3.2.2.2 Generation of clonal DNA (cDNA)

For qPCR analysis, the RNA must first be transcribed into cDNA. This was done using the Thermo Fisher Maxima First Strand c DNA synthesis kit for qPCR. To subscribe 20 ng/µl RNA in 20 µl H_20, 2 µl enzyme mix and 4 µl reaction buffer were added. Afterwards samples were placed in a LightCycler 480 device.

3.2.2.3 Quantitative real-time polymerase chain reaction for transcriptional analysis

The quantitative real-time polymerase chain reaction (qPCR) is a technique that enables the quantification of DNA copies in a sample by monitoring the amplification process in real-time. Polymerase chain reaction (PCR) comprises three stages, consisting of repeated cycles. The initial stage involves denaturation of the DNA, whereby the strands are separated by heating the DNA to 95 °C. Subsequently, a reduction in temperature enables the primer to hybridise with its complementary sequences. By raising the temperature to 70-75 °C, the Taq DNA polymerase adds matching nucleotides to the growing 3' end of the primer, thereby doubling the number of copies in each cycle.

qRT-PCR was performed to determine the relative amount of specific mRNA transcripts of interest by using LightCycler® 480 SYBR Green I Master (Roche). CDNA was used at a 1:5 dilution with 1 µl cDNA per sample. Then 9 µl of the master mix (LC480 kit) was added to each sample. The master mix consisted of 0.2 µl primer mix, 5 µl 2x SYBR Green Master, 3.8 µl H2O for each sample. In addition to measuring the samples, it is important to analyse the standard curves of the genes of interest for further analysis. For this purpose, all samples were pooled to a final volume of 15 µl before pipetting a serial dilution of this pooled sample for standard generation (100 %, 50 %, 10 %, ... to 0.1 % and 0 % sample in H_2O). 1 µl of each dilution of cDNA was pipetted into each well, adding 9 µl of master mix. Seal the plate with foil and vortex gently. Centrifuge the plate at 1000 rpm for 1 min and place directly into the LightCycler 480.

Table 13 LightCycler 480 programs

Name of Program	**Step**	**Time**	**Temperature**	**Cycles**
cDNA synthesis	1. 2. 3.	10 min 30 min 5 min	25 °C 50 °C 85 °C	
qPCR	1. Pre-incubation/Denaturation 2. Amplification	10 min 10 s 10 s 8 s	95 °C 95 °C 63 °C 72 °C	1 45 45 45

	3. Dissociation 4.Melting curve analysis stepwise rising from 65 °C to 95 °C	1 s 10 s 10 s	72 °C 95 °C 95 °C	45 1 1

Table 14 Primer for qRT-PCR

Gene	Forward (5'-3')	Reverse (5'-3')
IRG1	CAAGGAGTCCAAAGTTTTCTGG	GGAAGGGGGATGGAATCTC
IL-1β	TACCTGTCCTGCGTGTTGAA	TCTTTGGGAATTTTTGGGATCT
TNF-α	CTCCTTCCTGATCGTGGCAG	AAGATGATCTGACTGCCTGGG
RSP9	GAGCTGTACAGAAAGAGGGC	GAGCTGTATTACCACGTGCA

3.2.2.4 Control of RNA integrity using Fragment analyser Agilent 5200

The integrity of the RNA was controlled using an on-chip automated electrophoresis process, utilising an Agilent 5200 Bioanalyzer with an Agilent RNA kit and Agilent software. The RNA concentration of the previously diluted samples, as previously described in section 2.2.2.1, was analysed using a Quibit™ 4 Fluorometer and a Qubit™ RNA High Sensitivity (HS), Broad Range (BR) and Extended Range (XR) Assay Kit, in accordance with the instructions provided by the manufacturer. The samples were diluted to a final concentration between 0.2 ng/µl and 5 ng/µl with RNA/DNA free H_20, in accordance with the concentration obtained from the Quibit™.The integrity of the RNA was evaluated based on the RNA integrity number (RIN), which assigns a rating on a scale from 1 to 10. This evaluation process considers the various properties of the generated gel and electropherogram. Total degradation of the sample is equivalent to a RIN of 1, while intact RNA is equivalent to a RIN of 10. Samples with a RIN of 5 were deemed suitable for further processing. All samples that passed the quality measurements were subsequently processed by the next generation sequencing facility of the Niemann Lab.

3.2.2.5 Library preparations for RNA-bulk sequencing

Only RNA samples with high quality (RNA integrity number >7.0) as measured using the Aiglent5200 were used for library preparations. The following steps were performed by the NGS facility of the Niemann lab. The Zymo-Seq RiboFree® Total RNA Library Kit from Zymo research was used for universal rRNA depletion according to manufactures guidelines by the Niemann lab. Therefor total RNA (200 ng at a volume of 8 µl) were transferred into a 0.2 ml PCR tube. All procedures were performed on ice. For primer annealing, 2 µl of the cDNA synthesis reagent 1 was added to each sample, mixed thoroughly by pipetting and centrifuged briefly. Afterwards the samples were placed in a thermal cycle and step 1-2 of the program were run. For the Reverse transcription, again all samples were stored on ice while adding 10 µl cDNA Synthesis Reagent 2 before the samples were again placed into the thermal cycle and steps 3-5 were run. The next step was the RiboFree® Universal Depletion. Therefor 10 µl of Depletion Reagent 1 was added to each sample, kept on ice, mixed by pipetting and centrifuged briefly. Tubes were placed to the thermal cycle and Step 1-3 were run for the predilution incubation. While the tubes remain in the thermal cycler, 10 µl Depletion Reagent 2 were added and mixed by pipetting. Next Step 4 was run. Again, without removing the tube, 10 µl Depletion Reagent 3 was added and mixed by pipetting before continuing with Steps 6-7. Add 2 µl of the Depletion Reagent 4 to each tube, remove the tube from the cycler and flick the tube gently. Centrifuge samples briefly before placing them back into the thermos cycler to continue with Steps 8-10 of the program. Remove the tube from the thermal cycler and add 26 ml 95% ethanol at room temperature to obtain purified cDNA for the following steps.

3.2.2.6 Transcriptome sequencing using RNA-bulk sequencing

RNA was extracted from hMdMs 20 h post infection with *M. tuberculosis* H37Rv MOI=2 from untreated and hormone treated cells (DHT 10 nMol, E2 10 nMol as described in 3.1.7). As control RNA was also extracted from uninfected hMdMs with the same conditions and cells treated with phagocytic latex beads (as described in 3.2.1.17). For RNA extraction see 3.2.2.1. Samples were paired-end sequenced in cooperation with Prof. Stefan Niemann from the molecular and experimental mycobacteriology on the Illumina NextSeq 2000 using a read length of 100 bases. Sequencing results were analysed by Prof. Inken Wohlers from the Data Science group of the Research Center Borstel. Between 38.4 and 79.6 million

reads were generated per sample, with mapping rates between 33.7 and 58.8% (median 43.95%). Low transcript mapping rates are explained by insufficient DNA depletion. One expression PCA outlier with 13.3% mapping rate was removed (M_i_DHT_D14_B6). FastQC (https://www.bioinformatics.babraham.ac.uk/projects/fastqc) was run for sequencing data quality control and MultiQC (PMID: 27312411) for compiling a combined FASTQC report extended by kallisto mapping statistics.

3.2.2.7 Data availability

RNA sequencing data is currently stored at the Data Science Group of the Research Centre Borstel but will be available at EGA. Scripts and key results of the transcriptome analyses will also be available at FAIRDOMHub.

3.2.3 Biochemical methods

3.2.3.1 Enzyme-linked Immunosorbent Assay

The Enzyme-Linked Immunosorbent Assay (ELISA) is a widely used analytical technique in biochemistry and immunology for detecting and quantifying specific proteins, antibodies, antigens, hormones, and other substances in biological samples. The assay was conducted in accordance with the manufacturer's instructions. All procedures were conducted in a biosafety level 3 (BSL3) facility. The ELISA MAX™ deluxe sets from Biolegend were used to detect TNFα and IL-8. The samples were analysed without dilution or 1:50 dilution in assay buffer. Samples and the standards were measured in duplicates the mean was used for further analysis. The standard stock solution was diluted 1:4 for a total of six dilution steps (C1-C7). C0 only contained assay buffer. The day before running the experiment, 96-well plates were coated with 100 µL/well of capture antibody diluted in coating buffer and incubated overnight at 4 °C. The day of the experiment, all reagents were brought to RT. The plates were then washed four times with 300 µl wash buffer (DPBS + 0.05 % Tween-20) /well and 200 µL/well of assay diluent for 1 h at RT with shaking at 500 rpm to block unspecific binding and reduce background. After washing, 100 µL of standards and samples were added to the appropriate wells and incubated for 2 h at RT with shaking. Following incubation, the plates were washed and 100 µL of biotinylated detection antibody was added to each well. After 1 h of incubation, the plates were washed and 100 µL of Avidin-HRP solution was added for 30 min. The plates were then washed five times with incubation times of 30 sec, and 100 µL of substrate solution C was added to each well. Positive wells should now turn blue. The reaction was stopped after 15 min by adding 100 µL of stop solution (2N H_2SO_4). Absorbance was measured at 450 nm and 570 nm using a microplate reader Synergy HTX by Biotek. The 570 nm readings were subtracted from the 450 nm readings to correct for optical imperfections in the plate. Cytokine concentrations were calculated using a regression standard curve generated with the PRISM software.

3.2.3.2 Cytometric bead-based assay (Legendplex™)

The Legendplex™ analysis employs beads that have been pre-coated with antibodies that target specific cytokines, thereby enabling the simultaneous analysis of multiple analytes

within a single sample derived from the cell culture supernatant of infected monocyte-derived macrophages (MDMs). The assay was conducted in accordance with the manufacturer's instructions, utilising 96-well V-bottom plates. All procedures were conducted in a biosafety level 3 (BSL3) facility. The samples were analysed without dilution or 1:20 dilution in assay buffer, and the standards were measured in duplicates. the mean was used for further analysis. All reagents were brought to RT and the antibody-immobilised beads and wash buffer were prepared in advance. For the experiments an adapted costume wizard panel was used, adapted from the human inflammatory panel I. The standard solution was diluted 1:4 for a total of six dilution steps to prepare the standard (C1-C7). C0 only contains assay buffer. Prior to utilisation, the beads were vortexed for one minute, and all centrifugation steps were conducted at 1,000 x g for five minutes. Subsequently, 25 µl of the assay buffer was added to each well, followed by the addition of 25 µl of the supernatant samples. The standard wells were supplemented with 25 µl of Matrix B buffer and 25 µl of the prediluted standard, in duplicate. Subsequently, 10 µl of the vortexed beads were added to each well, after which the plate was sealed with sticky foil and incubated on a plate shaker (800 rpm). Following a period of two hours, the plates were subjected to centrifugation, after which the supernatant was discarded. The plate was then washed once with 1X washing buffer (200 µl/well), incubated for one minute at 800 rpm, and centrifuged. Subsequently, the supernatant was discarded, and 10 µl of antibodies were added. The plate was resealed with sticky foil and incubated for an additional hour at 800 rpm. Without washing, 10 µl of the SA-PE solution was added to each well, where it was incubated for a further 30 minutes at 800 rpm. Following centrifugation, the plates were washed once, after which 180 µl of 1X wash buffer was added to each well. The pellets were resuspended, and the solution was transferred to a 96-well U-bottom plate for analysis using the MACSQuant10 flow cytometric device with the PE and APC channels. Data analysis was performed using the Legendplex™ cloud-based analysis software.

Table 15: Custom Legendplex

Bead ID	Analyte	Bead
A4	IL-1β	A
A5	IFN-α2	A

A7	TNFα	A
A8	MCP-1	A
A10	IL-6	A
B2	IL-8	B
B3	IL-10	B
B4	IL-12(p70)	B
B6	IL-18	B
B7	IL-23	B

3.2.4 High-Content Screening (HCS) by automatic confocal microscopy

High content screening (HCS) by automatic confocal microscopy is a powerful laboratory technique used to simultaneously analyse multiple biological parameters in cells or tissues. It involves combining automated image acquisition and analysis with confocal microscopy to generate high-resolution, 3 dimensional (3D) images of biological samples. These images can then be analysed using specialized software to extract quantitative data about cellular processes such as proliferation, migration, and protein expression. HCS can be used in a variety of applications, including drug discovery, toxicity testing, and disease diagnosis. In our case we use HCS for analysing.

3.2.4.1.1 Immunocytochemical staining of the nuclei of human monocyte-derived macrophages

4',6-Diamidino-2-phenylindole (DAPI) staining is a widely utilized technique in cell biology and fluorescence microscopy for staining cellular nuclei. DAPI is a fluorescent dye that selectively binds to DNA by intercalating between base pairs, resulting in intense blue fluorescence upon excitation with ultraviolet light. The emitted blue fluorescence directly correlates with the presence and abundance of DNA within the cell nuclei, enabling precise visualization and quantification of nuclei across different experimental conditions. DAPI stock solution (1 mg/ml) was diluted 1:10.000 in DPBS for a final working concentration of 0.1 µg/ml. PFA fixed cells were washed twice to remove remaining fixation solution. 0.1 µg/ml DAPI solution was added for 5 min at RT. From this point forward, the cells were

shielded from light. If the cells were formerly infected with *M. tuberculosis dsRED*, they are constantly shielded from light. After the incubation period, the cells were rinsed twice with DPBS and stored at 4 °C in DPBS.

3.2.4.2 Image Acquisition

Images were acquired using the automatic Opera Phenix™ Nipkow confocal high-content screening (HCS) system (PerkinElmer, Rodgau, Germany) and a 20× water objective lens (NA 1.0; binning 1). In total 15 predefined fields per well were recorded with DAPI channel (excitation: 405 nm/emission 435-480 nm) for macrophage nuclei detection and either *dsRED* (excitation: nm/emission: nm) or *GFP* (excitation: nm/emission: nm) for *M. tuberculosis* and *BCG* GMO visualization at 100 % laser power. Seven different planes on the z axis were images to increase resolution (first plane=11 µm, last plane= 1 µm, difference between the planes=2 µm). The confluency of the cells was approximately 70-80 %, resulting in adequate numbers of macrophages (4000-6000) for quantification.

3.2.4.3 Image and Data Analysis

Image and Data Analysis is based on published work from Annika Bea and Helena Fehling et al. The images were analysed using a custom-designed image analysis sequence adapted from Fehling's sequence of the Harmony software. This analysis was originally implemented by Dr. Hanno Niss for his doctoral project for the detection of intracellular Leishmania parasite in host cells. The software's integrated analysis algorithm uses a building block approach. In step one (*find the nuclei* building block), MDMs were detected by their nuclei (DAPI; method; area > 40 µm2) defined by signal and size. The cytoplasm (*find cytoplasm* building block) was also defined using the DAP signal (DAPI; method A). Only cells with nuclei within the cytoplasm are considered representative; others were excluded. The bacteria *M. tuberculosis* or *bovis* (*dsRed, GFP*) were identified intracellularly as spots (*find spots* building block), while the cytoplasm was defined as the area of interest (ROI) to achieve high sensitivity for downstream analysis. Subsequently, the properties of the identified objects were calculated by selecting the 'Calculate Intensity Properties' and 'Calculate Morphology Properties' options for each individual segment. The previously calculated properties were then employed to distinguish between false-positive spots and bacteria, as well as uninfected and infected cells within the 'Select Population building

block'. Genetically modified organisms (GMOs) were used for infection protocols to prevent false-positive intracellular spots. Spot properties were defined by specific intensity and morphology of the subject. For the phenotypical analysis of the macrophages defining them either as proinflammatory M1 or anti-inflammatory M2. Based on the correlation between cell shape and macrophage activation upon specific stimuli Bea et al designed an image analysis sequence to either detect the roundish, homogenous M1 or spindle-shaped-elongated M2 cells. These results were verified by FACS analysis and published in Bea et al 2024. The final step was to utilise the 'Define Results building block' to calculate and display the desired readout values and parameters.

Main readouts (per well) generated with this image analysis sequence were:

1. total number of hMdMs/well in order to analyse host cell viability
2. number of *Mycobacteria*
3. total number of *Mycobacterium* infected hMdMs with and without hormone treatment
4. percentage of infected hMdMs with and without hormone treatment
5. hMdMs phenotype analysis

To ensure good signal-to-background ratios, we determined the quality and reliability of the assay and image analysis using the Z' values for each plate. Z' values between 0.3 and 1 are ideal, while values below 0.3 are considered significant for cellular screening. Microplates with total Z' values below 0.3 were excluded. The quantitative values obtained from the Harmony software were exported to Microsoft Excel for further analysis. The data were normalized to the negative control (infected, untreated hMdMs) and expressed as a percentage of the negative control (POC).

3.2.5 In silico methods

3.2.5.1 Analysis of bulk RNA-sequencing

Samples were generated from seven female and seven male donors under various conditions: uninfected; *M. tuberculosis* infected; and control bead-treated, with or without hormone treatment (DHT, E2 or untreated). This totalled 94 samples. The workflow outlines five sequential analysis steps: first comparing uninfected and infected states (Figure 6 Step 1); second evaluating sex differences after infection (interaction analysis)

(Figure 6 Step 2); next conducting sex-stratified comparisons for infection (Figure 6 Step 3); followed by assessing the influence of DHT and E2 treatments within infected samples (interaction analysis) (Figure 6 Step 4); and performing comparative analyses of hormone treated versus untreated samples, and infected versus infected/treated samples (Figure 6 Step 5). Interaction analysis investigates whether the effect of one variable (e.g., infection) differs depending on another variable (e.g., sex or hormone treatment), whereas simple comparative analysis directly compares two conditions without considering such combined effects. All successful analyses led to principal component analysis, identification of specific genes, and pathway enrichment and differential gene expression, providing a comprehensive view of sex- and hormone-specific immunomodulation in *M. tuberculosis* infected hMdMs. Results were name according to date of final analysis 20250715_.

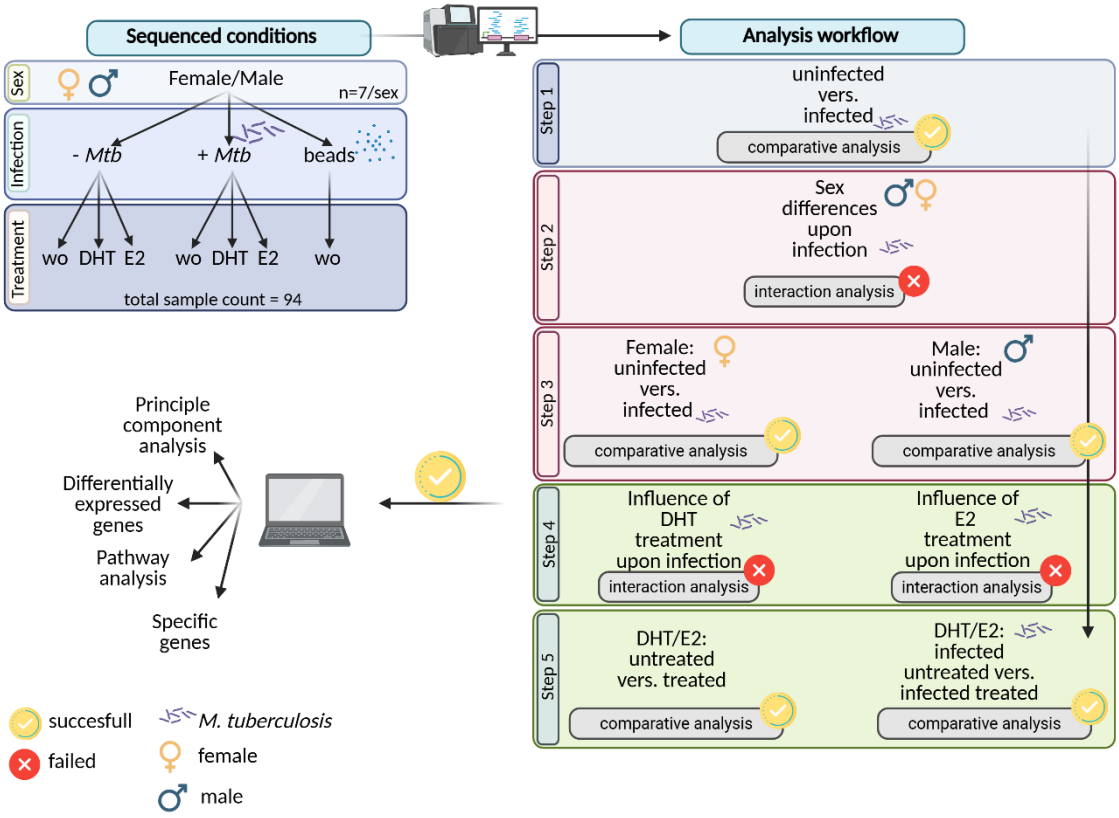

Figure 6 **Overview of experimental design and analysis workflow for sex- and hormone-specific transcriptomic profiling in *M. tuberculosis* infected hMdMs**

Transcriptome data was analysed by Prof. Inken Wohler from the Data Science group of the Research Center Borstel using a community workflow (https://github.com/snakemake-workflows/rna-seq-kallisto-sleuth, release 2.8.4) from the snakemake (PMID: 34035898)

workflow catalog (https://snakemake.github.io/snakemake-workflow-catalog). This workflow is based on transcript expression quantification using kallisto (PMID: 27043002) and differential expression testing using sleuth (PMID: 28581496) based on a model that considers sex, infection or treatment as primary variable and donor as batch variable. Isolation date, contrary to donor, was not a major batch effect according to expression PCA and thus not included in the model. The workflow is used with gene and transcript annotation from Ensemble release 113 and uses SPIA (PMID: 22321699) for computing enriched Reactome pathways, GOATOOLS (PMID: 30022098) for determining enriched Gene Ontology terms and fgsea (bioRxiv 060012) for enriched MSigDB (PMID: 16199517) gene sets. Statistical significance was assessed using both uncorrected p-values and FDR-adjusted q-values (Benjamini-Hochberg procedure). Given the conservative nature of FDR correction in large gene sets, we adopted a dual-threshold approach: $q < 0.01$ for highly stringent analysis and $q < 0.05$ for additional investigative approaches.

3.2.6 Statistical analysis

All statistical analyses and data visualization were performed using GraphPad Prism 10 (GraphPad Software, La Jolla, USA). Specific statistical tests are detailed in the respective figure legends. For comparisons involving three or more groups, a two-way ANOVA was applied, followed by Tukey's multiple comparisons test to evaluate all pairwise differences while controlling the family-wise error rate. For planned comparisons between two groups, Šídák's multiple comparisons test was used to adjust the significance level ($\alpha = 0.05$) and maintain a 95 % confidence interval, as this method provides greater power than Bonferroni while accounting for correlated comparisons. Unless otherwise specified, differences were considered statistically significant at p-values ≤ 0.05. Statistical significance is indicated in the figures using asterisks as follows: *p ≤ 0.05; **p ≤ 0.01; ***p ≤ 0.001; ****p ≤ 0.0001. Data are presented as means with corresponding standard deviations (SD).

4 Results

A striking and consistent epidemiological feature of TB is its male bias even after adjusting for socioeconomic and behavioural factors. Growing evidence points to biological sex and sex hormones as important modulators of immune responses to *M. tuberculosis*, but the mechanisms are not fully understood. As macrophages are central to *M. tuberculosis* control, this study investigates sex differences in human monocyte-derived macrophage (hMdMs) in response to *M. tuberculosis* infection and examines how estradiol and testosterone influence these responses, aiming to elucidate how sex and hormones influence macrophage-mediated immunity in TB.

4.1 Adaptation of a confocal high-content screening (HCS) system for quantifying *M. tuberculosis* infection dynamics in hMdMs

HCS microscopy is a powerful high-throughput technology that combines automated fluorescence imaging with advanced image analysis to quantify cellular and microbial dynamics with high precision and speed. Compared to traditional CFU assays, which involve manual plating and counting of bacterial colonies, HCS enables rapid, objective, and multiplexed analysis of *M. tuberculosis* infection at the single-cell level in hMdMs. This study adapts a confocal HCS system to accurately quantify infection dynamics, offering a scalable and detailed approach to investigate sex- and hormone-related differences in macrophage responses to *M. tuberculosis*.

4.1.1 Implementation of an *in vitro* infection model of hMdMs with *M. tuberculosis* to assess different aspects of host-pathogen interaction

To study the interaction with its primary host cell, the macrophage, monocytes from peripheral blood mononuclear cells (PBMCs) were isolated from whole blood collected from healthy male and female donors first. Therefore, $CD14^+$ monocytes were purified via immunomagnetic positive selection and differentiated into hMdMs over 10 days in the presence of M-CSF (Figure 7). HMdMs were infected with *M. tuberculosis* H37Rv at day 10 post-isolation, with standardized bacterial suspensions at different multiplicities of infection (MOI) for 4 h at 37 °C in a humidified atmosphere with 5-10 % CO_2.

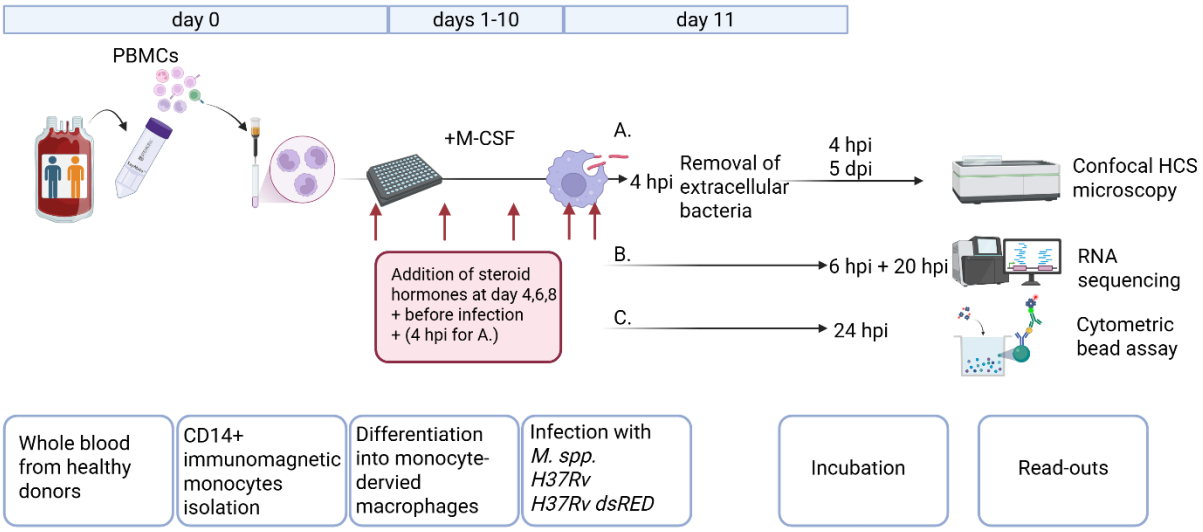

Figure 7 **Schematic workflow for in vitro infection of hMdMs with Mycobacteria**

Using whole blood from female and male human donors, CD14+ immunomagnetic positive bead-based selection was performed to isolate CD14+ monocytes. In the presence of M-CSF, monocytes were differentiated into monocyte-derived macrophages for 10 days. Mature hMdMs were infected with Mycobacterium. (A) For immunofluorescence analysis, infected hMdMs were washed at 4 hpi to remove extracellular bacteria and incubated for the respective time points, fixed and stained for characterisation by confocal microscopy. (B) *M. tuberculosis H37 Rv* infected hMdMs were used for RNA sequencing approaches and (C) the supernatant for cytokine profiling using cytometric bead-based assay (Legendplex®). Figure created with BioRender.com

The infection model incorporated three parallel analytical approaches with distinct temporal endpoints: To comprehensively assess the interaction between hMdMs and *M. tuberculosis*, microscopy-based analysis is used to quantify bacterial uptake and monitor intracellular replication dynamics over time (Figure 7 A). Complementary transcriptomic profiling reveals how host gene expression patterns shift during infection (Figure 7 B). Additionally, cytokine profiling provides insights into the host immune response (Figure 7 C). For microscopy-based cells were infected for 4 h, and washed to remove extracellular bacteria. This washing step was critical for ensuring4 h and sequent analyses reflected only intracellular bacteria. Infected cultures were either analysed directly after 4 hpi or maintained until 5 dpi to assess bacterial uptake and replication, respectively (Figure 7 A). To ensure accurate detection and prevent false-positive staining, dsRed expressing *M. tuberculosis* was used. Imaging was performed using the Opera Phenix Plus confocal high-content microscope (Revvity), and infection parameters, such as infection rate and

bacterial load per cell, were automatically quantified using a customized analysis pipeline in Harmony software as described in detail in supplementary table. (Figure 7 B) At 6 and 20 hpi RT-qPCR analysis was performed, allowing for targeted examination of specific genes of interest across the early infection timeline. RNA bulk sequencing, which provides comprehensive genome-wide transcriptional profiling, was conducted at the 20 hpi timepoint. (Figure 7 C) Culture supernatants were collected at 24 hpi for cytometric bead assay to measure secreted inflammatory mediators.

4.1.2 High-Content Confocal Pipeline for Multi-Parametric Analysis of *Mycobacterium tuberculosis* Infection in hMdMs: From Leishmania to Mycobacteria

Confocal HCS is an advanced imaging-based technique that enables the automated, quantitative analysis of cellular phenotypes and intracellular events in a high-throughput format. In this project, confocal HCS was utilised to evaluate the interaction between hMdMs and *M. tuberculosis* specifically quantifying bacterial uptake dynamics, intracellular replication patterns, and infection triggered phenotypic polarization of hMdMs. The system enables the quantification of multiple parameters, such as % infected hMdMs and *Mycobacterium* per infected hMdMs by analysing fluorescent confocal microscopy pictures with a customised image analysis sequence. Based on the defined parameters, this approach allows for the systematic evaluation of infectivity and persistence of *Mycobacterium* as well as the assessment of differences in susceptibility among donor-derived hMdMs.

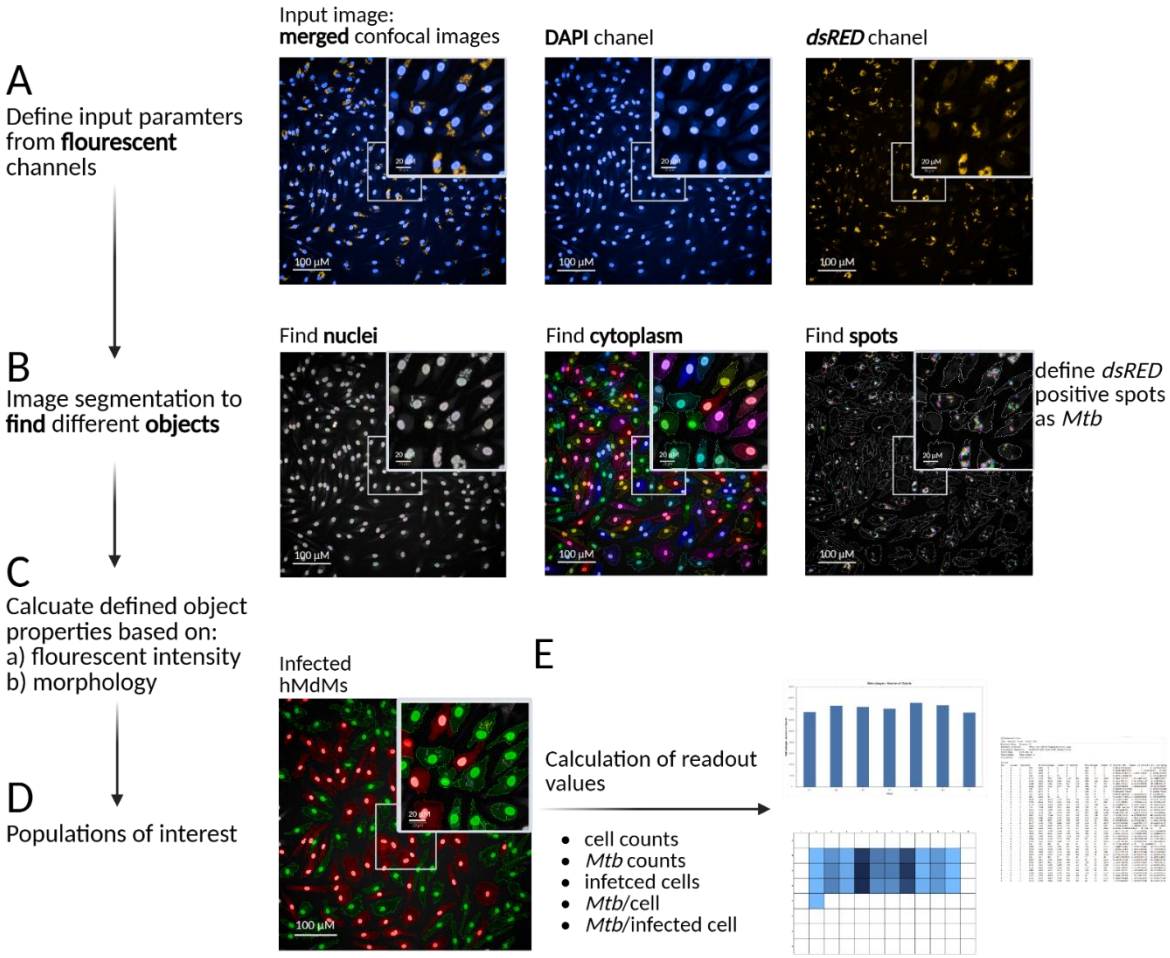

Figure 8 **Schematic depiction of customized image analysis algorithm in Harmony® software for hMdMs upon *Mycobacterium* infection**

Stepwise workflow of the customized image analysis algorithm in Harmony® software is illustrated with corresponding modules. Representative confocal microscopy images, captured using an Opera Phenix® microscope equipped with a 20X water-immersion objective, are shown. Main images display a scale bar of 100 µm, while close-up views include a 20 µm scale bar. Figure created with BioRender.com

In close collaboration with colleagues from the Lotter group at the BNITM, the pipeline they had established for the analysis of Leishmania infected macrophages was adapted to *Mycobacteria (144)*. To do so, the TB vaccine strain *Mycobacterium bovis BCG* expressing green fluorescent protein (*GFP*), was used. Figure 2 illustrates the workflow of the implemented image analysis pipeline for quantifying *Mycobacterium* infection in hMdMs using HCS microscopy. First input parameters were defined based on fluorescent channels (Figure 8 A). Secondly, the pipeline utilizes image segmentation to identify various objects, such as nuclei and cytoplasm (Figure 8 B). Nuclei and cytoplasm were visualized with DAPI-

staining, while bacteria were detected either in the GFP fluorescent channel for *BCG-GFP* or the *dsRED* fluorescent channel for *M. tuberculosis dsRED*. To identify intracellular bacteria, only fluorescent signal within the cytoplasm were used. The bacteria derived fluorescent signals were defined as “interesting spots” within the pipeline and adapted from the characteristic formats and dimensions of a Leishmania parasite to the specific properties of *Mycobacteria* (whole image analysis pipeline supplementary table). Next, fluorescent intensity and morphology were calculated, and populations of interest were identified (Figure 8 C, D). Lastly, from these segmented images, key quantitative readouts were generated, including total cell counts, bacterial counts, number of infected hMdMs, average bacteria per hMdMs, and additionally the counted number of bacteria per infected hMdMs (Figure 8 E).

4.1.3 Validation of High-Content Imaging Pipeline using BCG test Infection in hMdMs

To validate the adapted Harmony image analysis pipeline, hMdMs from healthy male and female donors were infected with BCG-GFP at rising MOI (Figure 9). After 4 and 24 hpi, respectively, fluorescence images from each donor were analysed for infection rates and bacterial loads (female: yellow, male: blue) (Figure 9 A, B). The percentage of infected hMdMs as well as the number of bacteria per infected hMdMs increased with rising MOI at both 4 hpi and 24 hpi, reaching approximately 80-100 % at the highest MOIs. Differences in terms of infection rates and the number of bacteria per infected cell were observed. Particularly at lower MOI, the number of infected macrophages was higher for male compared to female donors, while at the higher MOI, the number of *BCG* per infected cell was higher in male compared to female hMdMs. The uninfected control showed ±0 % infected hMdMs and ±0 *BCG*/infected hMdMs.

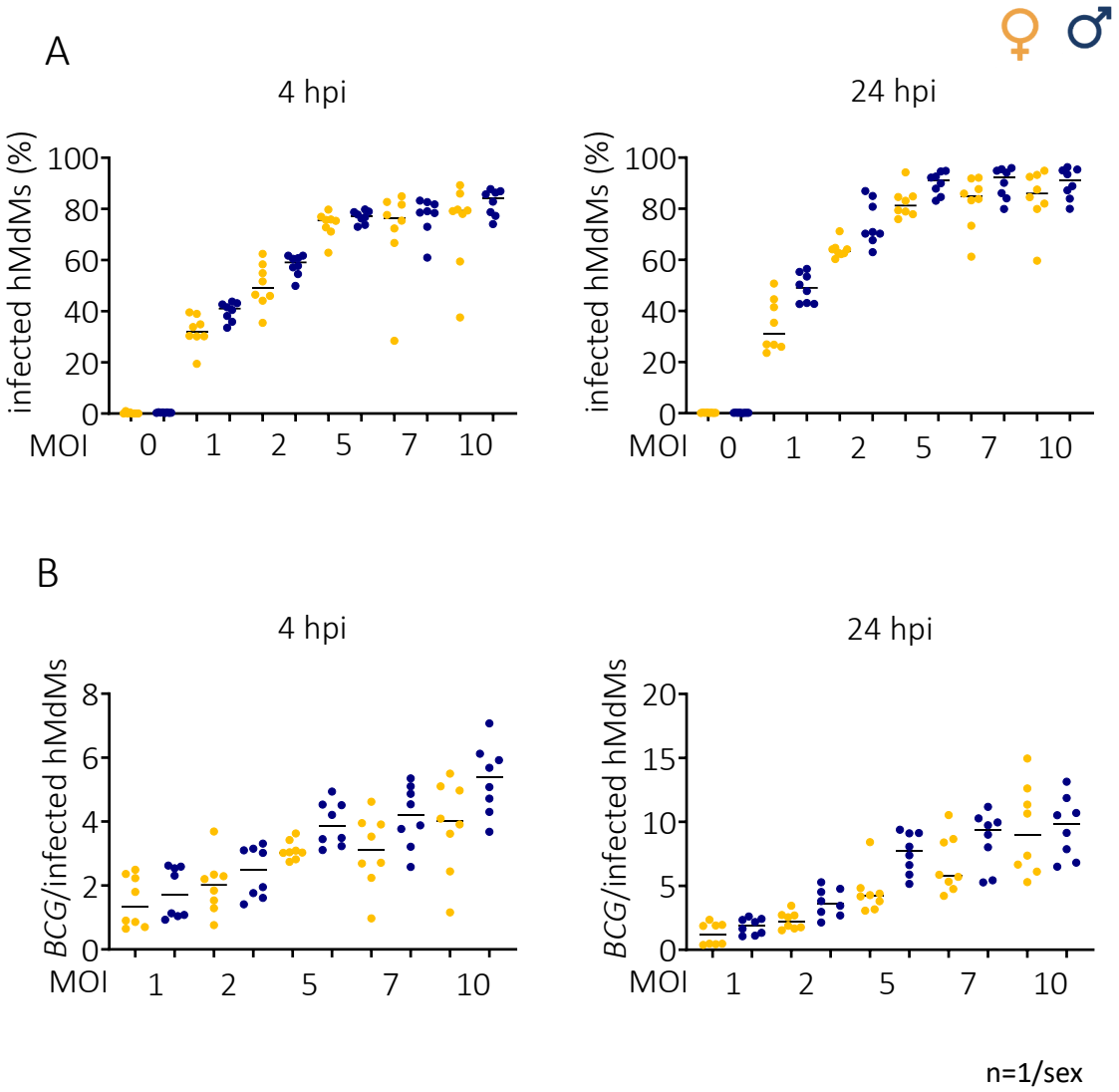

Figure 9 **Implementation of microscopy-based analysis using *BCG-GFP* infected hMdMs**

hMdMs were infected with (A) GFP-expressing BCG (green) (MOI 1-10), stained for cellular structures (DAPI) and analyzed by confocal microscopy at respective timepoints (4 hpi and 24 hpi). Image analysis was conducted using Harmony software to evaluate infected hMdMs (%) and BCGP per infected hMdMs. (B) Results from BCG-GFP infected hMdMs. Data reflects one test replicate with samples tested in quadruplicates of which the mean is shown. Images were taken using a 20x objective. (Scale bar= 50 µM)

In summary, test infections of primary hMdMs with *BCG-GFP* confirmed the successful adaptation of the HCS pipeline originally developed for Leishmania to Mycobacterium spp. To improve the specificity of infection detection compared to conventional immunohistochemistry a fluorescently labelled bacteria was used. The lack of fluorescence in uninfected control samples demonstrates a low background and confirms the specificity of the readout, minimizing the risk of false positives. This method ensures robust and

accurate quantification of infection rates across a range of bacterial MOIs, time points, and experimental conditions in both female and male donor cells, supporting its suitability for future studies of host-pathogen interactions in human macrophages.

4.1.4 Validation of High-Content Imaging Pipeline for Quantifying *M. tuberculosis* Infection in hMdMs

After the HCS Harmony analysis pipeline was established and validated with *BCG-GFP* infected hMdMs, it was subsequently adapted for application to *M. tuberculosis H37Rv.* Working with *M. tuberculosis* requires BSL-3 laboratory conditions. Consequently, BSL-3 containment is required to minimize the risk of laboratory-acquired infections, ensure the safety of personnel, and prevent environmental release of the pathogen. Since the Opera Phenix confocal microscope is located at the Leibniz Center for Virology, samples infected with *M. tuberculosis* must be sterilized before being removed from the BSL-3 facility at the Research Center Borstel for analysis to the Leibniz Center for Virology. Sterility, defined by the WHO as “the absence of all microorganisms capable of multiplying”, was assessed in accordance with standard guidelines for *Mycobacterium spp.* inactivation, as detailed in the Material and Method section (145, 146).

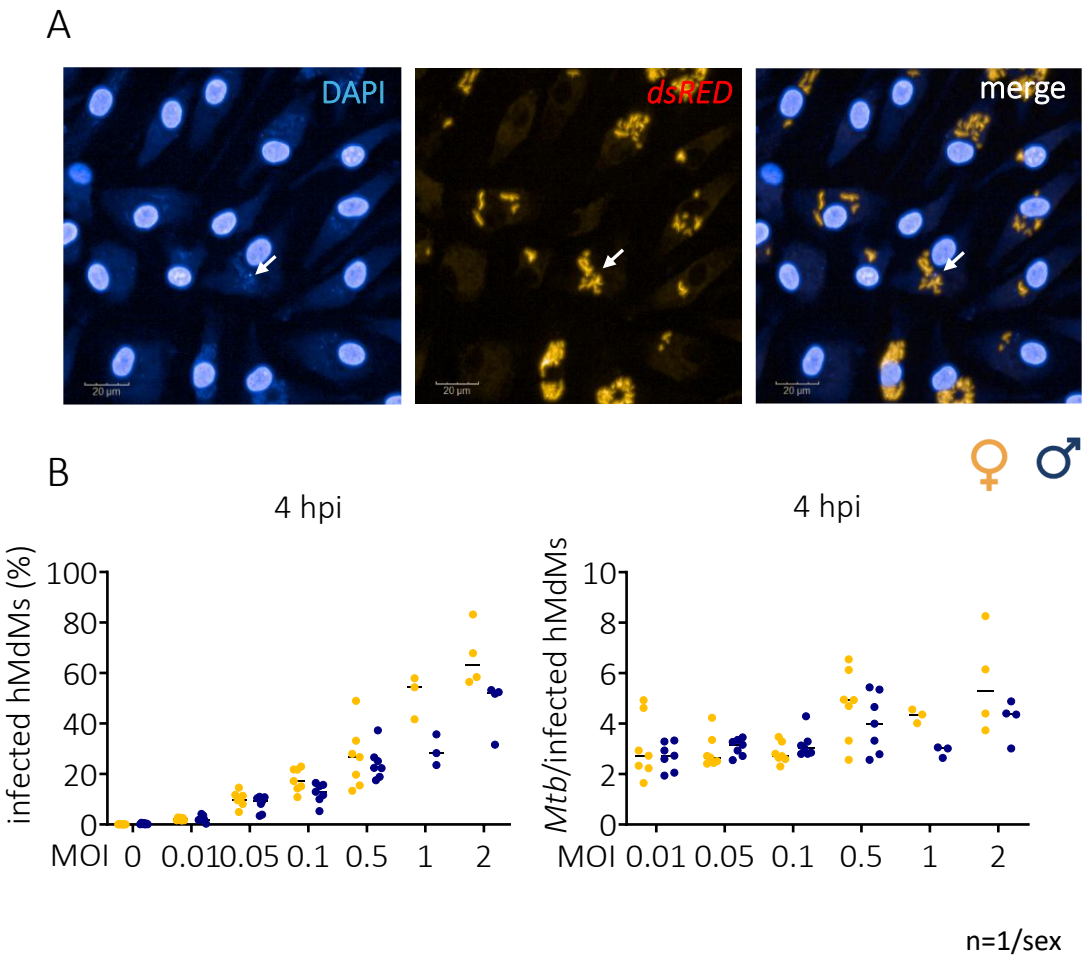

Figure 10 **Infection of hMdMs: Implementation of microscopy-based analysis for *M. tuberculosis dsRED* infected hMdMs**

hMdMs were infected with (A) *dsRED*-expressing *M. tuberculosis* (red) (MOI 0.01-2), stained for cellular structures (DAPI) and analyzed by confocal microscopy at 4 hpi. Image analysis was conducted using Harmony software to evaluate infected hMdMs (%) and *MTB*/infected hMdMs. (B) Results from *M. tuberculosis* infected hMdMs. Arrows highlight comparison of DAPI and *dsRed* positive signals of the bacteria. Each symbol represents an individual replicate, with yellow indicating the female donor and blue indicating the male donor. Data reflect one test replicate with samples tested in quadruplicates of which the mean is shown. Images were taken using a 20x objective. (Scale bar= 20 µM, n=1 per sex)

For the test infection, hMdMs from healthy male and female donors were infected with rising MOI of *M. tuberculosis* expressing *dsRed* and representative fluorescence images were taken after 4 hpi (Figure 10 A). Because the sterilization involved fixation in 2 % PFA for 20 hours, it was necessary to assess whether the bacterial fluorescence was preserved under these conditions. To do so, images of DAPI stained *M. tuberculosis dsRED* infected hMdMs were cross-compared across their respective fluorescent channels. Besides the

host cell nuclei, the bacteria themselves exhibited weak but detectable DAPI positive signals (Figure 10A). By aligning these DAPI signals with the corresponding *dsRED* fluorescence, it was confirmed that the *dsRED* fluorescence remained stable and unaffected by the fixation (Figure 10 A.). Figure 4B illustrates the infection rates and bacterial loads in male and female hMdMs 4 h post infection with *M. tuberculosis dsRED* at different MOIs (MOIs 0.01-2). A dose dependent increase in both the percentage of infected hMdMs and the number of bacteria per infected hMdMs was observed. Uninfected control showed ±0 % infected hMdMs and ±0 *M. tuberculosis*/infected hMdMs.

In conclusion, the adapted HCS analysis pipeline enables robust and reproducible identification and quantification of *M. tuberculosis dsRED* infection in hMdMs, with stable fluorescence signals maintained after fixation. Both infection rates and intracellular bacterial loads increased proportionally with MOI. These findings establish the pipeline as a reliable tool for quantitative, sex-stratified studies of intracellular *M. tuberculosis* infection.

4.1.5 Comparison of CFU to Microscopy based analysis (OPERA)

To confirm the accuracy and reliability of our HCS microscopy approach, we performed a direct comparison with conventional CFU analysis, enabling us to validate HCS as a robust alternative for quantifying viable cell populations. Therefore, hMdMs were infected with *M. tuberculosis H37Rv dsRED* at a MOI of 0.5 for 4 h. For uptake parameters, cells were either fixed immediately for HCS or directly lysed and plated for CFU analysis. For replication parameters, cells were washed and further incubated for 5 days before being fixed for HCS or lysed and plated for CFU analysis. For image analysis, we used the previously described TB pipeline for the Harmony software from Revvity. Notably, for CFU analysis, the entire well was plated, whereas for HCS analysis, 15 images per well were analysed.

Figure 11 A shows the CFU counts per well at 4 hpi (circles) and 5 dpi (triangles), separated by sex (yellow female, blue male). At 4 hpi, both groups show similar CFU values, while at 5 dpi, there is a slight increase in CFU counts. The mean fold increase in CFU per well from 4 hpi to 5 dpi of ~1.3 for both sexes indicates a modest increase in bacterial load over 5 days with no differences between the sexes (Figure 11 B). For the HCS analysis the number

of identified bacteria within the cytoplasm of each cell were count in 15 pre-defined areas of the well. The bacterial counts follow a similar trend to the CFU data, with both females and males showing increased bacterial numbers by 5 dpi (Figure 11 C). The mean fold change is around ~1.7 in both sexes, reflecting the trend observed in the CFU analysis (Figure 11 D). Although the absolute CFU counts and HCS bacterial counts are not directly comparable due to these methodological differences, both approaches reveal closely aligned trends in bacterial load dynamics across the conditions tested. Both CFU and HCS analyses yield comparable fold increases in bacterial load from 4 hpi to 5 dpi, supporting the reliability of HCS-based quantification as a valid alternative to classical CFU enumeration for assessing *M. tuberculosis* infection dynamics in hMdMs, especially for high-throughput approaches.

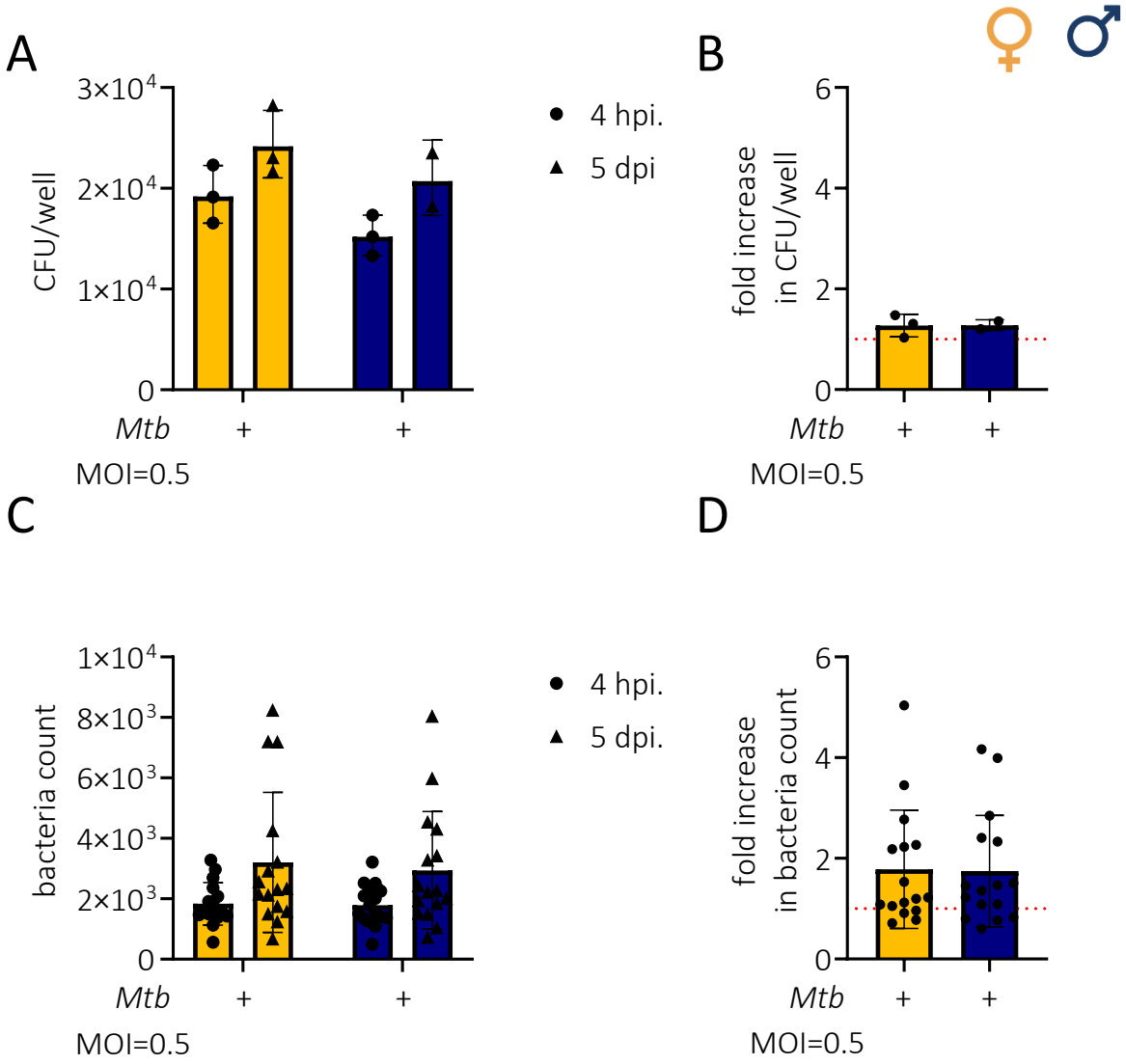

Figure 11 **Comparison of bacterial load of *M. tuberculosis* infected hMdMs analysed using CFU of HCS approach**

hMdMs were infected with *M. tuberculosis dsRED* at a MOI of 0.5. For CFU analysis, cells were lysed at 4 hpi or 5 dpi, plated on agar plates, and colonies were counted after 23 days. CFU counts per well (A) and the fold increase from 4 hpi to 5 dpi (B) are shown. For HCS analysis, cells were fixed with 2 % PFA for 20 h at both 4 hpi and 5 dpi. Image acquisition was performed using the Opera Phenix confocal microscope, and bacterial quantification was conducted using the TB dsRED pipeline in Harmony software. Bacterial counts were determined at 4 hpi and 5 dpi (C), and the fold increase in bacterial counts from 4 hpi to 5 dpi is shown (D). Female donors are represented in yellow, male donors in blue; circles indicate 4 hpi and triangles indicate 5 dpi. (CFU analysis n=3 per sex, HCS analysis n=16 per sex)

Results: Summary 1

- Implementation of an *in vitro* infection model providing basis for systematic study of *M. tuberculosis* interactions with human monocyte derived macrophages
- *M. tuberculosis H37Rv* infected hMdMs were fixed for 20 h with 2 % PFA which led to inactivation of the bacteria while preserving fluorescent signal of the bacteria
- Customized Harmony® image analysis pipeline enables precise quantification of mycobacterial infection via fluorescent labelling (*BCG-GFP*/*M. tuberculosis dsRED*), upon optimization of the detection thresholds for bacterial size and intensity which was successfully validated by MOI dependent titrations.
- Comparing CFU and HCS analyses revealed similar bacterial load trends over time, demonstrating that the HCS pipeline is a suitable alternative for high-throughput analysis.

4.2 Sex specific differences in hMdMs during infection with *M. tuberculosis*

Sex-specific differences in immune responses are recognized as important contributors to the susceptibility and progression of TB. To dissect these differences in detail, we employed HCS microscopy to accurately quantify *M. tuberculosis* infection parameters in hMdMs at the single-cell level. Building on this, we performed an analysis of macrophage phenotypes and examined cytokine secretion profiles. This integrated approach enables a comprehensive assessment of how biological sex shapes both the cellular infection dynamics and the immune functions of hMdMs in response to *M. tuberculosis*.

4.2.1 Analysis of *M. tuberculosis* infection dynamics in human macrophages stratified by donor sex

To investigate potential sex-specific differences in macrophage permissiveness, hMdMs from male and female donors were infected in vitro with red fluorescent *M. tuberculosis dsRED*. Infection parameters were assessed at 4 hpi to evaluate uptake and at 5 dpi to monitor infection progression. At 4 hpi, initial infection rates (percent of infected macrophages; Figure 12 A) as well as bacteria per macrophage (Figure 12 C) were similar between males and females, indicating comparable uptake. Over the subsequent five days, both the proportion of infected cells and the bacterial load per cell increased in macrophages from both sexes. In females, the mean infection rate increased by 5.14 %, while in males it rose by 6.97 %, with the increase in males being statistically significant (Figure 12 A). However, direct comparison of the percentage of infected hMdMs per time point across sexes did not reveal significant differences (Figure 12 B). The bacterial numbers per infected macrophages increased significantly over the 5-day course, reaching comparable levels between sexes with bacteria counts in infected female hMdMs rising from 1.45 to 2.832 ($p=0.0003$) and in infected male hMdMs from 1.742 to 2.68 ($p=0.0082$) (Figure 12 C). hMdMs harbouring more than three intracellular bacteria were classified as ‘massively infected hMdMs’. This threshold was established to address challenges in tracking bacterial proliferation over time, as traditional metrics (e.g., bacteria per infected hMdMs) showed limited sensitivity due to the difficulty of distinguishing single bacteria within dense intracellular aggregates. By focusing on hMdMs with high bacterial loads, this parameter provides a more robust indicator of replicative success, as it circumvents underestimation caused by clustered bacteria and better reflects bacterial proliferation

during the 5-day infection period. At 4 hpi, 4.411 % of infected female hMdMs were classified as massively infected, compared to 4.856 % in males. Over the subsequent 5-day infection period, the proportion of massively infected hMdMs increased significantly in both sexes, rising to 21.29 % in females ($p < 0.0001$) and 20.97 % in males ($p < 0.0002$). No significant difference between the sexes was observed either at 4 hpi or 5 dpi (Figure 12 F). This demonstrates comparable infection bacterial proliferation in hMdMs from both sexes under standardized conditions (Figure 11 E).

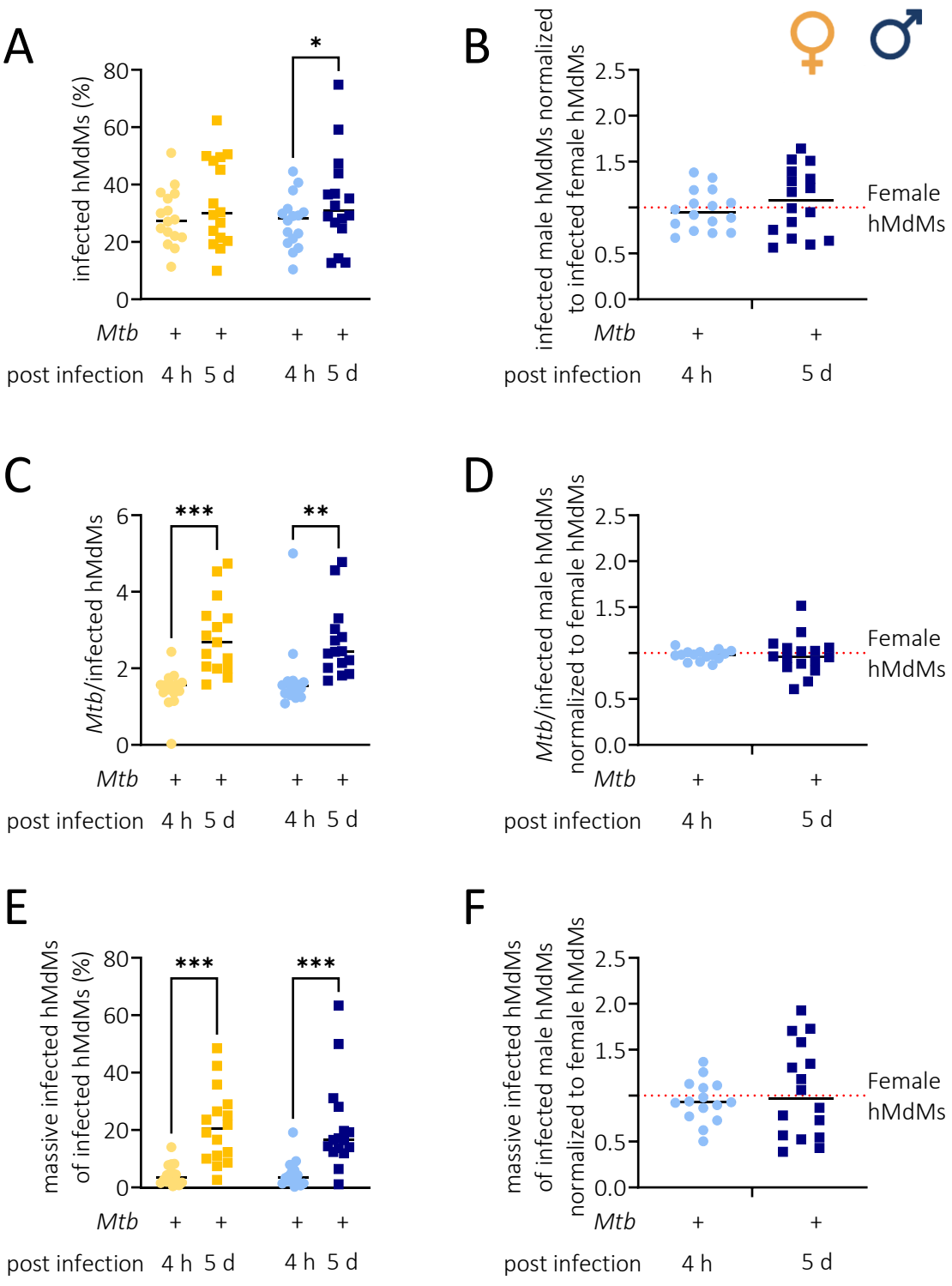

Figure 12 **Sex-specific differences in *M. tuberculosis* infected hMdMs**

hMdMs were infected with *M. tuberculosis dsRED* at a MOI 0.5, stained for cellular structures (DAPI) and analyzed by confocal microscopy at respective timepoints (4 hpi and 5 dpi). Image analysis was conducted using Harmony software to evaluate (A) infected hMdMs (%), (C) *Mtb*/infected hMdMs and (E) massive infected hMdMs of infected hMdMs (%). (B, D, F) Data from male hMdMs were additionally normalized to data generated from female hMdMs (=1, red dotted line). Each symbol

represents an individual donor, with yellow indicating female donors and blue indicating male donors. Data reflect 16 independent experiments per sex with samples tested in quadruplicates of which the mean is shown. (p*<0.05, p***<0.001 Two-Way-ANOVA multiple comparisons)

4.2.2 Macrophage polarisation in response to *M. tuberculosis* infection

Macrophages exhibit considerable functional plasticity, polarizing into pro-inflammatory (M1) or anti-inflammatory (M2) phenotypes in response to microenvironmental cues. Building on the Lotter group's protocol, which uses morphological parameters such as cell roundness and width to distinguish M1- and M2-like hMdMs during *Leishmania* infection (147), we adapted this approach for the analysis of hMdMs polarization in the context of *M. tuberculosis* infection using our custom Harmony® TB *dsRED* imaging pipeline (Figure A). First, the adapted imaging workflow employs a multi-step analysis approach using HCS microscopy to assess different infection parameters and cellular morphology simultaneously (Figure 13 A). Secondly, in this morphology-based classification system, M1-like macrophages characteristically display a round morphology with compact structure, reflecting their activated, pro-inflammatory state (Figure 13 B). Conversely, M2-like macrophages exhibit a distinct spindle-shaped, elongated appearance with prominent cytoplasmic extensions and irregular cell boundaries, consistent with their tissue-remodelling and anti-inflammatory functions (Figure 13 B). Lastly readout parameters like cell count and % infected cells were generated within the specific phenotype (Figure 13 C)

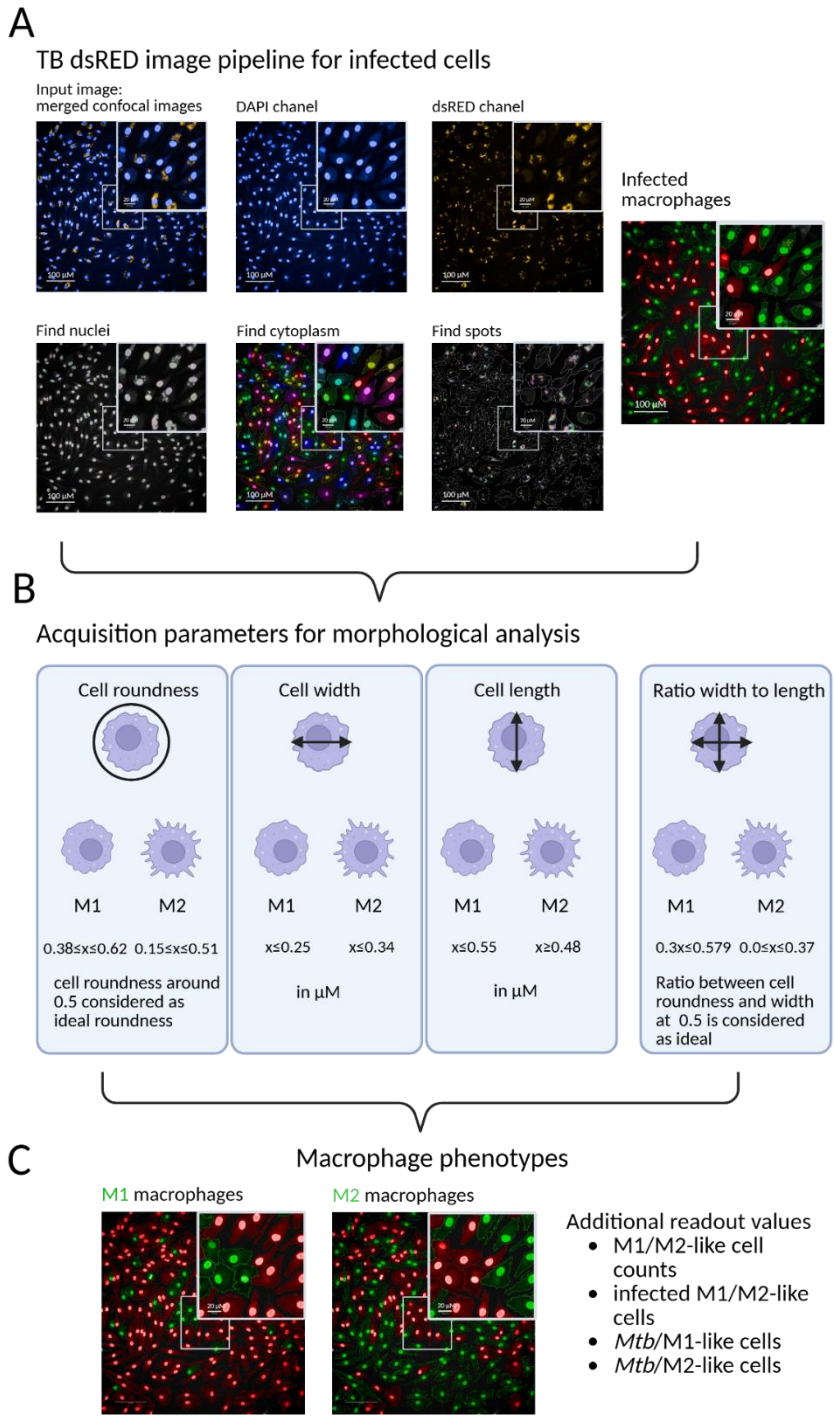

Figure 13 **Parameters for M1- and M2-like hMdMs phenotype in *M. tuberculosis* infected cells**

hMdMs were infected with *M. tuberculosis dsRED* at a MOI 0.5, stained for cellular structures (DAPI). (A) Image analysis was conducted using Harmony software for *M. tuberculosis dsRED* pipeline to further evaluate (B) M1- and M2-like hMdMs phenotypes according to cell roundness and cell width. As new defined populations M1- and M2-like hMdMs can be used for further analysis of infection parameters (C). (Phenotype pipeline was published in Bea…,Buer…,Schneider, Lotter et al (144)).

Figure 14A describes the identification of the two populations of interest: total hMdMs population and infected hMdMs only. In the absence of infection, hMdMs exhibit a mixed phenotype, with approximately 20 % displaying an M1 and 30 % an M2-like phenotype, and male hMdMs showing greater variability in M2 polarization compared to females (Figure 14B). In the presence of *M. tuberculosis*, the proportion of M2-polarized hMdMs increased significantly in both sexes over the 5-day infection period. Analysis of the infected cell populations revealed that both M1- and M2-like hMdMs internalize *M. tuberculosis*, with no marked preference or sex-specific differences observed at the 4 h time point (Figure 14C). However, 5 dpi, the proportion of infected M2-like hMdMs had significantly increased in both sexes, while the proportion of infected M1-like hMdMs remained unchanged. Together, these findings suggest that *M. tuberculosis* replicates more efficiently within M2-like hMdMs than in M1-like hMdMs, regardless of the macrophage's sex.

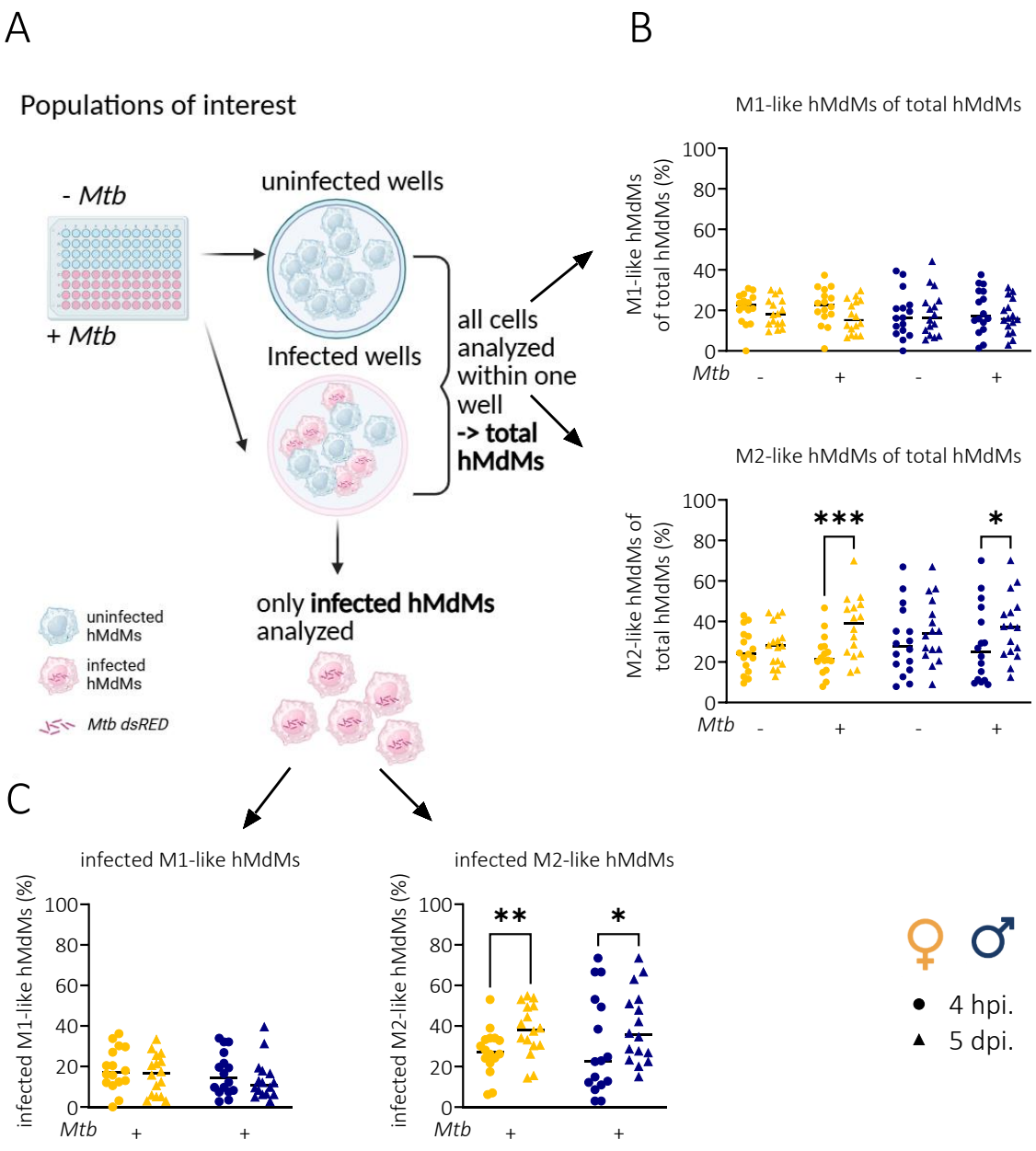

Figure 14 **Sex-differences in hMdMs phenotype upon *M. tuberculosis* infection**

hMdMs were infected with M. tuberculosis dsRED at a MOI 0.5, stained for cellular structures (DAPI) and analysed by confocal microscopy at respective timepoints (4 hpi round and 5 dpi triangle). Image analysis was conducted using Harmony software for *M. tuberculosis dsRED* pipeline to further evaluate M1- and M2-like hMdMs phenotypes. The distribution of M1- and M2-like hMdMs was analysed in the total population in uninfected and infected wells (A, B). Additionally, M1- and M2-like hMdMs distribution was analysed in infected hMdMs only (A, C). Each symbol represents an individual donor, with yellow indicating female donors and blue indicating male donors. Data reflect 16 independent experiments per sex with samples tested in quadruplicates of which the mean is shown. (p*<0.05 ,p***<0.001 Two-Way-ANOVA multiple comparisons)

4.2.3 Cytokine profiling of *M. tuberculosis* infected human macrophages reveals sex-specific trends amid high donor variability

Macrophages not only serve as host cells for *M. tuberculosis* but also act as effector cells by producing a variety of cytokines that influence inflammation, immune cell recruitment, and the balance between protective and pathological responses, ultimately shaping the outcome of the infection (58, 148). Therefore, the levels of cytokines and chemokines were measured in the cell culture supernatants 24 h post *M. tuberculosis H37Rv* infection (MOI=2) using the LEGENDplex™ Human Inflammation Panel 1 cytometric bead assay. The analysis included the cytokines IL-1β, TNF-α, IFN-α2, IL-6, IL-10, IL-17A, IL-23, IL-8 important in *M. tuberculosis* infection. The concentrations of IL-12p70 were below detection limit while concentrations of MCP-1 and IL-8 exceeded the detection range. Additionally, an IL-8 ELISA with higher sample dilutions was performed to accurately quantify IL-8 levels. Figure 15 highlights both the (Figure 15 A) absolute and (Figure 15 B) relative differences in cytokine production between female and male hMdMs in response to *M. tuberculosis* infection.

Absolute concentrations (Figure 15 A) revealed a trend toward higher IL-1β and IL-6 production in infected female hMdMs compared to infected males for IL-1β this was not reflected in the normalized male-to-female ratios but for IL-6 an increased production in infected female hMdMs was measured (Figure 15 B). In contrast, male hMdMs produced higher levels of TNF-a and IFN-a2 upon *M. tuberculosis* infection, with the normalized data showing marked male-biased increases, particularly for TNF-α (~7.5-fold). These cytokines are central to macrophage-driven inflammatory responses and are critical for orchestrating host defence and immune cell recruitment (36, 149-152) but also mediate immunopathology if produced in excess.

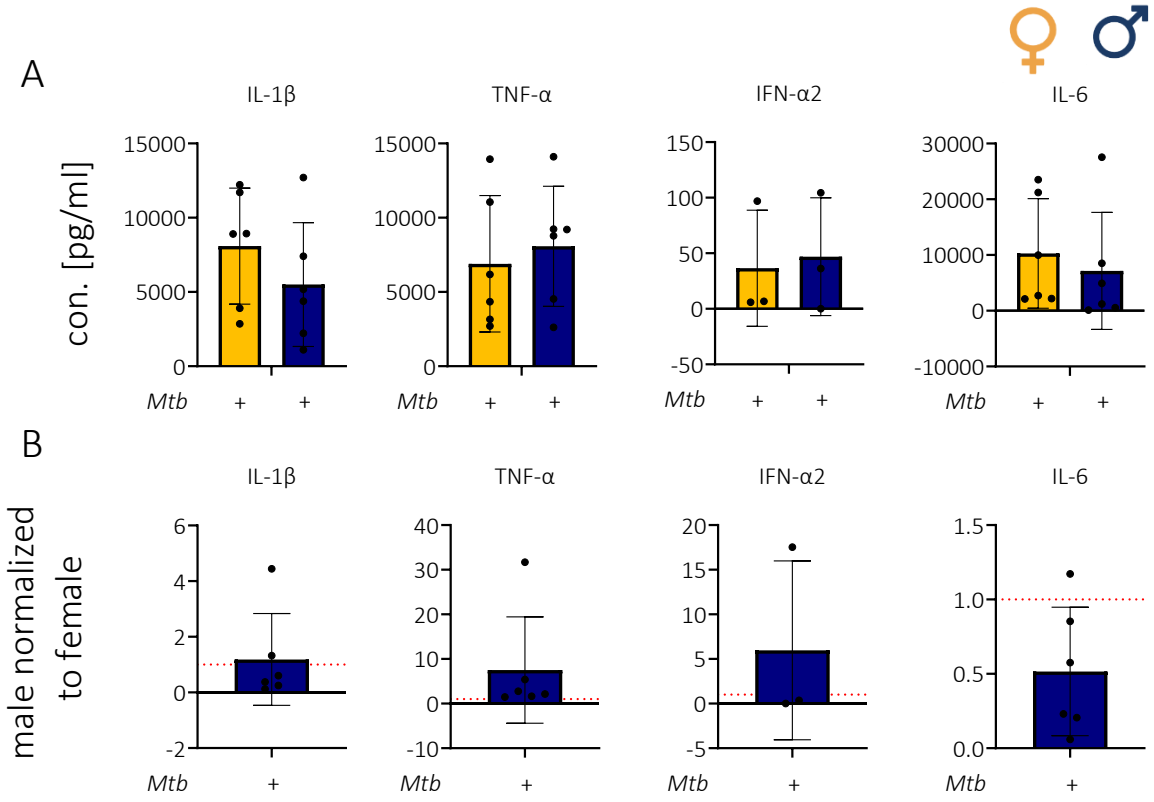

Figure 15 **Sex-specific IL-1β, TNF-α, IFNα2 and IL-6 cytokine responses to *M. tuberculosis* stimulation in hMdMs**

Concentrations of cytokines (IL-1β, TNF-α, IFNα2 and IL-6) were assessed in the supernatants of hMdMs derived from female (yellow) and male (blue) donors following infection with *M. tuberculosis H37Rv* (MOI=2). Samples were collected 24 hpi and analysed using a LEGENDplex™ assay. (B) Cytokine concentrations in male hMdMs were normalized to those in female hMdMs (red line) from the same isolation round (>1 upregulated in male compared to female, <1 downregulated in mal compared to female). Data are shown as mean ± SD for each group. Statistical analysis was carried out using Mann-Whitney test.

Figure 16 shows the results of cytokine IL -10 and IL-8 concentrations which were similar between sexes (Figure 16 A), and normalization (Figure 16 B) confirmed no consistent sex difference. Both are key mediators in modulating inflammation and neutrophil recruitment(153, 154).

For IL-17A and IL-23, both the absolute concentrations (Figure 16 A) and the normalized male-to-female ratios (Figure 16 B) indicate a trend toward higher production in female hMdMs compared to male hMdMs following *M. tuberculosis* infection. Both cytokines are central to granuloma formation, immune cell recruitment, and the regulation of

inflammation, but can also contribute to disease pathology if not properly regulated (155, 156).

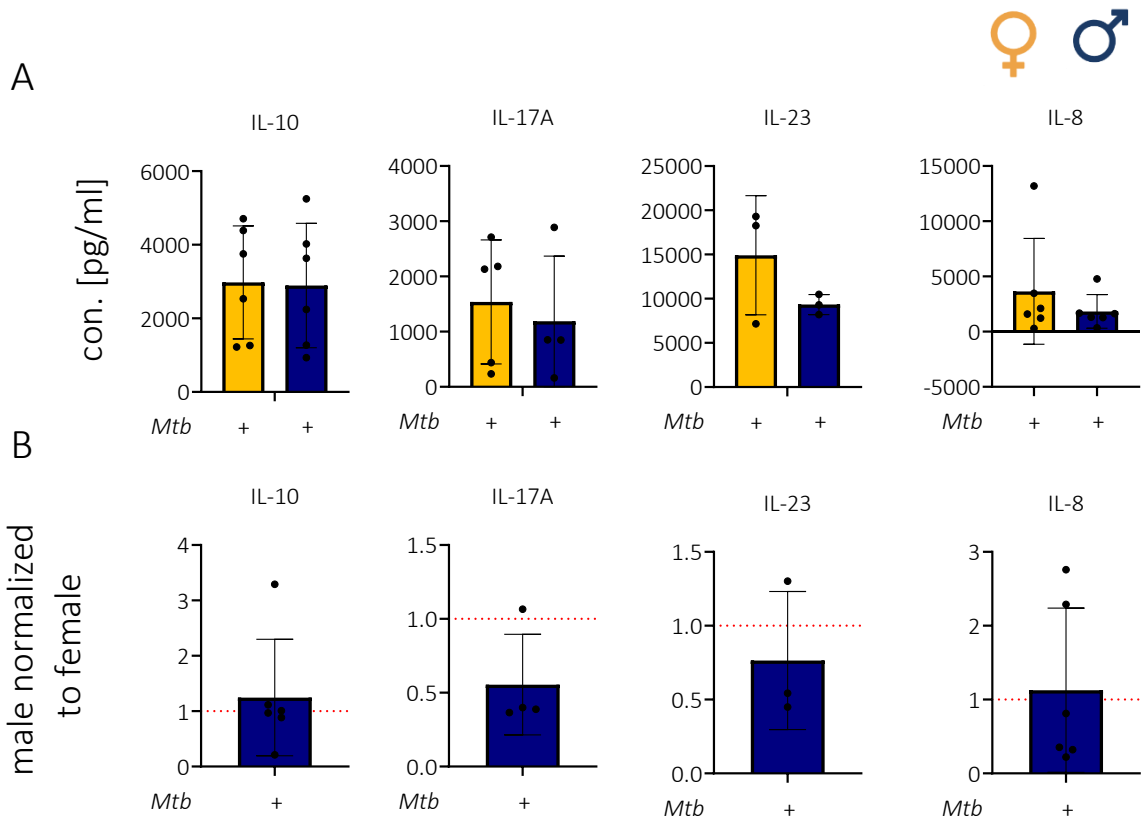

Figure 16 **Sex-specific IL-10, IL-17A, IL-23 and IL-8 cytokine responses to *M. tuberculosis* stimulation in hMdMs**

Concentrations of the cytokines IL-10, IL-17A, IL-23 and IL-8, which were assessed in the supernatants of hMdMs derived from female (yellow) and male (blue) donors following infection with *M. tuberculosis H37Rv* (MOI=2). Samples were collected 24 hpi and analysed using a LEGENDplex™ assay. (B) Cytokine concentrations in male hMdMs were normalized to those in female hMdMs (red line) from the same isolation. Data are shown as mean ± SD for each group. Statistical analysis was carried out using Mann-Whitney test.

Cytokine profiling of *M. tuberculosis* infected hMdMs reveals sex-specific differences. Female hMdMs show higher secretion of IL-17A and IL-23, while male hMdMs tend to produce more TNF-α and IFN-α2. No consistent sex differences are observed for IL-10, IL-8, IL-1β, or IL-6. These findings highlight distinct cytokine responses to *M. tuberculosis* infection between male and female hMdMs.

4.2.4 Sex-specific transcriptional response to *M. tuberculosis* infection in human macrophages

Sex-specific transcriptional responses to *M. tuberculosis* infection were examined via qRT-PCR in hMdMs from healthy male and female donors. hMdMs were infected with *M. tuberculosis* (MOI 2) and harvested at 6 h and 20 h post-infection to determine the optimal timepoint for subsequent transcriptome analysis (Figure 17). Our analysis focused on three key genes with central roles in antimycobacterial immunity: TNF-α, which is critical for granuloma formation and macrophage activation; IL-1β, a pro-inflammatory cytokine essential for recruiting immune hMdMs and promoting inflammatory responses during infection; and IRG1, which is one of the most highly upregulated genes under inflammatory conditions. It encodes for the enzyme aconitate decarboxylase 1, which converts cis-aconitate (an intermediate of the TCA cycle) into itaconate, a metabolite with important immunoregulatory and bactericidal properties. Gene expression from infected hMdMs was normalized to uninfected hMdMs from the same donor, ensuring baseline correction and minimizing inter-individual variability, highlighting infection-specific transcriptional changes between the sexes.

Figure 17 shows increased gene expression of all three target genes from 6 to 20 hpi for both sexes, with IRG1 expression being notably higher than TNF-α and IL-1β. Males exhibited a higher TNF-α expression at 20 hpi, while females showed a more pronounced increase in IRG1 expression. IL-1β expression increased similarly in both sexes. Based on the robust induction of gene expression observed at 20 hpi for all three target genes in both sexes, this timepoint was selected for RNA bulk sequencing to capture early transcriptional responses to *M. tuberculosis* infection.

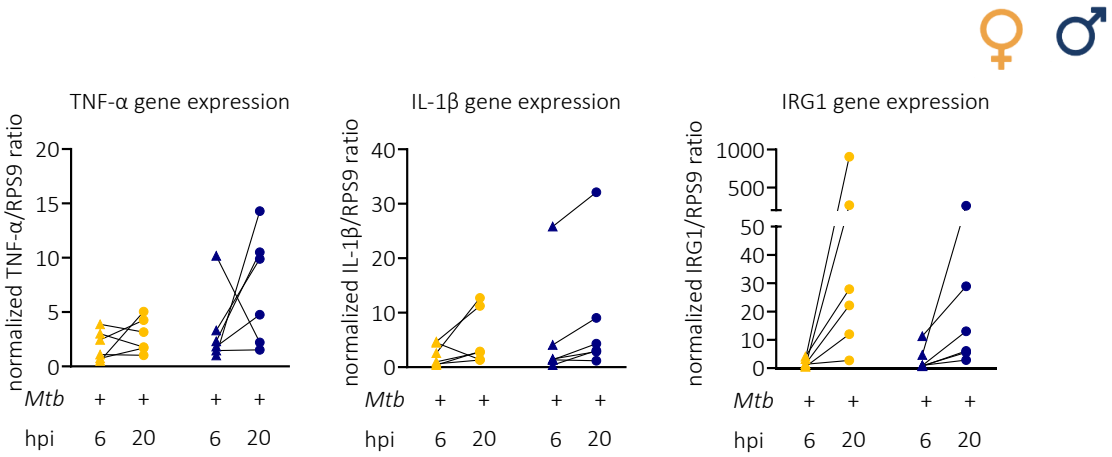

Figure 17 **Sex-specific differences in gene expression of TNFα, IL1β, and IRG1 in hMdMs induced by *M. tuberculosis***

hMdMs derived from healthy donors were infected with *M. tuberculosis H37Rv* at a MOI of 2 for 6 and 20 h. mRNA expression levels of TNF-α, IL-1β, and IRG1 were determined using qRT-PCR and normalized to the housekeeping gene RSP9. Each symbol represents an individual donor, with yellow indicating female donors and blue indicating male donors. Data show six independent experiments per sex.

Results: Summary 2

- Initial bacterial uptake (4 hpi) and five-day replication dynamics in hMdMs were similar between sexes, with no significant differences in infection rates, bacterial loads, or the proportion of heavily infected cells upon *M. tuberculosis* infection
- Both male and female hMdMs showed a significant increase in the proportion of M2-like hMdMs following *M. tuberculosis* infection, suggesting that M. tuberculosis preferentially expands within anti-inflammatory, M2-like hMdMs, independent of donor sex.
- Cytokine profiling revealed that male hMdMs produce higher levels of pro-inflammatory TNF-α and IFN-α2, whereas female hMdMs tend to secrete more IL-17A, IL-23 and IL-6 following infection with *M. tuberculosis*; no consistent sex differences were observed for IL-10, IL-8 or IL-1β.
- Transcriptional analysis showed increased expression of TNF-α in male and IRG1 in female hMdMs at 20 hpi, while IL-1β was similarly upregulated in both sexes, indicating differential gene regulation in response to *M. tuberculosis* in hMdMs.

4.3 Influence of sex hormones on *M. tuberculosis* infection

Sex differences in host-pathogen interactions arise from a complex interplay of genetic and hormonal factors that influence immune responses to *M. tuberculosis* infection. Hormonal influences, particularly from sex steroids such as estrogens and androgens, modulate innate and adaptive immunity by affecting cytokine production, macrophage activation, and immune cell recruitment (95, 123, 157). Investigating the role of sex hormones in this context helps to elucidate the mechanisms behind the observed sex-biased susceptibility.

4.3.1 Assessment of sex hormone induced cytotoxicity in *M. tuberculosis* infected macrophages

To assess potential cytotoxic effects of sex hormones on *M. tuberculosis* infected hMdMs, cell viability was evaluated using complementary cytotoxicity assays. The Lactate Dehydrogenase (LDH) assay quantified membrane integrity by measuring cytosolic enzyme release into culture supernatants following potential hormone-induced damage (Figure 18A), while the 3-(4,5-dimethylthiazol-2-yl)-2,5-diphenyltetrazolium bromide (MTT) assay assessed metabolic activity by measuring mitochondrial reduction of tetrazolium to formazan in viable hMdMs (Figure 18B). hMdMs differentiated in the presence of varying concentrations of DHT or E2 were analysed in the presence or absence of *M. tuberculosis* (MOI 0.5) to determine whether sex hormones affect macrophage viability. *In-vitro* doses often exceed serum concentrations due to bioavailability and experimental design. Physiological concentrations of DHT and E2 vary by sex and reproductive status, typically ranging from 1-50 nM depending on the specific hormone and population studied. Concentrations above this, particularly in the micromolar range such as 10 µM or higher, are regarded as supraphysiological and are often used to study pharmacological or cytotoxic effects. hMdMs showed minimal cytotoxicity at 4 hpi, with LDH levels remaining low in both uninfected and *M. tuberculosis*-infected hMdMs. In contrast, positive controls exhibited complete (100 %) cytotoxicity, confirming assay validity. At 5 dpi, a slight increase in LDH release was observed in infected hMdMs compared to uninfected controls; however, cytotoxicity remained below 10 % across all hormone concentrations tested. These findings were supported by MTT assays, which confirmed that cell viability was not compromised by hormone treatment, also not in the presence of infection. These results collectively demonstrate that both physiological and supraphysiological concentrations of

sex hormones do not compromise macrophage viability during differentiation or subsequent *M. tuberculosis* infection, validating the experimental conditions for downstream immunological analyses.

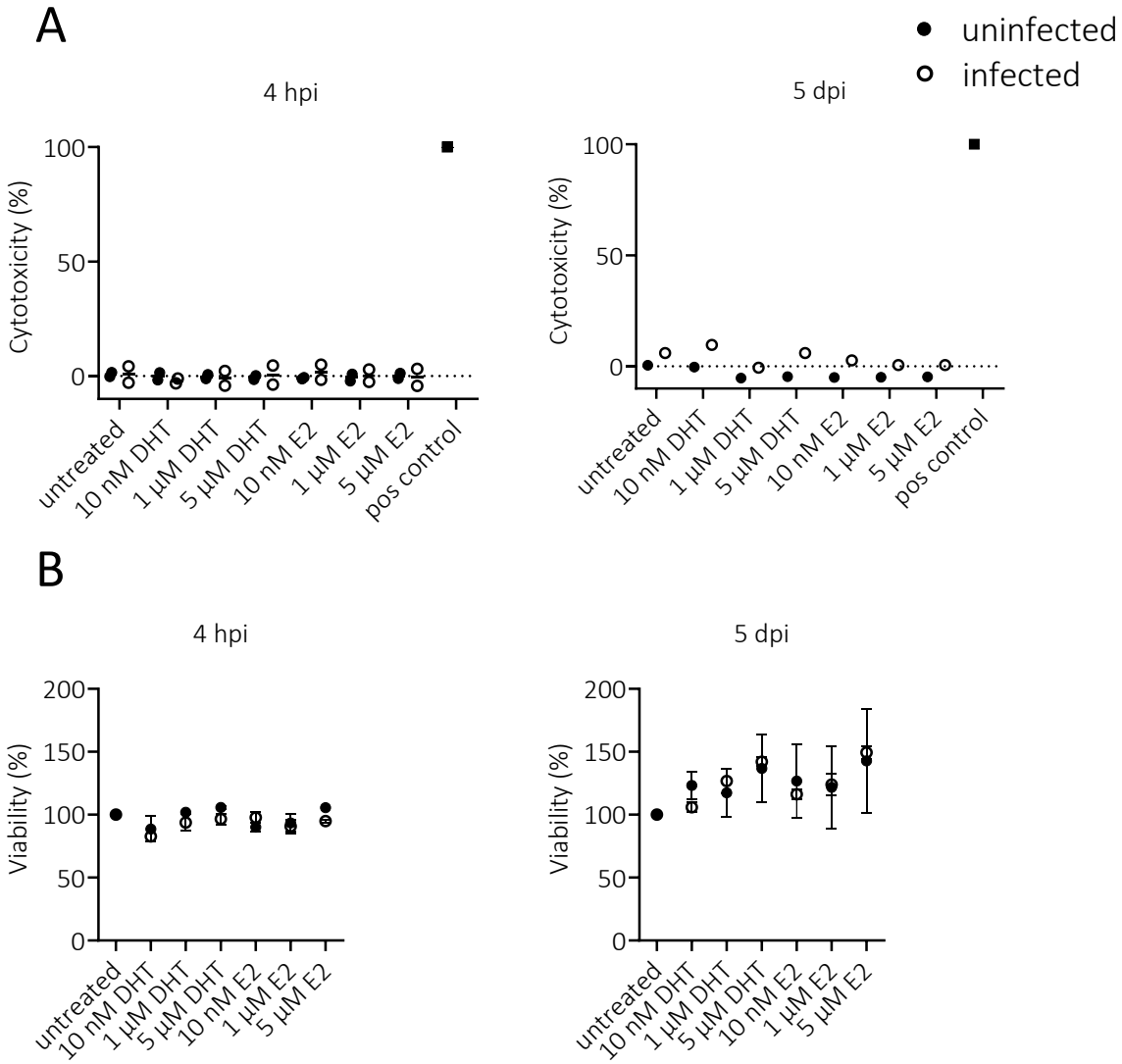

Figure 18 **LDH and MTT assay of hMdMs generated upon DHT and E2 treatment and infected with *M. tuberculosis***

hMdMs were generated under continuous treatment with the sex hormones DHT and E2 at varying concentrations, as detailed in the Materials and Methods section. (A) Cytotoxicity of DHT and E2 was assessed using an LDH assay, while (B) cell viability was evaluated via an MTT assay in both uninfected and *M. tuberculosis*-infected hMdMs at a MOI of 0.5. Analyses were performed at specific time points: 4 hours post-infection (hpi) and 5 days post-infection (dpi). Data reflects one test replicate with samples tested in triplicates for LDH assay and two replicates with samples tested in triplicates for MTT assay.

To complement LDH and MTT viability assessments, macrophage counts were quantified following hormone treatment using high-content confocal microscopy and image analysis within our customized Harmony pipeline (Figure 19). hMdMs from male and female donors were differentiated in the presence of varying concentrations (10 nM to 5 µM) of DHT or E2 and subsequently infected with *dsRED*-expressing *M. tuberculosis* (MOI = 0.5) for either 4 hours or 5 days. The analysis pooled data from multiple independent experiments with varying sample sizes for each condition and sex, untreated (n=16 per sex), 10-50 nM (n=6 per sex), 100-500 nM (n=12 per sex), and 1-5 µM (n=8 per sex), with each sample measured in triplicate or quadruplicate. Cell counts from infected, and hormone treated hMdMs were normalized to infected untreated hMdMs from the same donor, ensuring baseline correction and minimizing inter-individual variability, highlighting hormone-specific changes in cell counts. At 4 hpi, a slight increase in cell counts was observed with 10 and 50 nM DHT, while higher DHT concentrations did not change cell numbers in both sexes. In contrast, cell counts declined at higher E2 concentrations. At 5 dpi, female hMdMs treated with 10 to 50 nM DHT showed higher counts, which then plateaued at higher concentrations. While longer E2 treatment did not have a significant impact on cell counts, cell counts of female macrophages had slightly increased 5 dpi in the presence of low concentrations of DHT, while this increase was more pronounced for male macrophages at higher DHT concentrations only.

These findings suggest that while physiological hormone concentrations have minimal impact on hMdMs viability, supraphysiological levels may increase cell numbers during extended exposure.

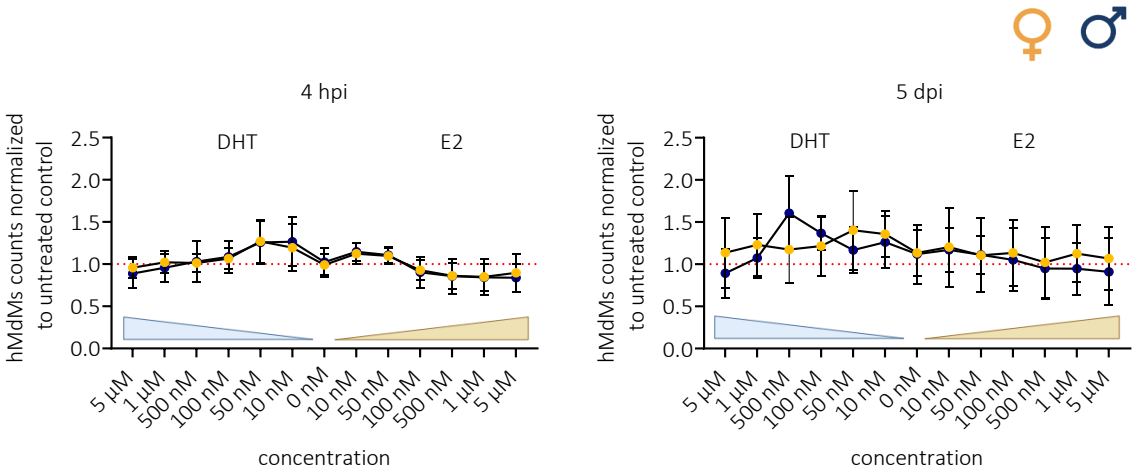

Figure 19 **Cell count of hMdMs generated upon DHT and E2 treatment and infected with *M. tuberculosis***

hMdMs were generated under continuous treatment of DHT and E2 at different concentrations, as detailed in the Materials and Methods section. hMdMs were infected with *M. tuberculosis dsRED* at a MOI 0.5, stained for cellular structures (DAPI) and analyzed by confocal microscopy at respective timepoints (4 hpi. and 5 dpi.). Image analysis was conducted using Harmony software for *M. tuberculosis dsRED* pipeline to further evaluate the number of hMdMs of each condition. (A) The number of hMdMs in the treated condition was normalised to the untreated control. Female donors are depicted in yellow, male in blue. The mean +SD of in total 16 independent experiments per sex with samples tested in quadruplicates are shown (n=16 untreated; n=12 100 nM, 500 nM; n=9 1 µM, 5 µM; n=7 10 nM, 50nM)

4.3.2 Impact of sex hormones on *M. tuberculosis* infection dynamics in human macrophages

To assess the impact of sex hormones on *M. tuberculosis* infection dynamics in hMdMs, hMdMs were infected at a MOI of 0.5 (Figure 20). Uptake was analysed at 4 hpi, while intracellular bacterial replication was evaluated at 5 dpi. Hormone treatments spanned a broad concentration range (10 nM to 5 µM for both DHT and E2) to capture dose-dependent effects. Key readouts were the proportion of infected hMdMs, the average bacterial load (*M. tuberculosis* per infected hMdMs) and hMdMs with ≥3 bacteria, indicating active replication (massively infected hMdMs). Hormone-treated groups were normalized to untreated controls (set as 1) to isolate hormone-specific effects. Data visualization positioned untreated controls centrally, with ascending DHT concentrations (androgen axis) to the left and E2 concentrations (estrogen axis) to the right, enabling direct comparison of hormone gradients across sexes.

While hormone treatment did not change the number of internalized bacteria per cell, the number of infected cells did slightly increase with increasing concentrations of both DHT or E2 (Figure 20 A, B) for both male and female macrophages. Conversely, with increasing concentrations of DHT or E2 the proportion of massively infected macrophages decreased, particularly for males. Interestingly, at 5 dpi, a concentration-dependent increase of infected male and female hMdMs as well as bacterial load per cell was observed in the presence of hormones, particularly DHT, in both sexes, indicating increased bacterial replication under these conditions. In contrast, presence of both hormones reduced the proportion of massively infected hMdMs.

Overall, the results suggest that supraphysiological levels of DHT may promote *M. tuberculosis* replication; however, this did not lead to an overall increase in the number of massively infected hMdMs. The effect of hormone treatment did not differ between male and female derived hMdMs.

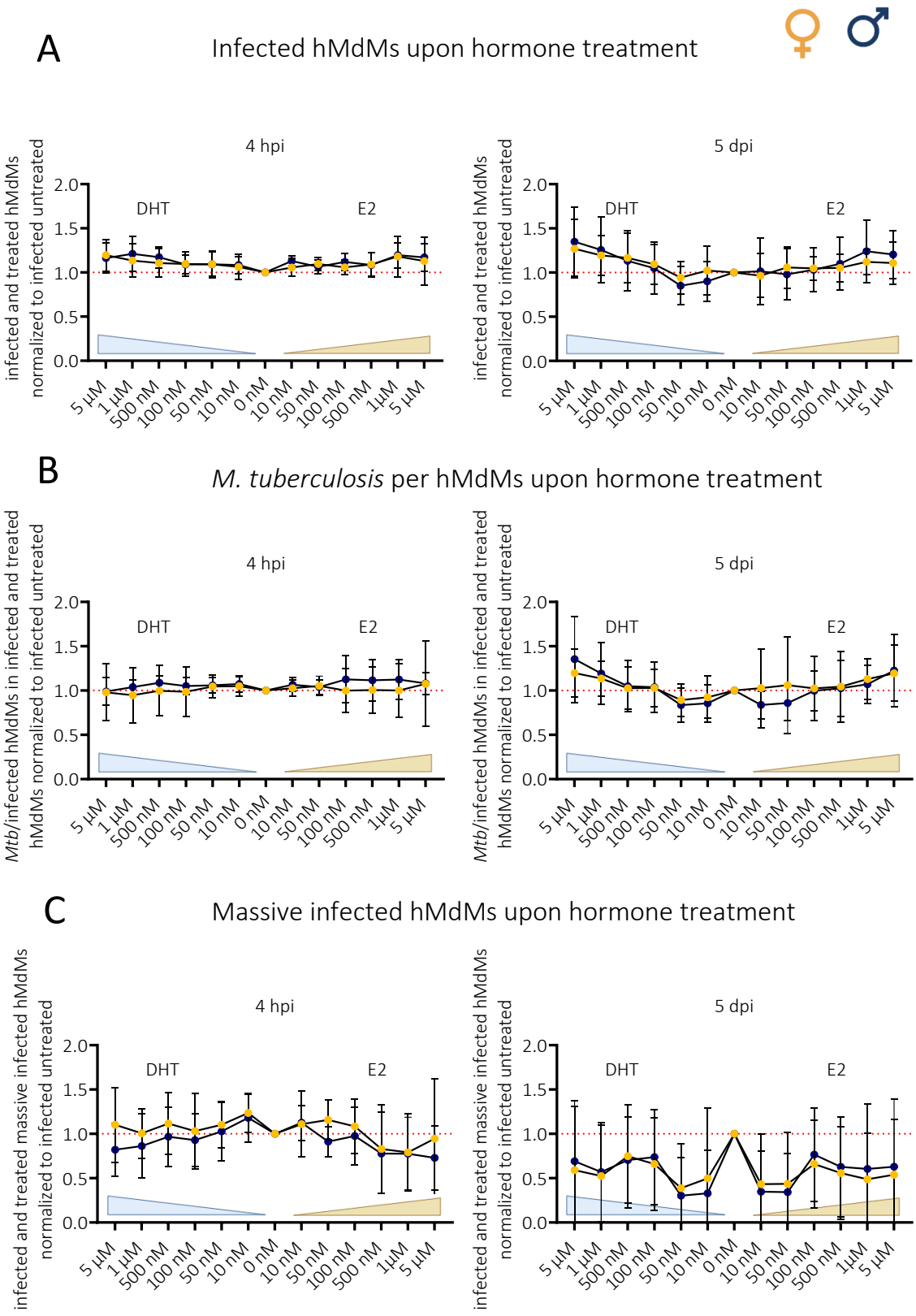

Figure 20 **Effect of DHT and E2 treatment on infection rates and bacterial burden in male and female human macrophages during *M. tuberculosis* infection**

hMdMs were generated under continuous treatment with the sex hormones DHT and E2 at different concentrations, as detailed in the Materials and Methods section. hMdMs were infected with *M. tuberculosis dsRED* at a MOI 0.5, stained for cellular structures (DAPI) and analyzed by confocal microscopy at respective timepoints (4 hpi. and 5 dpi.). Image analysis was conducted using Harmony software for *M. tuberculosis dsRED* pipeline. Image analysis was conducted using Harmony software to evaluate (A) infected hMdMs (%), (B) *MTB*/infected hMdMs and (C) massive infected hMdMs of infected cells (%). Female donors are depicted in yellow, male in blue. Results from the treated conditions were normalised to the untreated control to show the influence of the treatment. The mean +SD of in total 16 independent experiments per sex with samples tested in quadruplicates are shown (n=16 untreated; n=12 100 nM, 500 nM; n=9 1 µM, 5 µM; n=7 10 nM, 50nM).

4.3.3 Impact of sex hormones on macrophage polarization during *M. tuberculosis* infection

As shown previously (Figure 14), hMdMs initially display a balanced distribution of M1 and M2 phenotypes upon differentiation. However, over time and in response to *M. tuberculosis* infection, a shift toward the M2 phenotype was observed in both sexes. Figures 18 and 19 illustrate the impact of DHT and E2 treatment (10 nM to 5 µM) on hMdMs polarization during *M. tuberculosis dsRED* infection (MOI 0.5) within the whole cell population and within infected cells only. To assess the impact on bacterial uptake, analyses were performed at 4 hpi, while bacterial replication was evaluated at 5 dpi.

Initially, the focus was on analysing the polarization of the entire macrophage population, encompassing both infected and uninfected hMdMs, to highlight differences in hMdMs phenotypes influenced by sex hormones (Figure 21). All data were normalized to infected, untreated controls of the corresponding sex and timepoint to specifically highlight hormone induced effects. In the presence of DHT, a reduction in the M1 phenotype was observed at both time points, which was more prominent 5 dpi, while E2 had hardly any effect on the M1 polarization (Figure 21 A). In contrast, both E2 and DHT increased the proportion of M2 hMdMs, particularly in females, 4 hpi, while a reduction in M2 polarized hMdMs was observed in the presence of both hormones after 5 days (Figure 21 B).

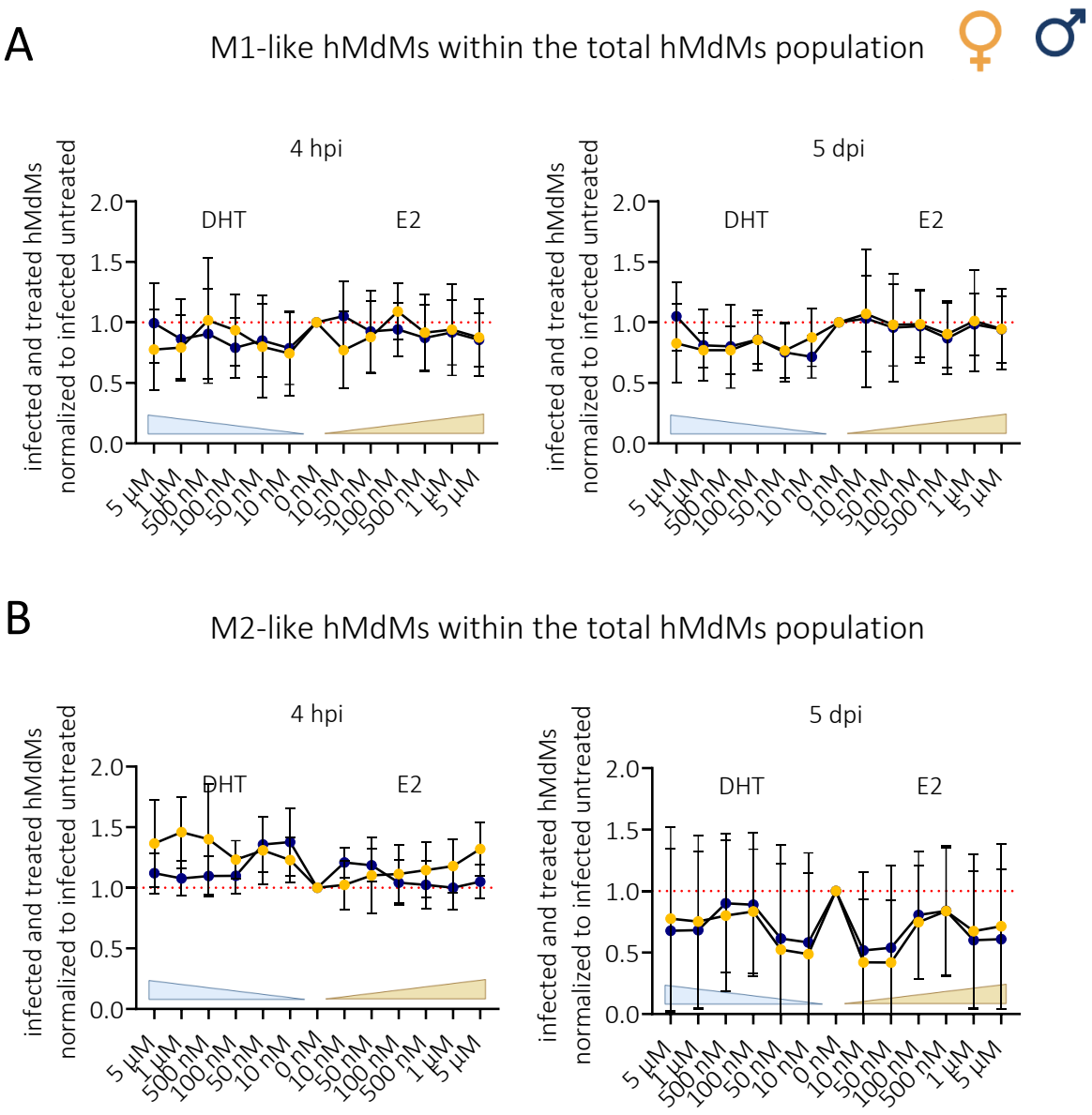

Figure 21 **Sex-specific differences of hormone treated and *M. tuberculosis* infected hMdMs phenotype in the whole cell population**

hMdMs differentiated upon hormone treatment with DHT and E2 were infected with *M. tuberculosis dsRED* at a MOI 0.5, stained for cellular structures (DAPI) and analyzed by confocal microscopy at respective timepoints (4 hpi. and 5 dpi.). Image analysis was conducted using Harmony software for *M. tuberculosis dsRED* pipeline to further evaluate M1- and M2-like hMdMs phenotypes as described in Material and Methods. (Phenotype pipeline (144)). Hormone concentration ranged from 10 nM to 5 µM. The distribution of (A) M1- and (B) M2-like hMdMs upon hormone treatment was analyzed within the whole cell population in one well. Female donors are depicted in yellow, male in blue. Results from the treated conditions were normalised to the untreated control to show the influence of the treatment. The mean +SD of in total 16 independent experiments per sex with samples tested in quadruplicates are shown (n=16 untreated; n=12 100 nM, 500 nM; n=9 1 µM, 5 µM; n=7 10 nM, 50nM).

Further analysis revealed that particularly DHT increased the proportion of M2 polarized hMdMs amongst those infected in both sexes at both time points, while E2 only increased the infected M2 polarized hMdMs population in females at the early time point (Figure. 22B). In contrast, the M1 phenotype was reduced amongst infected hMdMs in the presence of DHT (Figure. 22A).

Due to substantial donor-to-donor variability, statistically significant differences could not be established, highlighting the heterogeneity of primary human cell responses to hormonal modulation during mycobacterial infection.

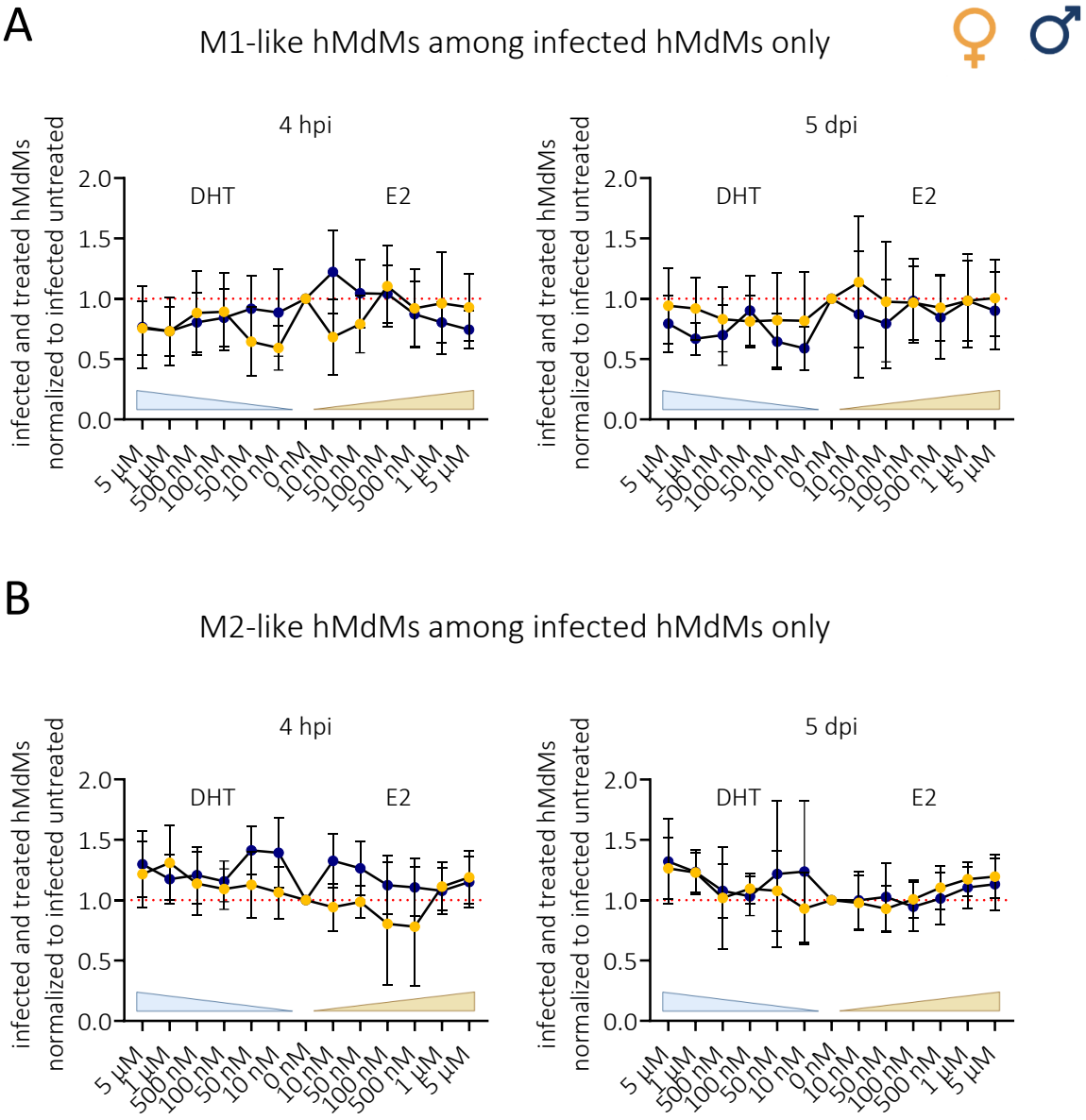

Figure 22 **Sex-specific differences of hormone treated and *M. tuberculosis* infected hMdMs phenotype in infected cells**

hMdMs differentiated upon hormone treatment with DHT and E2 were infected with *M. tuberculosis dsRED* at a MOI 0.5, stained for cellular structures (DAPI) and analyzed by confocal microscopy at respective timepoints (4 hpi. and 5 dpi.). Image analysis was conducted using Harmony software for *M. tuberculosis dsRED* pipeline to further evaluate M1- and M2-like hMdMs phenotypes as described in Material and Methods. (Phenotype pipeline was published (144)). Hormone concentration ranged from 10 nM to 5 µM. The distribution of (A) M1- and (B) M2-like hMdMs upon hormone treatment was analyzed in infected cells only. Female donors are depicted in yellow, male in blue. Results from the treated conditions were normalised to the untreated control to show the influence of the treatment. The mean +SD of in total 16 independent

experiments per sex with samples tested in quadruplicates are shown (n=16 untreated; n=12 100 nM, 500 nM; n=9 1 µM, 5 µM; n=7 10 nM, 50nM).

4.3.4 Cytokine profiling of *M. tuberculosis* infected human macrophages upon hormone treatment

To elucidate the impact of sex hormones on macrophage responses to *M. tuberculosis*, cytokine expression profiles in hMdMs treated with sex hormones before and during *M. tuberculosis* infection were analysed. The sex hormones DHT and E2 are known to differentially modulate intracellular signalling pathways and cytokine production in macrophages, shaping the balance between pro- and anti-inflammatory responses and potentially influencing infection processes (95, 158, 159) (Figure 23). Investigating cytokine responses under defined hormonal conditions thus provides valuable insight into how sex-specific immune regulation may contribute to differential susceptibility and outcomes in TB.

DHT and E2 treated (10 nM) hMdMs from male and female donors were infected with *M. tuberculosis H37Rv* (MOI=2) and supernatants were collected 24 hpi. Cytokines were analysed using the LEGENDplex™ Human Inflammation Panel 1 cytometric bead assay as described previously. The concentrations of IL-12p70 were again below detection limit and IL-8 and MCPI-1 were above detection limit. An additional ELISA with higher dilutions was performed to accurately quantify IL-8 levels. When comparing the measured cytokine concentrations in infected hMdMs upon DHT or E2 treatment, no differences were observed for TNF-α, IL-6, or IL-8. However, DHT treatment led to an increase in the production of IL-1β, IL-10, IL-17A, and IL-23 in female hMdMs, while in male hMdMs, DHT resulted in higher levels of IFN-α2 but a decrease in IL-23 production. Upon E2 treatment, cytokine production of IL-10 and IL-17A increased in female hMdMs, whereas IL-23 levels decreased compared to untreated controls. In male hMdMs, E2 treatment also led to an increase in IFN-α2 production.

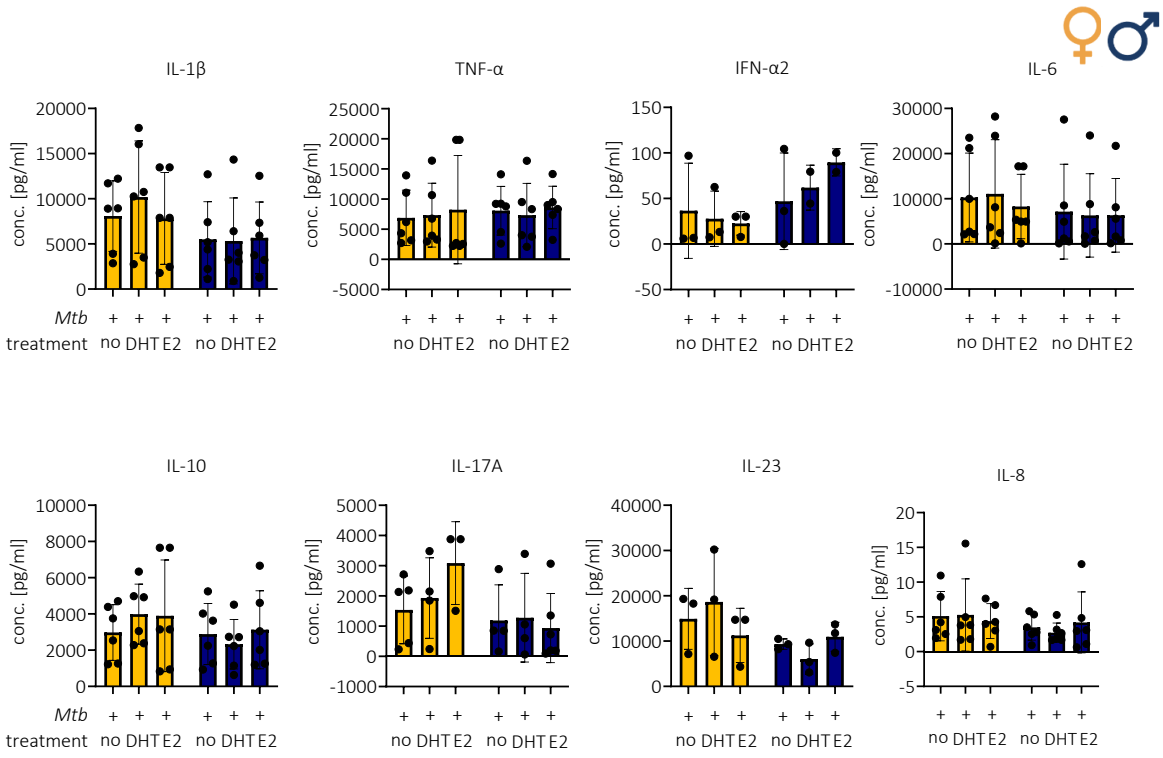

Figure 23 **Comparison of cytokine production in female and male donors after *M. tuberculosis* infection under different hormonal conditions**

Cytokine concentrations in supernatants from female (yellow bars) and male (blue bars) hMdMs treated with 10 nM DHT or E2 were measured 24 h post infection with *M. tuberculosis H37Rv* (MOI=2) via LEGENDplex™ analysis. Data show cytokine concentration in pg/ml. Cytokines were grouped in (A) classical inflammatory and (B) cytokines involved in adaptive immunity and immune regulation. Each dot represents an individual donor (n=3-6). Statistical analysis was carried out using Two-way ANOVA with Tukey's multiple comparison test.

To better assess/visualize the specific effects of DHT and E2 treatment on cytokine responses during *M. tuberculosis* infection in hMdMs, cytokine concentrations following hormone exposure were normalized to those of infected hMdMs from each donor, with results analysed separately by sex (Figure 24A female; Figure 24B male). Upon hormone treatment, infected female hMdMs exhibited higher levels of TNF-α compared to their male counterparts. In infected female hMdMs, the production of IL-1β and IL-6 did not show significant changes in response to either DHT or E2. In contrast, male hMdMs treated with E2 demonstrated increased IL-1β production compared to those treated with DHT, except for one outlier. For IL-6, DHT treatment resulted in higher levels than E2 treatment in infected male hMdMs, again with one outlier deviating from this trend. IFN-α2

production was not affected by hormone treatment but due to value below detection limit normalization decreased sample size.

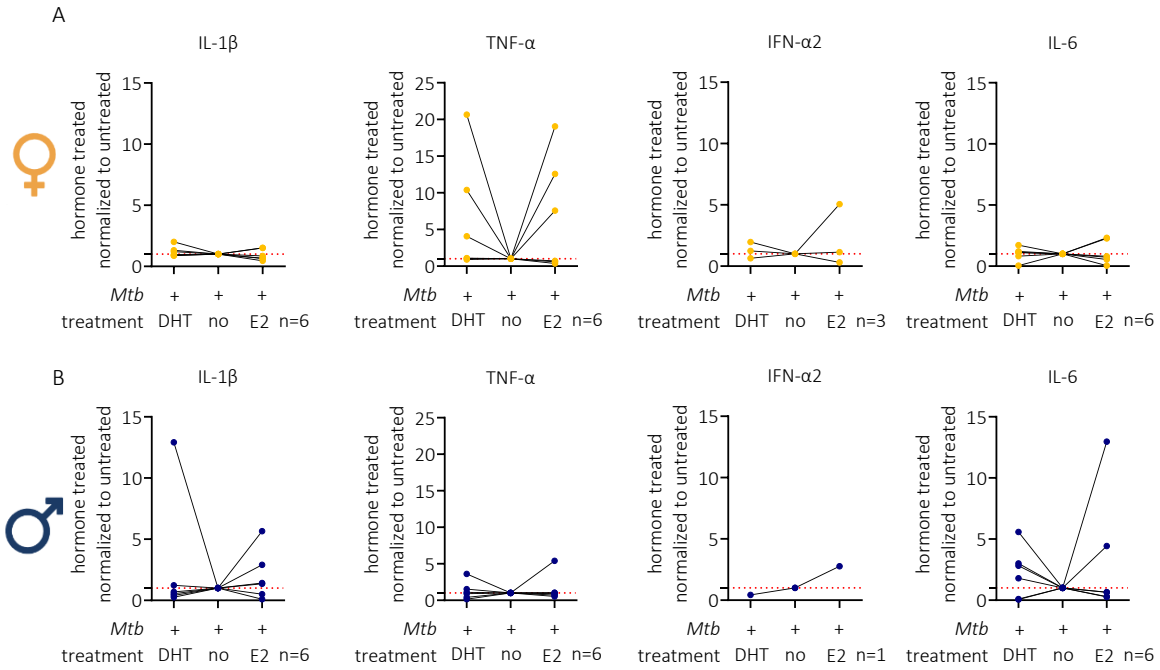

Figure 24 **Sex-specific effects of DHT and E2 on IL-1β, TNF-α, IFN-α2 and IL-6 cytokine production in *M. tuberculosis* infected hMdMs**

Cytokine concentrations (IL-1β, TNF-α, IFN-α2 and IL-6) were measured in supernatants from hMdMs treated with 10 nM DHT or E2 and infected with *M. tuberculosis H37Rv* (MOI=2) collected 24 hpi via LEGENDplex™ analysis. Data are normalized to untreated controls for each donor and separated by sex: (A) female donors (yellow), (B) male donors (blue). Each line represents an individual donor (n=6 per group).

Female hMdMs show a slight increase in IL-10 production following both DHT and E2 treatment, suggesting a modest upregulation of this regulatory cytokine in response to hormone exposure. However, the levels of IL-17A and IL-23 did not show significant changes in female hMdMs after either hormone treatment, indicating that these cytokines are not notably affected by DHT or E2 in this context (Figure 25A).

In male hMdMs, the response of IL-10 to hormone treatment was highly variable among donors. While some individuals exhibited a marked increase in IL-10 production following hormone exposure, others did not, resulting in a diverse overall pattern. Nevertheless, there was a general trend toward increased IL-10 levels upon hormone treatment in male

hMdMs. For IL-17A and IL-23, no consistent effects of DHT or E2 treatment were observed in male hMdMs, which may be attributed to the smaller sample size in this group due to normalization challenges when cytokine values fell below the detection limit. For IL-8 a slight increase upon hormone treatment can be observed in infected female hMdMs but not in males (Figure 25B).

In summary, our results demonstrate that DHT and E2 exert sex-specific effects on cytokine responses in *M. tuberculosis* infected hMdMs. However, due to high donor variability, our findings primarily reflect observable trends rather than statistically significant differences. These findings highlight the importance of considering both sex and hormonal environment when investigating immune responses to *M. tuberculosis*.

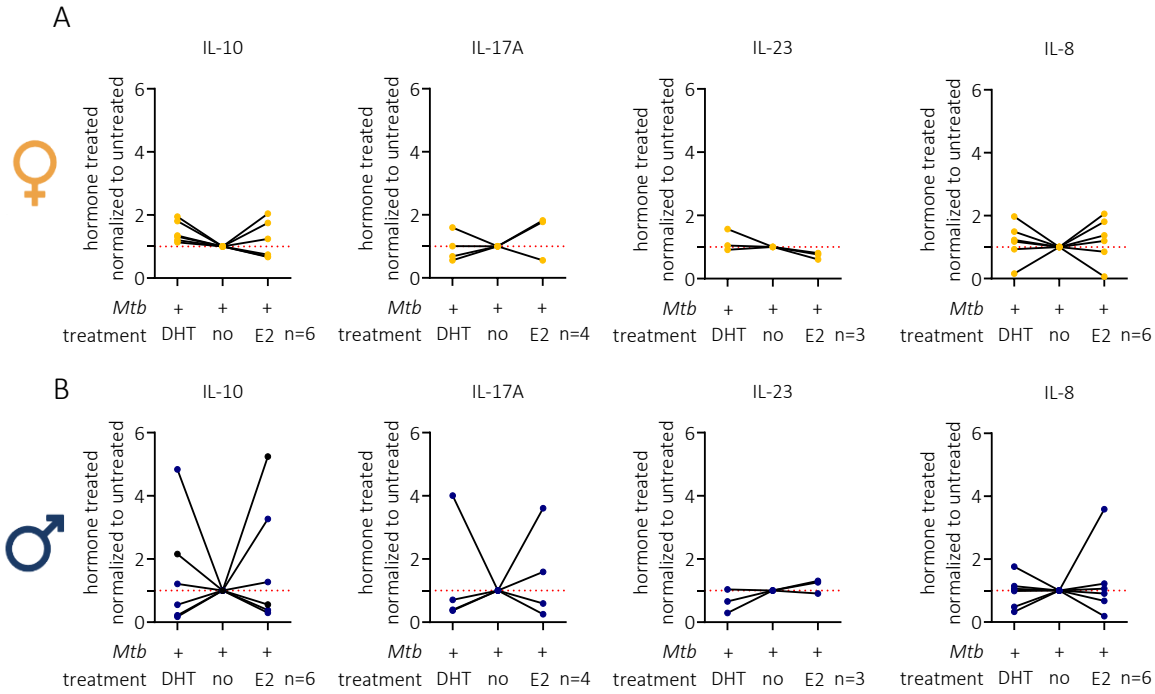

Figure 25 **Sex-specific effects of DHT and E2 on IL-10, IL-17A, IL-23 and IFN-α2 cytokine production in *M. tuberculosis* infected hMdMs**

Cytokine concentrations (IL-10, IL-17A, IL-23, IFN-α2) were measured in supernatants from hMdMs treated with 10 nM DHT or E2 and infected with *M. tuberculosis H37Rv* (MOI=2) collected 24 hpi via LEGENDplex™ analysis. Data are normalized to untreated controls for each donor and separated by sex: (A) female donors (yellow), (B) male donors (blue). Each line represents an individual donor (n=varies per group).

Results: Summary 3

- Both physiological and supraphysiological concentrations of DHT and E2 do not compromise hMdMs viability or metabolic activity, either during differentiation or after *M. tuberculosis* infection, as confirmed by LDH and MTT assays.
- Treatment with supraphysiological concentrations of DHT and E2 led to a modest increase in the proportion of infected macrophages and bacterial load per cell at 5 dpi but decreased the proportion of massively infected hMdMs, with no consistent sex differences observed.
- DHT reduced the proportion of pro-inflammatory M1-like macrophages and increased M2 polarization, especially among hMdMs infected with *M. tuberculosis* in both sexes, whereas E2's effects were less pronounced and mainly observed in females at 4 hpi however, donor variability limited statistical significance.
- DHT increased production of IL-1β, IL-10, IL-17A, and IL-23 in infected female hMdMs, while in males, DHT boosted IFN-α2 but reduced IL-23; E2 generally enhanced IL-10 and IL-17A in females and IFN-α2 in males. Due to high inter-donor variability, most effects were observed as trends rather than statistically significant differences, underlining the complexity of hormone-mediated immune modulation.

4.4 Transcriptome analysis of hMdMs in naïve and *M. tuberculosis*-infected hMdMs to study sex and hormone specific gene regulations

The previous experiments demonstrated that hMdMs from male and female donors do not differ in their susceptibility to *M. tuberculosis* infection. Over the course of infection, however, there was a notable increase in the proportion of M2-like hMdMs among both the total and infected hMdMs populations, while the proportion of M1-like hMdMs remained stable. Additionally, sex-specific differences in the production of selected cytokines by male and female hMdMs upon *M. tuberculosis* infection were observed. qPCR analyses further revealed that males exhibited a higher TNF-α expression at 20 hpi, while females showed a more pronounced increase in IRG1 expression. To further investigate how biological sex and sex hormones influence the molecular response of hMdMs to *M. tuberculosis* infection, bulk RNA sequencing was performed. Bulk RNA sequencing is a technique that measures the average gene expression levels across a population of cells by extracting RNA from cell cultures of interest and sequencing it using NGS technologies. This approach provides a comprehensive overview of which genes are active and at what levels over the entire population, making it possible to identify differentially expressed genes (DEGs) and pathways between experimental conditions, such as between infected and uninfected cells or between sexes. In our study we analysed gene expression profiles in hMdMs derived from healthy male and female donors who were left uninfected or infected with *M. tuberculosis H37Rv* (MOI = 2) for 20 h, aiming to uncover sex specific transcriptional signatures and pathways that may contribute to differences in susceptibility or immune response. Additionally, both uninfected and infected hMdMs were treated with the sex hormones DHT or estradiol E2 at physiological concentration (10 nM), to investigate the influence of these hormones on gene expression in the context of infection. HMDMs exposed to latex beads were included as a phagocytosis control to distinguish infection driven changes from those related to general phagocytic activity. This approach allows us to directly compare how male and female hMdMs, as well as hormone treated hMdMs, respond at the transcriptomic level to *M. tuberculosis* infection, providing valuable insight into the role of sex and sex hormones as a biological variable in TB pathogenesis.

4.4.1 *M. tuberculosis* infection drives distinct and robust innate immune transcriptional responses in hMdMs

To visualize the effect of *M. tuberculosis* infection on macrophage gene expression, PCA of the 1000 genes with most variable expression was performed (Figure 26 A). Here the first and second principal components (PC1 and PC2), which together explain 75.96 % of the total variance are shown. The plot reveals two clear clusters, uninfected (blue) and infected (red) hMdMs, with no overlapping. PC1 accounts for 66.51 % and reflects transcriptomic differences between uninfected and infected hMdMs. In total 9,930 canonical gene transcripts were differentially expressed between uninfected and infected samples of which 690 genes were downregulated DEGs (q-value < 0.01) in *M. tuberculosis* infected hMdMs compared to uninfected, while 774 DEGs were upregulated (Figure 26 B).

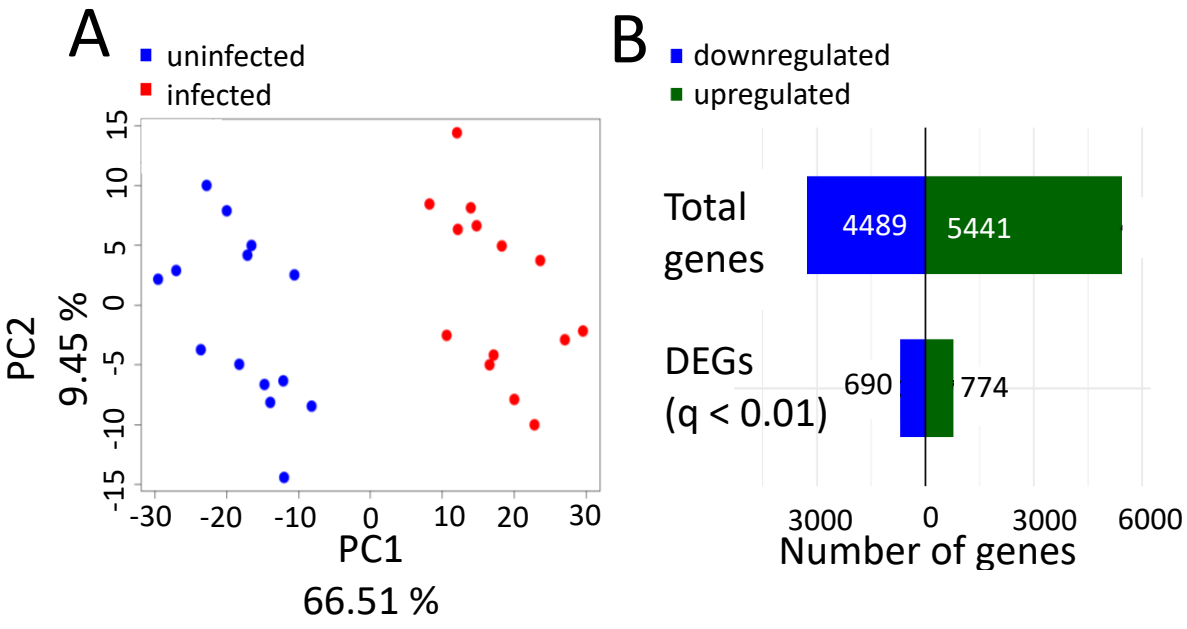

Figure 26 **Principal component analysis and differential gene expression in *M. tuberculosis* infected hMdMs**

Transcriptome analysis of *M. tuberculosis H37Rv* (MOI=2) infected hMdMs after 20 hpi. (A) PCA of transcriptomic profiles of 1,000 most variable genes separates uninfected (blue) and *M. tuberculosis* infected (red) hMdMs samples along PC1 (66.51%). (B) Bar plots show the total number of upregulated (green) and downregulated (blue) canonical gene transcripts, as well as the subset of DEGs (q < 0.01) in upon *M. tuberculosis* infection in hMdMs.

The heatmap shows the hierarchical clustering analysis comparing canonical gene transcripts expression profiles of uninfected and *M. tuberculosis* infected hMdMs. The samples are organized along the horizontal axis, with color-coded annotations indicating

infection status (red for infected, blue for uninfected) and sex (yellow for female, blue for male). The vertical axis shows the 50 transcripts with maximum variability across samples (identified by Ensembl IDs with their respective gene), which is a hypothesis-free selection (Figure 27). Expression levels are represented by a colour gradient from blue (low expression) to red (high expression). The dendrogram at the top of the map reveals that the samples cluster primarily based on infection status, with infected and uninfected samples forming relatively distinct groups, though some overlap exists. Most variable genes show increased expression in infected samples compared to uninfected samples, indicating that the predominant effect of infection on transcriptome is upregulation of canonical gene transcripts expression. PCA and clustering further show that infection status is a stronger driver of transcriptional variation than sex differences in this experimental system, as the primary separation occurs based on infection rather than sex. Several key canonical gene transcripts important for *M. tuberculosis* infection and immunology are among the most variable transcripts. Among the most prominently upregulated genes are key immune mediators including CXCL8 (IL-8), a critical neutrophil chemoattractant essential for inflammatory cell recruitment and IL-1β, a central pro-inflammatory cytokine crucial for granuloma formation. Additional upregulated canonical gene transcripts include CCL2, which encodes a monocyte chemoattractant protein vital for macrophage recruitment, and STAT2, a component of interferon signalling pathways important for antimicrobial responses. Transcriptional regulators and signalling molecules show coordinated activation, including various transcription factors, THBD (thrombomodulin) for coagulation regulation, and PRPF38B (pre-mRNA processing factor) for RNA processing. Additionally, metabolic and cellular remodelling pathways and membrane and adhesion proteins are upregulated underlining the cellular reorganization during infection.

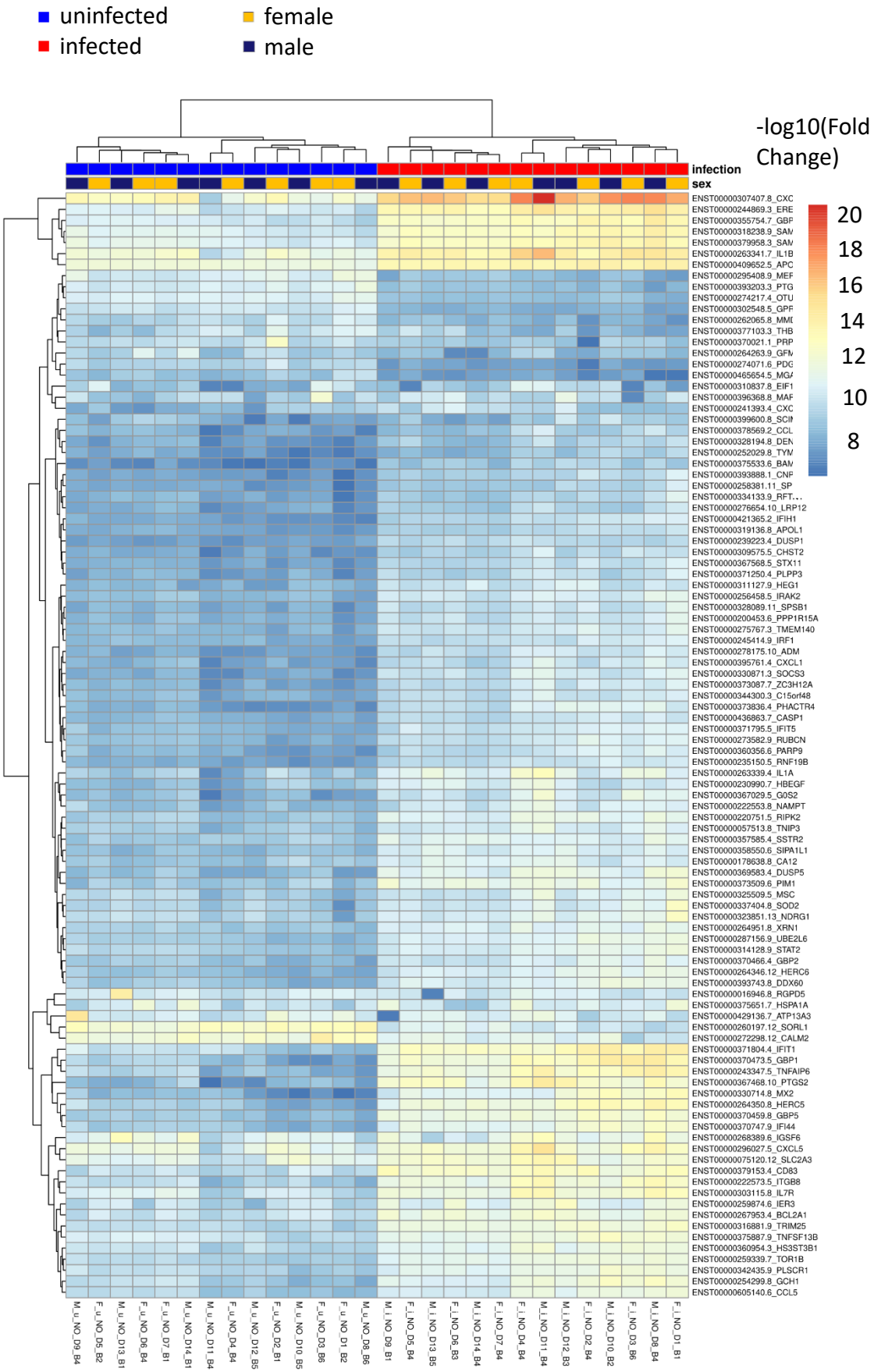

Figure 27 **Heatmap of top 100 most variable genes in naïve hMdMs and *M. tuberculosis* infected hMdMs**

Hierarchical clustering heatmap showing expression levels of the 100 most variable canonical gene transcripts across naïve and *M. tuberculosis H37Rv* infected hMdMs (MOI=2) samples. Samples are classified by infection status (red: infected, blue: uninfected) and donor sex (yellow: female, blue: male). Rows represent the 50 transcripts of maximum variability in expression (using ENSEMBL IDs) and their respective gene. Columns represent individual donors (D1–D14), each included with uninfected (u) and infected (i) samples (n=14 donors (n=7 female, n=7 male), 28 samples). The colour scale indicates gene expression.

After identifying the most variable canonical gene transcripts that capture the greatest expression differences across samples in a hypothesis-free manner, next DEG analysis was performed to pinpoint genes whose expression levels differ significantly between specific experimental conditions, here uninfected to *M. tuberculosis* infected hMdMs. The volcano plot summarizes both the statistical significance and the magnitude of canonical gene transcripts expression changes, with the x-axis representing log2 fold change and the y-axis showing the -log10(q-value) (Figure 28 A). Only genes meeting the significance threshold and with at least a ±1.5 log2 fold change are highlighted. Upon *M. tuberculosis* infection, several canonical gene transcripts known to play crucial roles in the immune response become strongly upregulated. Key upregulated genes (green) in the infected state include classic pro-inflammatory cytokines such as IL-6, IL-1β, and canonical gene transcripts of the TNF pathway, which mediate inflammatory responses and activate other immune cells. Chemokines like CXCL8 (IL-8), CCL2, and CCL5, as well as the colony-stimulating factors CSF2 and CSF3, are also upregulated and play crucial roles in attracting and expanding myeloid cells at the site of infection. The immunometabolism gene ACOD1, which is essential for itaconate production and host defence, is another key gene upregulated during infection. Additionally, the IFN pathway is strongly induced, as shown by the upregulation of several interferon-stimulated canonical gene transcripts (ISGs), including IFIT2, MX1, OASL, and ISG20. Further, a substantial subset of canonical gene transcripts are markedly downregulated upon infection (blue). Among the significantly downregulated genes relevant for TB or macrophage function are SELENOP, SLC46A1, and GPR34 (Figure 28 A). SELENOP supports antioxidant defence and modulates macrophage function which has been shown to influence susceptibility to intracellular pathogens like *M. tuberculosis*. GPR34, a G protein-coupled receptor expressed in immune cells, is involved in modulating immune signalling, which can impact the overall responsiveness of the macrophages during infection with TB.

To further investigate the functional consequences of the observed transcriptional changes in hMdMs following *M. tuberculosis* infection, Gene Ontology (GO) enrichment analysis was performed (Figure 28 B). The bubble dot plot shows the top enriched biological processes (y-axis), with fold enrichment values depicted on the x-axis. The dot size indicates the number of the genes associated with that pathway, while the colour gradient from blue to red reflects the statistical significance (-log10 false discovery rate, FDR). The analysis reveals prominent enrichment for processes related to antiviral and antibacterial immunity. Among the most significant GO terms are “regulation of viral genome replication”, “response to type II interferon”, “regulation of viral life cycle”, and “defence response to virus”, highlighting that genes modulated by *M. tuberculosis* infection in macrophages are heavily implicated in broad antiviral defence mechanisms. The enrichment for “response to type II interferon” is notable, given the central role of IFN-γ in activating macrophage antimicrobial pathways during infection. Processes central to the response against bacterial pathogens are also represented, such as “cellular response to lipopolysaccharide”, “response to molecule of bacterial origin”, and “pattern recognition receptor signalling pathway.” These pathways include processes connected to well-known components of the innate immune system and signalling pathways that are activated when macrophages recognize and respond to mycobacteria. Further, the GO analysis underscores the activation and regulation of innate immunity, with enriched pathways like “leukocyte proliferation”, “activation of innate immune response”, “regulation of innate immune response”, and “innate immune response-activating signalling pathway.” These categories include biological processes related to the increase in immune cell numbers, attraction of immune cells, and enhanced activity of defence mechanisms as reflected in the gene expression data. Other overrepresented pathways include “defence response to virus”, “positive regulation of leukocyte activation”, and “regulation of inflammatory response”. Together, these categories include biological processes related to the initiation of inflammation, regulation of leukocyte function, and adjustment of immune system activity during interaction with the pathogen.

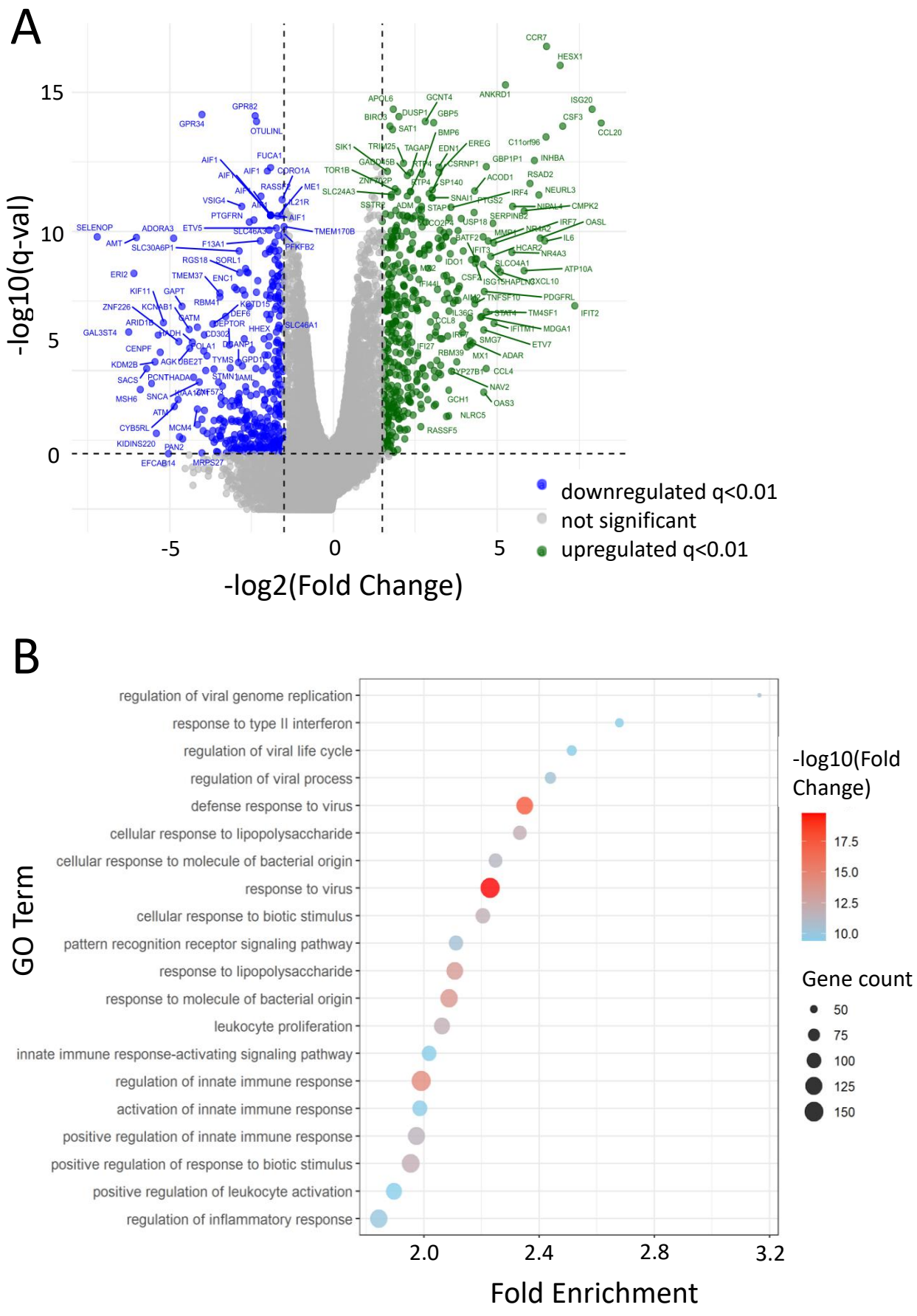

Figure 28 **Changes in canonical gene transcripts expression and biological processes in hMdMs**

upon infection with *M. tuberculosis*

hMdMs were infected with *M. tuberculosis H37Rv* (MOI=2, 7 replicates) for 20 h. (A) Volcano plot displaying DEGs between uninfected and *M. tuberculosis* infected hMdMs. Each point represents a canonical gene transcript; significantly downregulated (blue, q < 0.01) and upregulated (green, q < 0.01) genes are highlighted, with non-significant genes shown in grey. The x-axis shows the log2 fold change, and the y-axis shows -log10(q-value) for significance. (B) Bubble plot of the top 20 enriched GO terms with their respective fold enrichment, canonical gene transcripts count of DEGs in the GO gene set (bubble size), and significance (bubble colour, -log10 fold change).

Overall, these analyses reveal that *M. tuberculosis* infection of hMdMs induces pronounced and coordinated transcriptional changes, clearly distinguishing infected from uninfected cells characterized by widespread upregulation of immune response genes and activation of innate immune processes such as IFN signalling and leukocyte recruitment, while also suppressing key regulatory genes, highlighting a transcriptional landscape dominated by antimicrobial defence and inflammatory pathways.

4.4.2 Sex-specific transcriptional responses to *M. tuberculosis* infection in hMdMs reveal both shared and distinct gene regulation patterns

Our focus was to investigate the differences between male and female hMdMs upon *M. tuberculosis* infection. To explore potential sex-specific differences in the transcriptional response of hMdMs to *M. tuberculosis* infection, an interaction analysis model was first applied. This linear model included terms for sex, infection status, and their interaction (sex:infection), aiming to identify genes whose expression upon infection differed significantly between males and females. Such interaction models are designed to directly capture sex-dependent infection effects and are increasingly recognized as biologically informative for RNA-seq studies involving multifactorial designs (Method II, Duda et al.,) (160). However, consistent with challenges highlighted in Duda et al., the limited number of donor samples and high donor variability in gene expression resulted in insufficient statistical power to detect significant interaction effects. Due to these limitations, it was decided to analyse male and female samples separately in subsequent analyses. This separate comparison of the sexes was employed to identify sex-specific transcriptional responses to the infection (Method I according to Duda et al.). To visualize the sex-specific effect of *M. tuberculosis* infection on canonical gene transcripts expression, PCA was performed as described above Again, a clear separation along the PC1 (70,51 %) indicated a major shift in transcriptional profile associated with infection (Figure 29 A and B). For

both sexes, the samples within each infection status group relatively tight, and the pattern of variance explained by PC1 and PC2 is comparable (female 79,03 %, male 74,8 %).

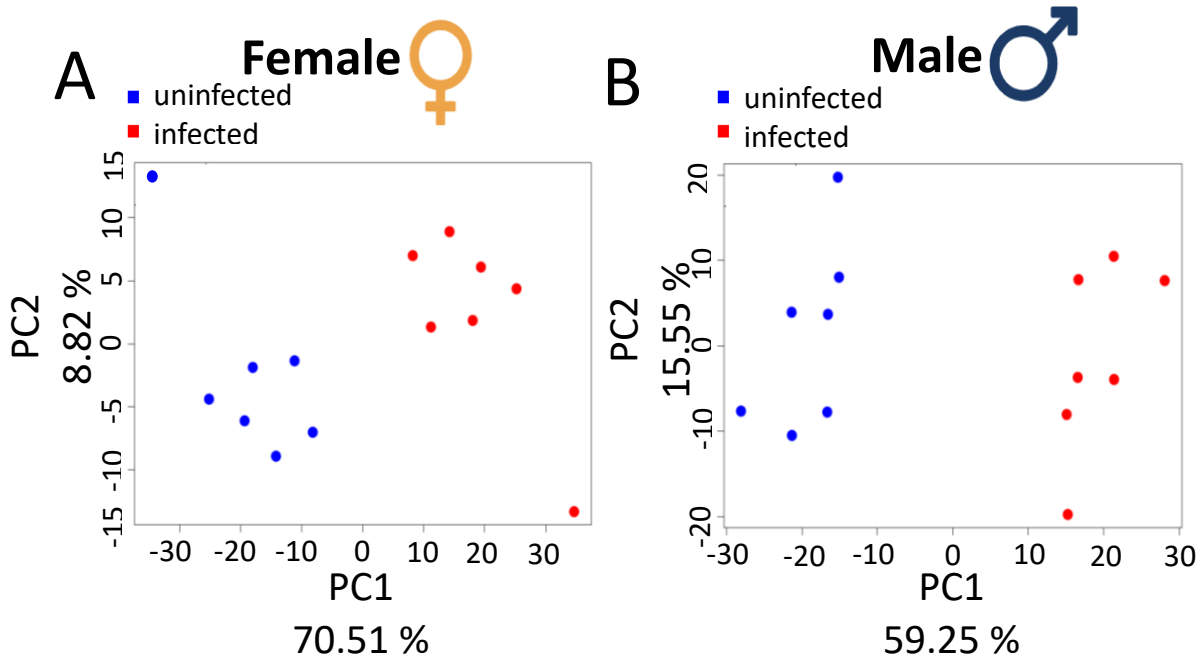

Figure 29 **Principal component analysis of naïve and *M. tuberculosis* infected hMdMs separated by sex**

hMdMs were infected with *M. tuberculosis H37Rv* (MOI=2) for 20 h. RNA-bulk sequencing was performed for transcriptome analysis and samples were separated according to donor sex for further analysis.(A) PCA plot of transcriptomic data from female donor hMdMs, showing separation between uninfected (blue) and *M. tuberculosis* infected (red) samples along PC1 (70.51%) and PC2 (8.82%). (B) PCA plot of male donor hMdMs, with uninfected (blue) and infected (red) samples separated along PC1 (59.25%) and PC2 (15.55%). Each point represents an individual donor sample (n=7/sex).

In total there were 10028 canonical gene transcripts that are differentially expressed in male hMdMs upon infection and 7473 in female (Figure 30 A female, B male). Of those 936 were classified as DEGs regulated in male (385 down, 478 up), whereas there have been 898 DEGs in female (548 up, 350 down)(q-val < 0.01). While the overall response, like robust upregulation of immune and IFN pathway canonical gene transcripts and downregulation of certain metabolic or homeostatic canonical gene transcripts is similar between the sexes, direct comparison may reveal differences in the identity and function of DEGs. The Venn diagram illustrates the overlap and exclusivity of DEGs in response to *M. tuberculosis* infection in hMdMs from female and male donors (Figure 29 C). The yellow circle on the left represents DEGs identified exclusively in female hMdMs (354 genes). The blue circle on the right represents DEGs identified exclusively in male hMdMs (319 genes).

The overlapping region in purple denotes DEGs that are shared between both sexes (544 genes). This visualization shows that while a substantial number of canonical gene transcripts are differentially regulated by infection in both male and female hMdMs, there are also considerable sets of DEGs uniquely found in either males or females.

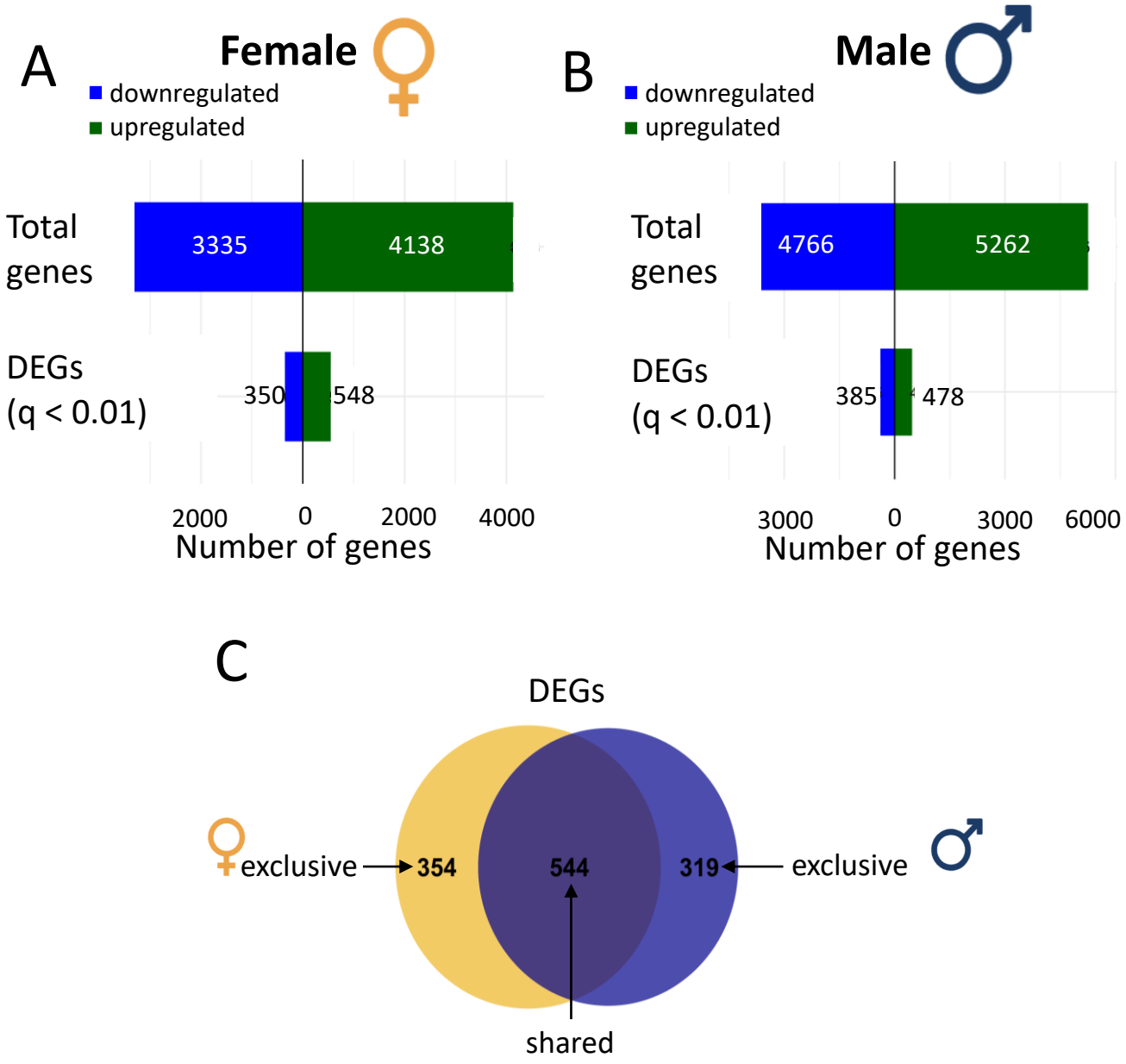

Figure 30 **Sex-specific and shared differential gene expression in hMdMs upon *M. tuberculosis* infection**

hMdMs were infected with *M. tuberculosis H37Rv* (MOI=2) for 20 h. RNA-bulk sequencing was performed for transcriptome analysis and samples were separated according to donor sex for further analysis. Bar plots show the total number of upregulated (green) and downregulated (blue) genes, as well as DEGs (q < 0.01), in female (A) and male (B) hMdMs following infection with *M. tuberculosis H37 Rv* (MOI=2, 20 h). (C) Venn diagram illustrating overlap of DEGs between female (yellow) and male (blue) hMdMs, with numbers of exclusive and shared genes shown (n=7/sex).

Volcano plot analysis of female only (Figure 31 A) and male only (Figure 31 B) DEGs (q-val < 0.05) revealed distinct sex-specific expression patterns in *M. tuberculosis* infected hMdMs. Female exclusive canonical gene transcripts showed predominant upregulation of Type I IFN stimulated genes (IFI16, IFI27, IFI44, IFITM2/3/10, MX2), RNA sensors (ADAR, DHX58, IFIH1), and IFN regulatory factors (IRF1, IRF2, IRF9). Chemokine expression included neutrophil-recruiting factors (CXCL1-3, CXCL9) and T-cell costimulatory molecules (CD40, CD69, CD80, CD274). Additional female-specific canonical gene transcripts encompassed Class I MHC molecules (HLA-B, HLA-C, HLA-E), PRRs (TLR3, TLR4, IRAK2), and antimicrobial genes (CYP27B1, LAMP3, G3BP1). Male-exclusive canonical gene transcripts demonstrated upregulation of JAK-STAT signalling components (JAK2, STAT1, STAT2, STAT3), classical cytokines (IL-10, IL-12B, IL-36G), and distinct chemokine profiles (CCL1, CCL3, CCL5, CCL22). Male-specific expression included T-cell markers (CD4, CD52), antigen presentation machinery (HLA-A, HLA-DMB), and lipopeptide recognition receptors (TLR6).

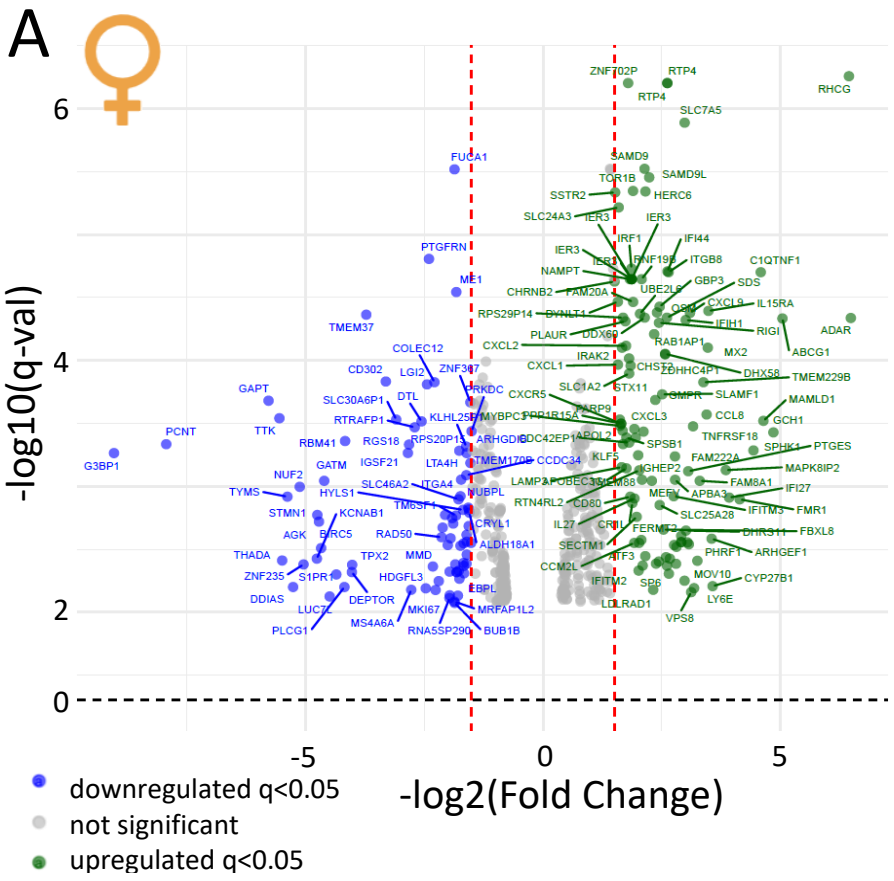
A
-log10(q-val)
-log2(Fold Change)
downregulated q<0.05
not significant
upregulated q<0.05

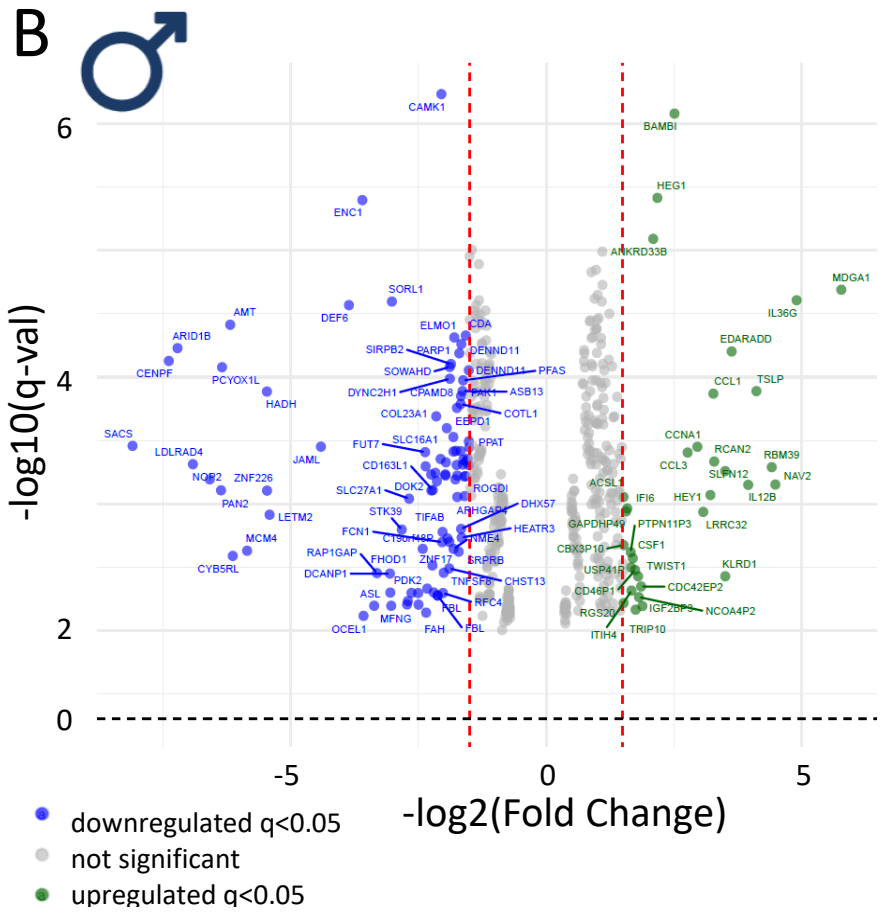
B
-log10(q-val)
-log2(Fold Change)
downregulated q<0.05
not significant
upregulated q<0.05

Figure 31 **Sex-exclusive differentially expressed genes in *M. tuberculosis* infected hMdMs**

hMdMs were infected with *M. tuberculosis H37Rv* (MOI=2) for 20 h. RNA-bulk sequencing was performed for transcriptome analysis and samples were separated according to donor sex for further analysis. Volcano plots of DEGs uniquely regulated in hMdMs from female donors (A) and male donors (B). Significantly upregulated (green, $q < 0.05$) and downregulated (blue, $q < 0.05$) exclusive DEGs are labelled, with log2(fold change) on the x-axis and -log10(q-value) on the y-axis. Red dashed lines indicate the fold change threshold of ±1 (corresponding to fold change of 2) additionally used for DEG selection.

To systematically characterize the functional significance of these sex-specific expression patterns, GO enrichment analysis on the DEGs sets was performed. Notable distinctions emerge between the female and male GO profiles. In the female exclusively DEG set, there is a pronounced enrichment for biological processes involving "T cell activation", "positive regulation of interferon-gamma production", and specific pathways governing lymphocyte proliferation and differentiation (Figure 32 A). This suggests that in females, the sex-specific transcriptional response may more strongly favour pathways enhancing T cell-mediated immunity and interferon signalling. Conversely, the male exclusively DEG enrichment highlights processes such as "cellular response to lipopolysaccharide", "cellular response to molecule of bacterial origin", and broader innate immune activation pathways including heightened responses to bacterial patterns and TLR signalling (Figure 32 B). The male specific profile appears to be more weighted toward initial innate immune sensing and inflammation, perhaps reflecting differences in early pathogen recognition and response cascades between sexes. Despite the differences in the GO enrichment analysis between the sexes, significant DEGs are predominantly enriched in both sexes in processes related to the regulation and activation of immune signalling pathways. Notably, pathways such as "positive regulation of leukocyte activation", "positive regulation of immune effector process", and "positive regulation of cytokine production" appear on both sides, highlighting a conserved upregulation of genes driving leukocyte function and immune effector activity in both sexes.

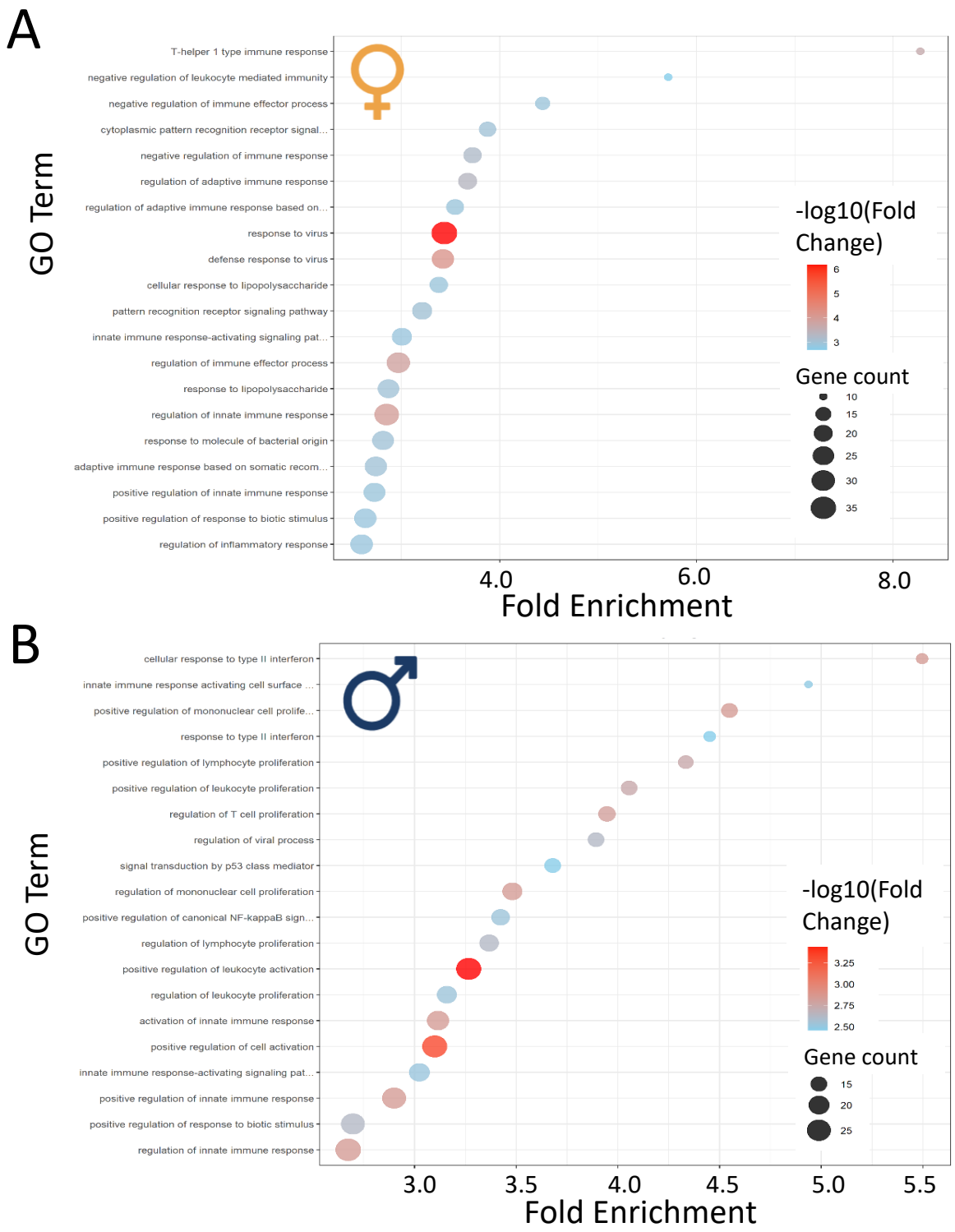

Figure 32 **Sex-specific enriched biological processes of exclusively DEGs in hMdMs infected with *M. tuberculosis***

hMdMs were infected with *M. tuberculosis H37Rv* (MOI=2) for 20 h. RNA-bulk sequencing was performed for transcriptome analysis and samples were separated according to donor sex for

further analysis. Bubble plot showing the top 20 GO terms enriched among DEGs exclusively regulated in infected female (A) and male (B) donor hMdMs. GO terms are ordered by fold enrichment (x-axis), with bubble size reflecting the number of genes and colour indicating significance (-log10 fold change) (n=7/sex).

Results Summary 4

- Naïve and infected hMdMs from male and female donors show largely similar global canonical gene transcripts expression profiles, with only very few canonical gene transcripts (mostly Y-chromosome linked) significantly differing between sexes.
- *M. tuberculosis* infection induces pronounced and widespread transcriptional changes in hMdMs, with DEGs highlighting strong activation of immune, inflammatory, and IFN related pathways.
- PCA and hierarchical clustering of most variable canonical gene transcripts reveal that infection status is the main factor separating samples on transcriptomic level, outweighing sex-related differences.
- Uniquely regulated DEGs in male (354 genes) or female (319 genes) hMdMs indicate distinct molecular mechanisms and immune adaptations between sexes.
- Female-specific DEGs are enriched in pathways related to stronger antiviral and pro-inflammatory responses, such as interferon signalling and leukocyte activation, whereas male-specific DEGs show enrichment in metabolic and immunomodulatory pathways, suggesting different modes of immune regulation between sexes.

4.5 Androgen and estrogen differentially modulate transcriptomes in naïve and *M. tuberculosis* infected hMdMs

First, RNA sequencing data from male and female hMdMs were analysed to identify sex-specific transcriptional responses to *M. tuberculosis* infection. Subsequently, the impact of sex hormones on these responses was investigated to further elucidate their modulatory roles. Therefore, hMdMs were exposed to either DHT or E2 to investigate how androgens and estrogens modulate gene expression and infection responses. This allows for a comparative evaluation of the combined influence of sex, infection, and hormonal environment on the macrophage transcriptome.

4.5.1 DHT and E2-specific effects on the transcriptome of uninfected hMdMs

To first assess the direct impact of DHT and E2 sex hormone treatments on the baseline state, canonical gene transcripts expression profiles of naïve, uninfected hMdMs were compared between untreated controls and cells treated with either DHT or E2. This comparison provides insight into how androgens and estrogens modulate the macrophage transcriptome independently of infection. PCA was performed to assess the effects of DHT and E2 treatments on the transcriptional profiles (Figure 33 A, B). The dispersion of data points reflecting individual donors and the absence of clearly separated clusters suggest that neither DHT nor E2 lead to pronounced differences in canonical gene transcripts expression within these experimental conditions.

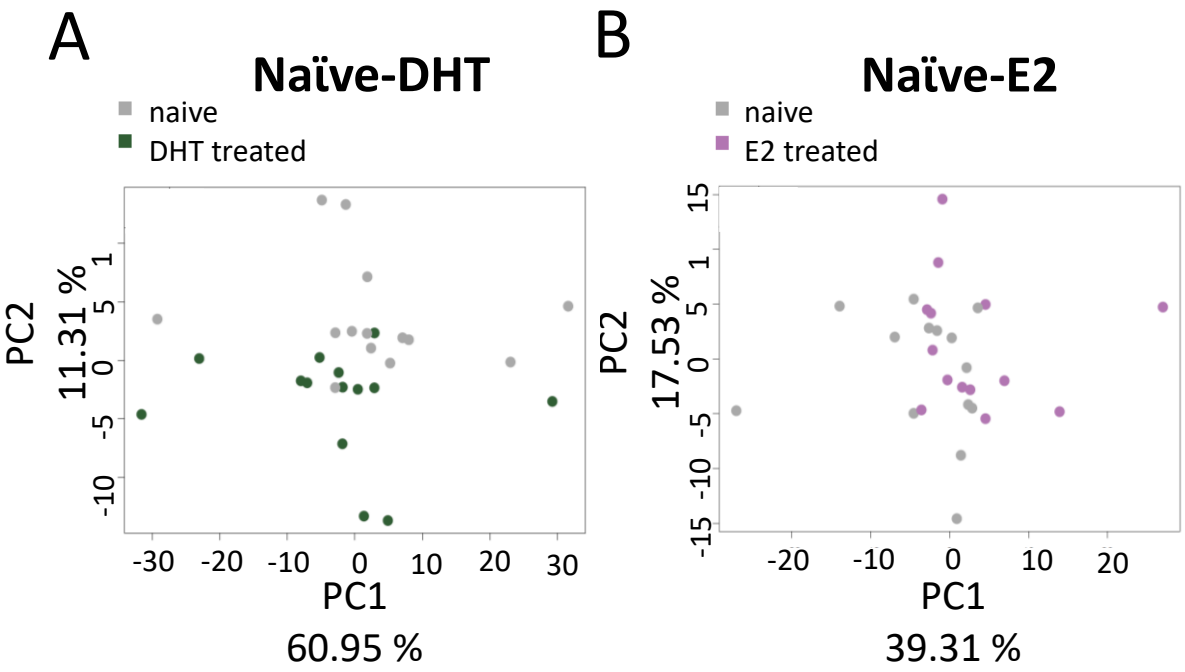

Figure 33 **Principal component analysis of naïve and DHT or E2 treated hMdMs**

hMdMs were differentiated under constant DHT or E2 (10 nM) treatment. RNA-bulk sequencing was performed for transcriptome analysis comparing naïve and DHT or E2 treated hMdMs. (A) PCA plot of transcriptomic data showing infected samples in grey and infected + DHT treated samples in green. Samples separated along PC1 (60.95 %) and PC2 (11.31 %). (B) PCA plot of transcriptomic data showing infected samples in grey and infected + E2 treated samples in purple. Samples separated along PC1 (39.31 %) and PC2 (17.53 %). Each point represents an individual donor sample (n=7/treatment).

DEG analysis identified significantly regulated genes (q-val < 0.05, log2 fold change > 1) between hormone treated and untreated conditions (Figure 34 A, B). At first glance, E2 exerted a more pronounced effect, reflected by a greater number of DEGs, particularly upregulated ones, whereas DHT treatment had minimal impact, primarily causing downregulation of only a few genes (Figure 34 C). HBEGF encodes a growth factor promoting cell proliferation and repair, while TRIM73 belongs to a protein family involved in regulation and immune responses (161, 162). PPFIA1 functions as a scaffolding protein for cell adhesion and cytoskeletal organization, and GOLGA4 is essential for Golgi apparatus function and protein trafficking (163, 164). Most notably, IL1RAP encodes a component of the interleukin-1 receptor complex involved in inflammatory signalling (165). The coordinated suppression of these genes suggests DHT broadly influences cellular processes including growth signalling, structural organization, protein trafficking, and inflammatory responses. In contrast, E2 treatment induces predominantly upregulation across the transcriptome, with relatively few canonical gene transcripts showing significant

downregulation (Figure 34 D). The barplot shows upregulated canonical gene transcripts for genes including KDM1A, a histone demethylase involved in epigenetic regulation; CIRBP, a cold-inducible RNA-binding protein; and multiple canonical gene transcripts for genes such as DENND1A, IFT172, and VPS8 involved in cellular processes such as membrane trafficking and endocytosis (DENND1A), cilia assembly and intraflagellar transport essential for cell signalling and development (IFT172), and endosomal fusion and integrin trafficking important for cell adhesion and migration (VPS8) (166-169). Notable upregulated canonical gene transcripts also include cell cycle regulators like KIF15 and PAK5, histone variants (H3C1, H3C4, H2AC15, H2AC14), and metabolic enzymes such as MT1L and FES. In contrast, only a small subset of canonical gene transcripts was downregulated, including CCL1, a chemokine involved in immune cell recruitment; SERPINB2, a serine protease inhibitor; CXCL11, a chemokine involved in T-cell activation; MMP12, a matrix metalloproteinase involved in tissue remodelling; and ATF7IP2, a transcriptional repressor (170-173).

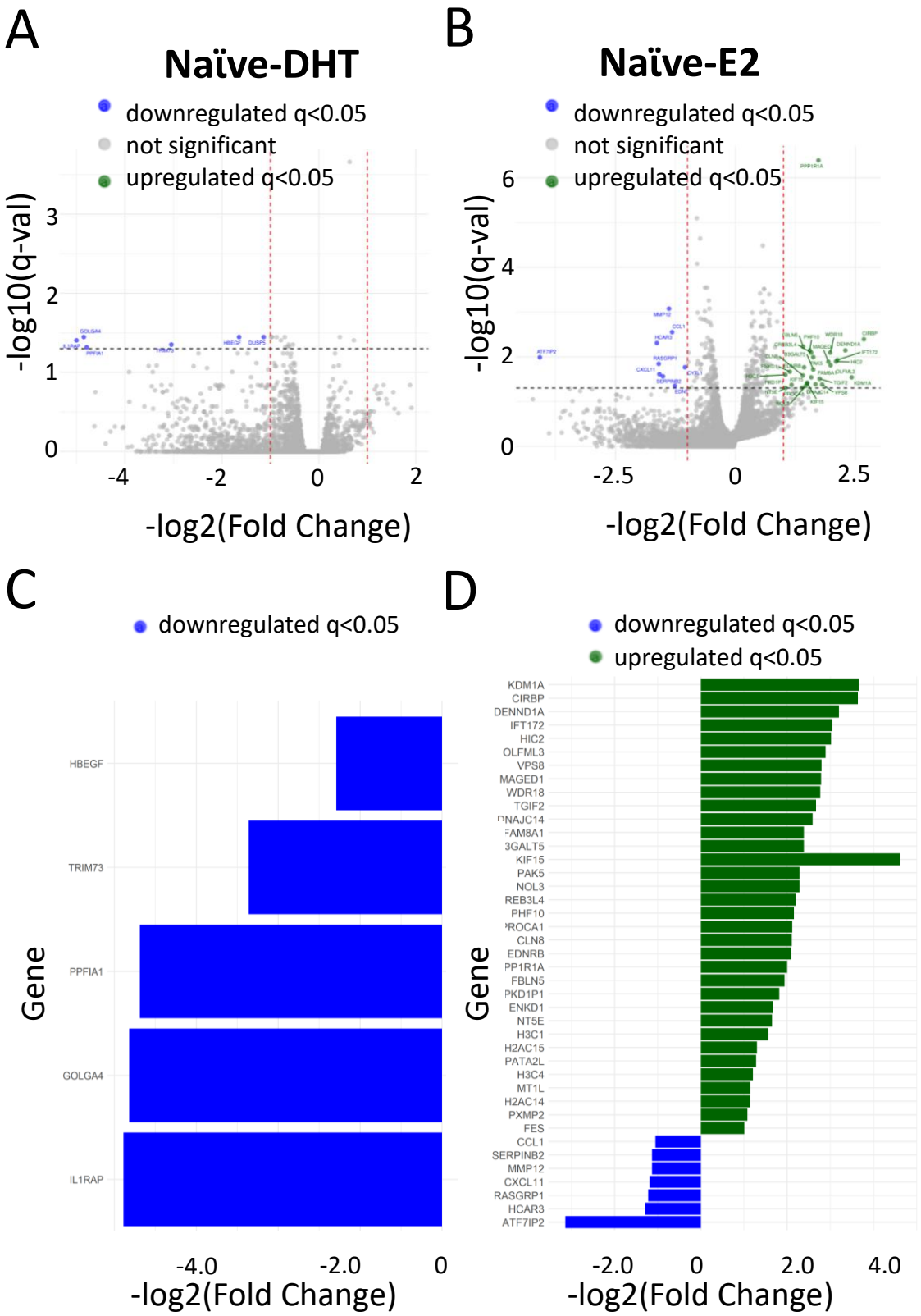

Figure 34 **Differential gene expression of DHT or E2 treated naïve hMdMs**

hMdMs were differentiated under constant DHT or E2 (10 nM) treatment. RNA-bulk sequencing was performed for transcriptome analysis. Volcano plot showing DEGs hMdMs differentiated under 10 nM DHT (A) or 10 nM E2 (B) treatment compared to naïve hMdMs. Downregulated genes (blue, q < 0.05), upregulated canonical gene transcripts (green, q < 0.05), and non-significant

canonical gene transcripts (grey) are depicted, with log2 fold change and -log10(q-value) on the axes. Bar plot displaying log2 fold change values (x-axes) for the DEGs following DHT treatment (C) and E2 treatment (D). Gene names are depicted on the y-axes (n=7/treatment).

These findings demonstrate that DHT and E2 exert distinct transcriptional effects on resting hMdMs, with DHT selectively suppressing key inflammatory and cellular organization pathways while E2 broadly activates metabolic, proliferative, and epigenetic programs, establishing hormone-specific baseline states that may influence subsequent immune responses.

4.5.2 DHT and E2-specific effects on the transcriptome of *M. tuberculosis*-infected hMdMs

To further investigate how the sex hormones DHT and E2 influence the hMdMs response to *M. tuberculosis* infection, analyses were conducted comparing untreated *M. tuberculosis* infected hMdMs with DHT and E treated *M. tuberculosis* infected hMdMs. This approach allows evaluation of the combined effects of infection and hormone exposure on canonical gene transcripts regulation. PCA was performed to examine the effects of DHT and E2 treatments on the transcriptional profiles. In both the DHT (Figure 35 A) and E2 (Figure 35 B) PCA plots, each point represents an individual *M. tuberculosis*-infected sample, either treated or untreated with the respective sex hormone, plotted by their position along the first two principal components (PC1 and PC2). DHT-treated samples cluster slightly distinct from the untreated control samples along the horizontal (PC1) axis, forming a separation with only a few overlaps. The E2-treated and untreated samples show some dispersion from each other, yet the two groups largely overlap and do not form separate clusters. In contrast to naïve cells, where DHT had minimal impact (Figure 33).

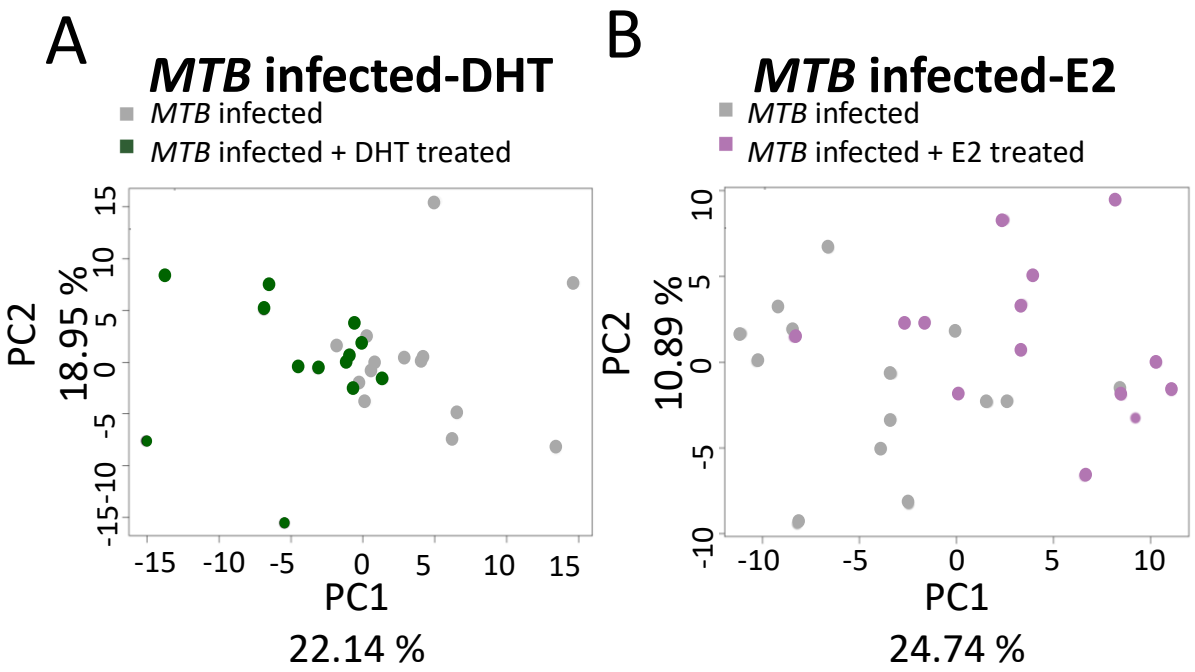

Figure 35 **Principal component analysis of DHT or E2 treated *M. tuberculosis* infected hMdMs**

hMdMs were differentiated under constant DHT or E2 (10 nM) treatment and infected with *M. tuberculosis H37Rv* (MOI=2) for 20 h. RNA-bulk sequencing was performed for transcriptome analysis. (A) PCA plot of transcriptomic data showing infected samples in grey and infected + DHT treated samples in green. Samples separated along PC1 (22.14 %) and PC2 (18.95 %). (B) PCA plot of transcriptomic data showing infected samples in grey and infected + E2 treated samples in purple. Samples separated along PC1 (22.14 %) and PC2 (18.95 %). Each point represents an individual donor sample (n=7/treatment).

Both DHT and E2 induced significant up- and downregulation of canonical gene transcripts in *M. tuberculosis*-infected hMdMs, with E2 consistently producing a greater number of DEGs and more pronounced effects (Figure 36 A, B). Upon DHT treatment in total six DEGs were significantly (q-val <0.05, log2 fold change >1) up- and 15 were downregulated (Figure 36 C). Among the DEGs significantly downregulated are MMP1, a matrix metalloproteinase involved in tissue remodelling and granuloma formation; CSF2, a key cytokine for macrophage activation and survival; LIF, leukemia inhibitory factor involved in inflammatory responses; and DLL4, a notch signalling ligand important for immune cell differentiation and several genes involved in cellular signalling and metabolism (173-176). Upon E2 treatment 12 DEGs were significantly up- and 25 were downregulated (Figure 36 D). Upregulated genes include KIDINS220, NEB, EPHAS, GSG1, ZNF235, PTPDC1, ORC1L3, NPEPPS1, LAMB1TS, DEPDC1, and SGO1, which are involved in cellular signalling,

cytoskeletal organization, and cell cycle regulation. Among the downregulated genes in E2 treated *M. tuberculosis* infected hMdMs are several key inflammatory mediators like TNFRSF18 important for immune regulation by enhancing T cell activation and proliferation, CSF2 which is essential for macrophage activation, CCL1 a chemokine for immune cell recruitment, and TARP a T-cell receptor-associated protein (177, 178) Other notable downregulated genes include IL-23A, the interleukin-23 subunit involved in Th17 responses, genes involved in metabolism (CYB5B, ANGPTL6, ABCG1), cell cycle control (CCNE1), protein degradation (ZYG11A), transcriptional regulation (MED25), and cellular signalling pathways (DOCK7, AKT1S1, ITPRID2) (156).

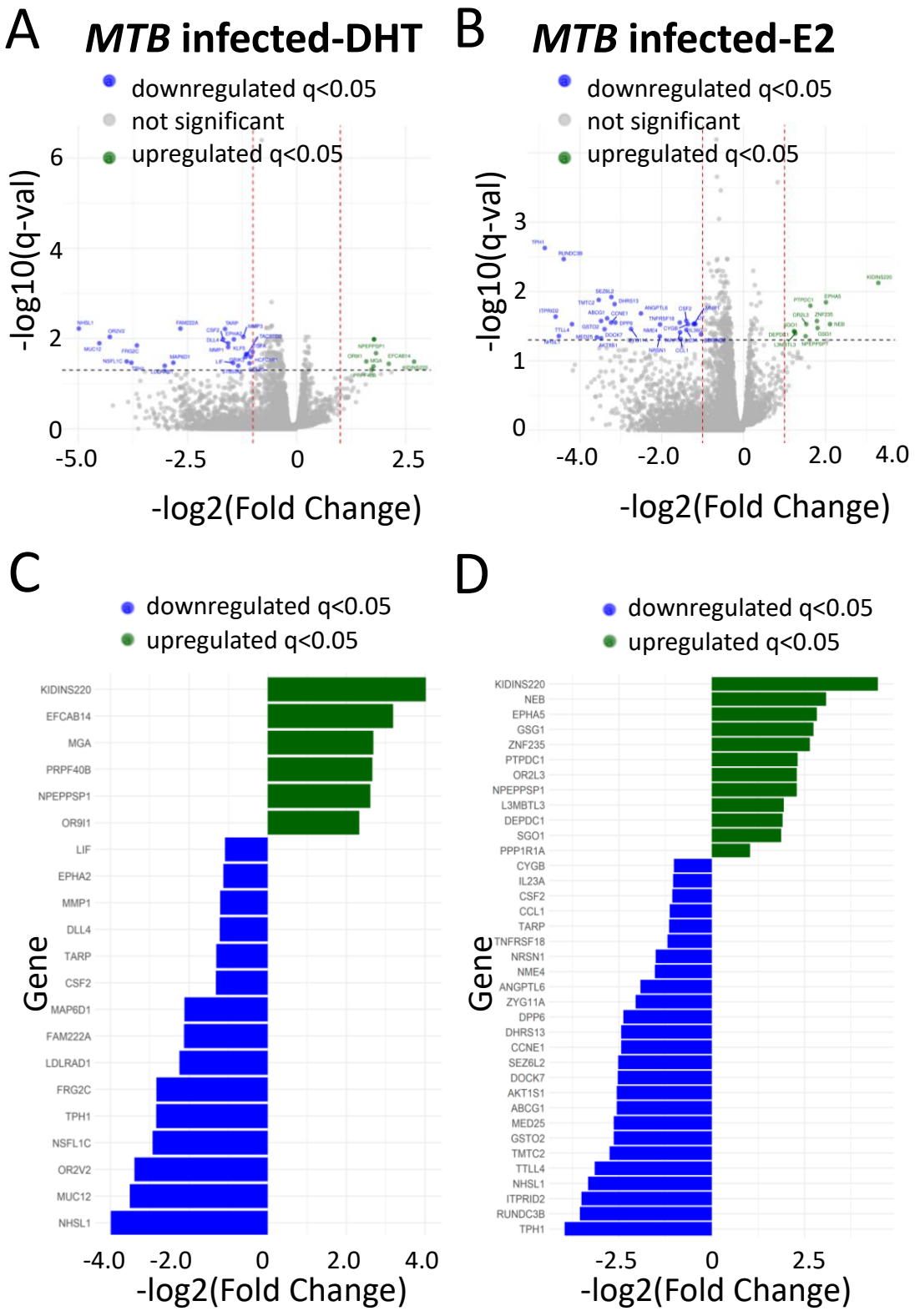

Figure 36 **Differential gene expression of DHT or E2 treated *M. tuberculosis* infected hMdMs**

hMdMs were differentiated under constant DHT or E2 (10 nM) treatment and infected with *M. tuberculosis H37Rv* (MOI=2) for 20 h. RNA-bulk sequencing was performed for transcriptome analysis. Volcano plot showing DEGs of infected hMdMs differentiated under 10 nM DHT (A) or 10

nM E2 (B) treatment compared to naïve hMdMs. Downregulated genes (blue, $q < 0.05$), upregulated genes (green, $q < 0.05$), and non-significant genes (grey) are depicted, with log2 fold change and -log10(q-value) on the axes. Bar plot displaying log2 fold change values (x-axes) for the DEGs following DHT treatment (C) and E2 treatment (D). Gene names are depicted on the y-axes (n=7/treatment).

These results demonstrate that both DHT and E2 treatments significantly alter the transcriptional response of hMdMs to *M. tuberculosis* infection, with DHT predominantly suppressing immune activation and inflammatory pathways while E2 exhibits a more complex pattern of selectively downregulating key immune mediators and T-cell regulatory factors while upregulating cellular structural and metabolic genes.

Results: Summary 5

In naïve hMdMs

- DHT treatment selectively downregulates canonical gene transcripts involved in inflammation, cellular organization, and protein trafficking. Specifically, it suppresses genes related to growth signalling (e.g., HBEGF), immune regulation (e.g., TRIM73), cytoskeletal architecture (e.g., PPFIA1), protein trafficking (e.g., GOLGA4), and inflammatory signalling (e.g., IL1RAP).
- E2 treatment broadly upregulates canonical gene transcripts associated with metabolism, proliferation, epigenetic regulation, and cell cycle. Examples include epigenetic modification genes (e.g., KDM1A), cell cycle/proliferation genes (e.g., KIF15, PAK5), and RNA-binding/regulatory genes (e.g., CIRBP, histone variants), with only a few immune or tissue remodelling genes being downregulated.

In *M. tuberculosis* infected hMdMs

- DHT treatment during infection significantly downregulates canonical gene transcripts crucial for macrophage activation and tissue remodelling, including MMP1, CSF2, LIF, and DLL4, suggesting a dampening of inflammatory and immune responses.
- E2 treatment during infection both downregulates important inflammatory and immune regulatory canonical gene transcripts (e.g., TNFRSF18, CSF2, CCL1, IL-23A) and upregulates canonical gene transcripts related to cytoskeletal organization, cell cycle, and metabolism, indicating a nuanced remodelling of infected macrophages' transcriptional programs.

5 Discussion

Tuberculosis (TB) infection remains a significant global health threat, despite advances in diagnostics and treatment. The ongoing high global burden of TB underscores the urgent need for innovative strategies to improve disease management. Interdisciplinary research is increasingly enhancing our understanding of individualized therapeutic approaches, paving the way for patient tailored interventions that may optimize patient outcomes and address the diverse needs of affected populations. Among the many factors that influence the course of TB, male sex is recognized by the WHO as an independent risk factor (2). Globally, the reported male-to-female ratio of TB cases is approximately 2:1, with even higher disparities observed in certain regions (2, 71). While sociocultural and behavioural factors, such as healthcare access, risk behaviours, and occupational exposure partly account for this difference, accumulating evidence suggests that biological determinants also play a critical role (71, 179-181). In particular, hormonal influences and genetic differences, including functional impact of immune genes on the X and Y chromosomes, contribute to sex-specific variations in immune responses and disease progression (95). As a result, the importance of sex as a modulator of infectious and immunological diseases is gaining increasing attention in research and the development of individualized therapeutic approaches.

As the primary host cell for *M. tuberculosis*, macrophages play a central role in both controlling and shaping the immune response to TB. However, the molecular mechanisms driving sex differences in macrophage-*M. tuberculosis* interactions remain poorly characterized (71). This study investigates how biological sex and sex hormones shape macrophage functional states during *M. tuberculosis* infection, with the goal of identifying pathways that in a long-term perspective may result in sex-tailored therapeutic strategies.

5.1 Advancing High-Content screening (HCS) for *M. tuberculosis* infected hMdMs

HCS is an automated imaging technology that enables quantitative analysis of diverse cellular features such as morphology, infection rates, and bacterial burden in thousands of cells per assay. Published workflows by Fehling et al. for murine macrophages and Bea et al. for hMdMs infected with *L. mexicana* have adapted this approach for robust phenotypic analysis using a high-throughput 96-well format (144, 147). Building on these

methodologies, the pipeline has been further refined for application to hMdMs infected with *M. tuberculosis*. Traditional staining methods for mycobacteria can be challenging due to the small size of the bacteria, their waxy cell wall, and the potential for background staining or cross-reactivity of the antibodies with cellular debris. The use of genetically modified Mycobacterium strains expressing engineered fluorescence markers prevents false-positive staining, allowing specific differentiation between fluorescent bacteria, cellular debris, or other sources of background fluorescence. To validate the HCS system for *M. tuberculosis* infected hMdMs HCS was compared with conventional CFU analysis demonstrating that HCS is a robust alternative for monitoring infection dynamics, as it revealed similar trends in bacterial fold-increase over time (CFU: ~1.3-fold; HCS: ~1.7-fold from 4 hpi to 5 dpi). These initially modest growths align with findings from Simone Tazoll's doctoral thesis, who showed that *M. tuberculosis* exhibits limited replication within hMdMs during the first 3 dpi, with bacterial load increasing approximately ~4-fold between days 3 and 7, using MOIs of 0.05 and 0.1. Notably, no significant difference was observed at 3 days, whereas the marked bacterial expansion around day 7 reflects the delayed intracellular replication typical of *M. tuberculosis* in hMdMs (182). This comparison further supports the robustness and reliability of HCS in capturing the dynamic intracellular growth phases of *M. tuberculosis*. However, absolute infection values between the two methods are not directly comparable, mainly because CFU assays quantify bacteria from the entire well, while HCS covers only 15 selected imaging fields. Moreover, a central limitation of the HCS method in detecting bacteria is its restricted ability to reliably identify individual bacteria within highly infected cells. Mycobacteria tend to form aggregates which complicates automated single-bacterium detection. This problem has been discussed by Ayla et al who noted the challenge of resolving individual mycobacteria within such clusters (183). Consequently, the HCS system may detect bacterial aggregates as single events or underestimate the actual bacterial count. To account for this limitation, hMdMs containing more than three *M. tuberculosis* bacilli were classified as "massively infected" and quantified separately.

Interestingly, there was no increase in the overall proportion of *M. tuberculosis*-infected cells during the five-day time course. However, the number of bacteria counted within infected hMdMs and the proportion of massively infected hMdMs rose, indicating

successful intracellular replication. These observations could be explained by efficient bacterial replication within individual host cells without immediate transmission to neighbouring cells. However, it remains speculative whether bacterial spread is truly limited in this way. Infected cells may undergo necrotic or apoptotic death and be lost, affecting bacterial transmission dynamics – a scenario that may differ in vivo, where intracellular replication can lead to cell death, facilitating bacterial spread to adjacent cells and contributing to pathogenesis (25, 35, 184). Another factor that could impair the escape of *M. tuberculosis* from phagosomes and restrict dissemination after host cell death is the absence of the PDIM motif which is essential for both host cell exit and subsequent cell-to-cell transmission (56, 185, 186). PDIM is recognized as an essential mycobacterial virulence factor that effectively masks underlying PAMPs on the bacterial surface, thereby inhibiting host innate immune recognition and facilitating immune evasion during infection(56). For the HCS experiments a genetically modified *M. tuberculosis H37Rv dsRed* was used, which was tested negative for the PDIM motif during the study[1]. Although this study did not investigate the causal relationship, the absence of PDIM may explain the limited spread of *M. tuberculosis* across the cell culture during in vitro infection.

HCS enables detailed analysis of infected primary human macrophages beyond bacterial replication dynamics, such as cell polarization. The remarkable plasticity of macrophages enables them to respond to external stimuli by adopting distinct polarization states, most notably the pro-inflammatory M1 and the anti-inflammatory M2 phenotypes, which play a critical role in determining the outcome of infection. Functionally M2-macrophages have increased phagocytosis rates and tissue remodelling function whereas M1 macrophages are associated with microbial and anti-tumoral function (68). In TB, M1-polarized macrophages contribute to host defence by producing reactive nitrogen intermediates (RNI) and pro-inflammatory cytokines (e.g., TNF-α, IL-12), which are critical for controlling intracellular *M. tuberculosis* growth. However, excessive M1 activity can drive immunopathology, leading to tissue necrosis and cavitation (187). Conversely, M2-polarized macrophages promote tissue repair and dampen inflammation but may foster a permissive environment for *M. tuberculosis* persistence by suppressing antimicrobial

[1] During study strain was tested negative for PDIM (Gareth Prosser), re-genome sequencing still to be done

mechanisms (148). Dysregulated polarization, whether skewed toward hyperinflammatory M1 or immunosuppressive M2 phenotypes, can disrupt immune homeostasis, exacerbate TB progression or contributing to comorbidities such as fibrosis or reactivation of latent infection (69).

This study assessed macrophage polarization based on morphological features, which was validated using cell surface markers linked to the morphological phenotype via flow cytometry analysis (144). While naïve hMdMs were of a mixed phenotype, *M. tuberculosis* infection induced polarization towards M2-like phenotype, suggesting a preferential expansion of *M. tuberculosis* within anti-inflammatory macrophage subsets. These findings are in line with previous studies showing that *M. tuberculosis* infection promotes a shift towards the M2 phenotype (148, 188, 189). By inducing M2 polarization, *M. tuberculosis* employs a key immune evasion strategy, as this shift suppresses the bactericidal activity of M1 macrophages, which are essential for controlling infection through their production of reactive oxygen and nitrogen species, including NO (187). In mice, M1 and M2 macrophages show different susceptibilities to *M. tuberculosis* which can be broadly characterized as inhibitive M1 and permissive M2 phenotypes (187, 190, 191). Upon *M. tuberculosis* infection in vivo, the first cells that become infected are AMs, which are known to exhibit a more growth-permissive M2-like phenotype(1, 35). A shift toward M2 polarization is also evident in lung tissues of TB patients with active TB and is a characteristic finding in in vitro models of TB granulomas, where *M. tuberculosis* infection drives a time dependent transition of macrophages from an M1 to an M2 phenotype (148, 192). However, this binary classification of M1 and M2 macrophages in vitro may not fully capture the complex phenotypic spectrum observed in vivo, and differences arising from the extreme plasticity of macrophages are challenging to analyse comprehensively (193). The dichotomous M1/M2 framework, while useful for experimental purposes, oversimplifies the continuous spectrum of macrophage activation states that exist in physiological conditions, where macrophages can exhibit mixed or intermediate phenotypes depending on the local microenvironment and temporal dynamics of infection (148, 188, 189, 194-196).

5.2 Sex-specific differences in *M. tuberculosis* infection dynamics and hMdMs polarization

The main objective of this thesis was to assess the impact of the biological sex on the interaction of *M. tuberculosis* with human macrophages. Having adapted the HCS-analysis pipeline for *M. tuberculosis*-infected hMdMs as described, it was then used to investigate bacterial growth and macrophage polarization in hMdMs derived from healthy male and female donors. Bacterial uptake did not differ between sexes, as reflected by comparable initial infection rates. Moreover, although the proportion of infected hMdMs significantly increased from 4 h to 5 dpi in males but not in females, there were no differences between sexes in the bacterial load per infected cell or in the proportion of heavily infected macrophages. Likewise, macrophage polarization did not differ between the sexes – both male and female macrophages exhibited a shift towards M2 polarization upon *M. tuberculosis* infection. Overall, the data do not indicate a substantial difference in the permissiveness or polarization of male or female macrophages to *M. tuberculosis*.

The analysed data stand in contrast to findings from other studies. For example, sex differences in macrophage infection dynamics have been reported in Leishmania infection, where male-derived macrophages exhibit higher susceptibility and parasite loads compared to those from female donors (197). Furthermore, female human AMs exhibited enhanced killing of ingested *S. pneumoniae*, the bacterial pathogen responsible for pneumococcal pneumonia, a disease in which males experience higher incidence and severity (198). Although epidemiological data show that men have a higher incidence of active TB than women, the cellular basis for sex differences in susceptibility is complex and multifactorial (2, 71). Previous work in mouse models has confirmed the male bias as observed in humans. Male mice of different genetic background exhibit increased susceptibility to *M. tuberculosis* infection. Increased susceptibility is characterized by accelerated disease progression, increased mortality and overt differences in granulomatous lesions in males compared to females (71, 136, 137, 142). Although males showed higher bacterial loads in the lungs than females, these studies did not specifically analyse macrophage-intrinsic differences (137). Studies on sex differences in immune control of *M. tuberculosis* in humans are scarce. In a cohort of 100 healthy individuals, BCG-vaccinated females exhibited higher CD4+/CD8+ T cell ratios and their PBMCs controlled

M. tuberculosis growth more effectively than those from males (199). While this suggests potential sex differences in systemic immune responses, the specific role of macrophages was not directly investigated.

Importantly, macrophages play essential roles beyond bacterial uptake, particularly through their regulatory functions. By cytokine and chemokine production, macrophages shape downstream immune responses and influence the balance between protective immunity and pathological inflammation (58, 148, 200, 201). This raises the question of how macrophages may contribute to the observed sex differences in TB outcomes if not through differences in initial infection susceptibility and killing. These considerations align with growing evidence that disease severity and pathology in TB are often more closely linked to differences in host inflammatory responses rather than bacterial burden alone (28, 202, 203). Macrophages, through their orchestration of innate immune signals, play a crucial role in directing adaptive immunity, potentially shaping the overall course of infection in a sex-dependent manner (37, 148).

5.3 Cytokine profiles reveal divergent inflammatory profiles between the sexes

Macrophages play a central role in the immune response to *M. tuberculosis* infection by producing a range of cytokines and activating antimicrobial pathways. Assessing these secreted mediators and gene expression profiles provides critical insights into infection dependent functional differences in macrophage responses. Given the substantial donor-to-donor variability and the low sample sizes, sometimes with as few as three biological replicates, it is challenging to draw definitive conclusions from these data; however, certain trends can still be observed. TNF-α, IFN-α2, IL-1β, IL-6, IL-8, IL-10, IL-17A and IL-23 were induced upon *M. tuberculosis* infection. The data indicate increased production of TNF in male macrophages in response to *M. tuberculosis* compared to females on cytokine and transcriptional level. TNF is a key proinflammatory cytokine involved in TB that contributes to macrophage activation, recruitment of immune cells to the infection site, and the maintenance of granuloma structure, which plays a critical role in containing *M. tuberculosis*. Although TNF has a crucial protective function in granuloma formation and macrophage activation during TB, excessive or insufficient TNF signalling can be detrimental. Traditionally, TB has been regarded as a consequence of failed immune responses, but recent research highlights that excessive inflammation can also drive

increased TB susceptibility. In zebrafish models' susceptibility to *M. marinum* results not only from insufficient but also from excessive acute inflammatory responses linked to TNF dysregulation (204). Too little TNF impairs granuloma integrity and increases the risk of disseminated and reactivated infection, while excessive TNF may cause tissue damage and pathology (205). Thus, an optimal balance of TNF activity, is essential for effective host defence against *M. tuberculosis* (206). Studies on *M. tuberculosis* as well as other infections have shown that TNF-α production can be differentially regulated between the sexes. Human studies have shown that PBMCs from males produce higher levels of TNF-α upon stimulation compared to those from females (71, 207). Additionally, clinical research involving male TB patients has reported elevated TNF-α concentrations during specific treatment stages relative to females, indicating sex-related differences in inflammatory responses (208). Sex-specific secretion of TNF-α has also been shown with a male predominance in a murine *L. mexicana* infection model (209). These opposing trends underscore the complex influence of sex on immunity, which varies depending on the pathogen and immune context.

In contrast to TNF which tends to be higher in males, IL-23 and IL-17 production were reduced in male compared to female macrophages. This is in line with data from mouse models showing higher levels of both IL17 and IL23 in female compared to male lungs during Mtb infection (142). IL-23 drives protective TH17 responses and is required for the long-term containment of *M. tuberculosis* infection by bridging innate and adaptive immunity (142, 210). Interestingly, estrogen amplifies IL-23-induced IL-17A production through transcriptional upregulation and immune cell sensitization, while testosterone dampens this axis (211). Although these measurements have been done in the absence of sex hormones, one cannot rule out hormone effects on . Higher IFN-α2 secretion in male macrophages during *M. tuberculosis* infection may promote disease by enhancing macrophage necrosis and bacterial replication. Although sex differences in IFN-α2 during TB are not well-studied, increased type I IFN signalling has been linked to sex-biased immune responses in other infections, where females often show stronger IFN-I pathway activation, affecting pathogen control and immune regulation differentially between sexes (117, 212). On transcriptional level, female bias in IRG1 expression was observed in female macrophages. IRG1 is induced via TLR-2, STING, and type I IFN signalling after bacterial

phagocytosis, produces itaconate, which limits bacterial growth and modulates inflammation suggesting that female macrophages may have an enhanced capacity for itaconate mediated immune modulation during TB infection which needs further investigations (213, 214).

5.4 Infection driven transcriptomic signatures in macrophages

While the measurement of individual cytokines provided valuable insights into specific aspects of the immune response, it offered only a limited view of the broader regulatory landscape. To gain a more comprehensive understanding of macrophage activation, the analysis was extended to the transcriptome level. Comprehensive unbiased transcriptome-wide analyses revealed infection as the primary driver of transcriptomic changes. PCA analysis and hierarchical clustering of the most variable canonical gene transcripts revealed that the infection status is the primary factor for clustering. Top 100 most variable gene transcripts were selected based on expression variability across all samples regardless of condition, focusing on gene transcripts with the highest overall variation. This helps identify gene transcripts that show strong expression changes and are likely biologically informative for unsupervised analyses like clustering or visualization. Analysis of the top 100 most variable gene transcripts revealed broad upregulation in infected samples from both sexes, highlighting the activation of key antimicrobial response pathways such as IFN signalling, inflammatory cytokine production, and immune cell activation. Notably, there was a prominent induction of interferon-stimulated genes (ISGs), including members of the IFIT family, MX1, OASL, and ISG20, which reflects strong type I IFN responses. Such responses are fundamental to both antiviral and antimycobacterial defences, however in TB, type I IFN signatures, unlike in viral infections, often correlate with unfavourable outcomes and can modulate cytokine expression and immune responses in a detrimental way in TB (212, 215). Additionally, transcripts of genes involved in key inflammatory pathways (IL-1B, IL-6, and TNF pathways), as well as chemokine ligands like CXCL8 (IL-8), CCL2, and CCL5, are markedly upregulated. These molecules are known to mediate immune cell recruitment and activation in TB infection, reflecting the typical inflammatory response. This is accompanied by increased expression of direct antimicrobial effectors, such as ACOD1 (encoding aconitate decarboxylase responsible for itaconate synthesis=IRG1), complement components, and antimicrobial peptides. Only to mention a few.

DEG analysis (comparative analysis between predefined groups) revealed numerous genes that showed statistically significant changes in expression between uninfected and *M. tuberculosis* infected samples. DEG analysis results were in line with the results from the variable canonical gene transcript expression. Upregulated DEGs include chemokines and cytokines (CXCL8, CCL2, CCL5, CCL20, IL-6) which facilitate immune cell recruitment and systemic activation, ISGs (ISG20, IFIT2, MX1) indicating robust type I IFN responses, antimicrobial effectors such as ACOD1, complement components, and other direct defence factors; genes involved in glycolysis and immunometabolism reprogramming, and transcriptional regulators (STAT1, IRF, NF-κB) coordinating immune gene expression (212-214, 216). Conversely, downregulated DEGs were linked to tissue homeostasis (SELENOP), oxidative metabolism, and cell cycle/growth factor pathways, potentially reflecting a metabolic shift from homeostatic maintenance to active immune defence and reduced cell proliferation. Taken together these results reveal broad upregulation of ISGs (IFIT family, MX1, OASL, ISG20), inflammatory cytokines (IL-1β, IL-6, TNF-α), and chemokines (CXCL8, CCL2, CCL5), alongside antimicrobial effectors (ACOD1/IRG1, complement components, peptides), reflecting robust type I IFN–mediated and pro-inflammatory responses.

GO enrichment highlights both antibacterial (e.g., 'cellular response to lipopolysaccharide,' 'pattern recognition receptor signaling') and surprisingly strong antiviral pathways ('regulation of viral genome replication,' 'defense response to virus'; $-\log_{10}$[FDR] ~15–18). This antiviral signature is driven by ISG20 and type I IFNs. ISG20 is an RNase that degrades viral RNA and is characteristically expressed in M2 macrophages (217), corroborating our HCS finding of an infection-induced M2 shift. While counterintuitive for a bacterial infection, this aligns with evidence that *M. tuberculosis* deliberately triggers type I IFN responses to impair antibacterial immunity (218). Gene expression analysis of active TB patients shows similar activation of type I IFN in the peripheral blood (219, 220),(218)). The IFN system is the first line of defence against microbial infections, also against *M. tuberculosis*. During infection, cells detect PAMPs via PRRs, triggering signalling cascades that activate transcription factors such as IRF3, IRF7, and NF-κB. These factors drive the production of type I IFNs (IFN-α/β), which broadly induce antiviral defences and initiate innate immune responses (55, 217). Upon *M. tuberculosis* infection in human macrophages, a strong type I IFN response suppresses key antibacterial immunity,

exacerbating disease. IFN1 signalling limits protective cytokines (such as IL-1β), promotes immunoregulatory cytokine expression, and may facilitate pathogen persistence and disease progression (212).

GO analysis further revealed significant enrichment of key bacterial recognition pathways, including "cellular response to lipopolysaccharide" and "pattern recognition receptor signaling pathway," highlighting the central role of PAMP detection in initiating host defence against *M. tuberculosis* (55). These pathways activate TLR signalling cascades that drive transcriptional programs producing pro-inflammatory cytokines, chemokines, and type I IFNs essential for effective immune responses. Robust enrichment of innate immunity terms such as "activation of innate immune response" and "regulation of innate immune response" (fold enrichment 2.0-3.2; 50-150 canonical gene transcripts per pathway) demonstrates coordinated upregulation of innate immune activation. Additionally, enrichment of "leukocyte proliferation" and "positive regulation of leukocyte activation" indicates broader immune cell mobilization beyond local macrophage responses, suggesting systemic inflammatory cascades crucial for pathogen containment. These findings align with established literature demonstrating TLR signalling's critical role in *M. tuberculosis* infection and confirm that the pathogen triggers comprehensive innate immune responses across broader immune networks, contributing to bacterial containment and granuloma formation (50, 55).

5.5 Sex-specific transcriptomic signatures indicate divergent immune strategies

In this study particular attention was given to identifying sex-specific signatures at the transcriptomic level. To investigate sex-specific transcriptomic differences in hMdMs following *M. tuberculosis* infection, initially an interaction analysis was performed following the approach described by Duda et al. (160). However, no DEGs were identified in this complex setup, likely due to the high sample sizes required to achieve statistical significance in interaction studies. Consequently, the analysis was focused on examining each sex separately in response to *M. tuberculosis* infection. This approach, which has been used in other studies before (221) , enabled the identification of 334 DEGs shared between female and male samples, along with a number of sex-specific DEGs, 522 unique to females and 493 unique to males (221).

GO enrichment analysis of female-exclusive DEGs revealed a different immune strategy compared to males, characterized by regulatory and antiviral responses rather than inflammation. Overall, male hMdMs exhibited enrichment of innate responses including NF-kb signalling and type II IFNs. This analysis revealed a pronounced inflammatory response to *M. tuberculosis* infection. Alongside this, a strong type I IFN response was observed, characterized by 11 DEGs and significant enrichment of pathways associated with type I IFN signalling. ("response to virus" fold enrichment ~4.5). From an evolutionary standpoint, females may have developed stronger IFN responses as a protective mechanism to enhance antiviral and antibacterial immunity, including against *M. tuberculosis* infection. This heightened IFN response, partly linked to X chromosome-encoded genes such as TLR7 and influenced by sex hormones, likely provided females with a survival advantage by promoting early pathogen detection and immune activation (81, 95, 222). However, this increased immune responsiveness may come with a trade-off, as stronger type I IFN signalling can also drive immune-mediated pathology, reflecting a balance shaped by pathogen pressure and reproductive fitness in female hosts. Recent work by Kotov et al showed that type I IFNs promote susceptibility to *M. tuberculosis* through increasing the permissiveness of recruited myeloid cells to *M. tuberculosis* growth in mice (37, 223). Although females generally exhibit stronger type I IFN responses that enhance antiviral immunity and vaccine responsiveness, the role of type I IFN in TB is complex (224-226). Elevated type I IFN responses have been linked to pathogen persistence and worsening disease by suppressing protective immunity (212). However, despite stronger IFN signalling, females are less susceptible to active TB, suggesting that factors beyond type I IFN, such as immune regulation, hormones, and genetics, contribute to sex-biased TB outcomes (71, 82, 95). In addition, female gene expression profile suggests a suppression of excessive inflammatory responses that could cause tissue damage, as shown by the enrichment of negative regulatory pathways (GO "negative regulation of leukocyte mediated immunity," "negative regulation of immune effector process," and "negative regulation of immune response") supporting the hypothesis of a more balanced response.

Female gene expression profiles indicate a suppression of excessive inflammation, while maintaining the potential for protective Th1-type immune responses (GO term 'T-helper 1

type immune response,' fold enrichment ~8). Although our system did not include T cells, the observed macrophage gene expression patterns may reflect how macrophages influence T cell activation and the broader immune response. Protective immunity correlates with IFNγ and TNF-α, which promote phagosome maturation and NO production (227). Females typically mount stronger Th1 responses than males, aided by E2-driven Th1 polarization and macrophage activation, while sustaining IL-10 production to limit immunopathology (95). Further, females exhibit strong pathogen detection and balanced immune regulation, responding to bacterial components within a controlled framework (GO "cytoplasmic pattern recognition receptor signaling", "pattern recognition receptor signaling pathway", "regulation of adaptive immune response").

Interestingly, female macrophages upregulate a set of genes that encode for specific transport systems. ABCG1 (log2FC: 6.05) encodes ATP-binding cassette subfamily G member 1, a cholesterol efflux pump that transports cholesterol and phospholipids out of the cell, both of which serve as nutrients for *M. tuberculosis*. This activity likely reduces intracellular cholesterol availability, which may act protectively by limiting the nutrients accessible to intracellular *M. tuberculosis*, thereby contributing to a form of nutritional immunity (228, 229). It has been shown that *M. tuberculosis* activates ABCG1 to regulate the process of foamy macrophage formation. Although *M. tuberculosis* infection initially activates ABCG1 to regulate lipid efflux, subsequent infection-associated can reduce ABCG1 function (230, 231).

Female hMdMs further upregulated the substrate transporters SLC7A5 (LAT1) and SLC30A4 (zinc transporter), likely reflecting enhanced nutrient and metal ion handling, which can play dual roles (232). While these transporters may provide essential amino acids and metal cofactors that both host and bacteria need for their metabolism, they may also contribute to antimicrobial defence by delivering toxic levels of metals like zinc into the phagosome to kill pathogens, a process known as metal poisoning (233).To prevent poisoning by metal ions such as ZN^{2+}, *M. tuberculosis* requires a variety of metal efflux and detoxification systems in order to survive inside their host cell (234). Therefore, this upregulation could represent a complex balancing act between supporting host cell metabolism and actively restricting or poisoning intracellular bacteria.

hMdMs from male donors exhibited enrichment of innate immune pathways including NF-κB signalling, and type II IFNs in line with a strong inflammatory signature characterized by upregulation of pro-inflammatory cytokine genes including IL-12β (log_2FC: 5.24) and IL-36γ (log_2FC: 5.83). IL-12β is critical for protective immunity against *M. tuberculosis* by driving Th1 responses (235). IL-36γ has a dual role. While it promotes macrophage autophagy and inflammatory cytokine production that aid bacterial control, excessive or prolonged IL-36γ-driven inflammation can contribute to tissue damage and pathology (236, 237). This heightened inflammatory response may contribute to effective bacterial clearance but also, if dysregulated, to severe tissue damage and immunopathology. NF-κB is a central regulator of macrophage activation and orchestrates the expression of multiple inflammatory mediators upon *M. tuberculosis* infection, including TNFα, IL-1, and IL-6. This is in line with the results from the qPCR, which also showed a trend toward higher TNFα expression in male-derived hMdMs, supporting the transcriptomic evidence of a heightened NF-κB-driven inflammatory response.

In addition, a robust immune cell activation was indicated (GO "positive regulation of leukocyte activation" fold enrichment ~3.2, "activation of innate immune response" fold enrichment ~3.2). Together with the positive regulation of mononuclear cell and lymphocyte proliferation, this heightened activation could lead to enhanced immune surveillance but also increased inflammation and tissue pathology if not properly controlled. This observation aligns well with the mouse studies from the Schneider lab, where female mice demonstrate better long-term control of *M. tuberculosis* infection, whereas males, especially in the H37Rv model, showed increased inflammation and greater infiltration of innate immune cells such as $CD68^+$ macrophages and $iNOS^+$ cells (136). This inflammatory milieu is compounded by a strong type II IFN response which, while essential for antimycobacterial immunity, can become pathological when excessive (212, 238). The resultant heightened inflammation profile could result in increased cavitation and lung tissue destruction, creating a scenario where host immune responses inflict more damage than the pathogen. Supporting this, the Schneider laboratory reported that male mice developed more extensive lung lesions than females following *M. tuberculosis* H37Rv infection (136). Further infected hMdMs from males expressed higher levels of matrix metalloproteinase-1 (MMP-1) (log_2 fold change 6.87) compared to those from females (log_2

fold change 5.22). MMP-1, a collagen-degrading enzyme pivotal to TB pathogenesis, inducing lung tissue destruction and cavitation (28, 239). In good agreement, clinical studies showed that plasma MMP-8 is significantly higher in males than females with TB, independently of disease severity markers or delayed presentation, indicating a sex-specific inflammatory response rather than an artefact of more advanced disease or later diagnosis (240).

Notably, males express fewer negative immune regulators compared to females, who appear better able to counterbalance inflammation through enhanced expression of inhibitory pathways. This reduced expression of negative regulators in males may diminish their capacity to restrain excessive inflammation, contributing to greater immunopathology. Literature supports that males generally exhibit higher inflammatory responses and impaired counter-regulation, especially with aging, which exacerbates disease severity (81, 95, 241).

The X chromosome contains the highest density of immune-related genes in the human genome, many of which play critical roles in regulating immune responses and susceptibility to autoimmune diseases (95, 242). Interestingly X-linked immune-related genes were found among female DEGs (ARMCX1, TMSB4X) in response to *M. tuberculosis* infection. While some of these genes have immune-related functions, none were found to have documented roles in TB pathogenesis or immune responses. To balance gene expression between males (XY) and females (XX), one X chromosome in females undergoes epigenetic silencing through X-chromosome inactivation (XCI), ensuring dosage compensation. However, XCI is a complex and dynamic process; not all genes on the inactive X are fully silenced, with an estimated 15-30 % escaping inactivation to varying degrees across tissues and individuals. This variability in escape and patterns of XCI skewing contribute to the nuanced differences in gene expression between sexes and complicate the straightforward interpretation of sex differences based solely on gene copy number (95, 104, 243). As expected, Y-chromosomal genes were found to be uniquely expressed in male hMdMs, although none were differentially regulated upon *M. tuberculosis* infection in the dataset. Nevertheless, they could play a role in the infected cell as they are only expressed in the male sex, even if the expression level does not increase upon infection. Still, they are absent in females. Compared to X-linked genes, Y-chromosomal genes are

less extensively studied, but growing evidence suggests that they contribute notably to male immune function and susceptibility to diseases (244). Advances in sequencing technologies have revealed the immunological relevance of Y-linked genes, emphasizing the need for more focused research to elucidate their specific roles in infectious diseases such as TB.

These findings reveal a complex picture of sex-specific hMdM responses to *M. tuberculosis* infection, characterized by distinct transcriptional signatures, immune regulatory pathways, metabolic adaptations, and genetic contributions.

5.6 The impact of sex hormones on *M. tuberculosis*-macrophage interaction

Sex differences in host-pathogen interaction can arise from multiple factors, including genetic and hormonal influences. The fact that the male bias in TB manifests post-puberty strongly implicates that sex hormones influence host-pathogen interactions and disease outcomes. In good agreement, Bini et al showed that castration rendered male mice more resistant to *Mtb* infection (137). Extensive evidence from clinical and experimental studies highlights the significant modulatory role of estrogens, androgens, and their respective receptors in shaping both innate and adaptive immunity, mediating the differences in inflammatory responses, tissue tolerance, and pathogen susceptibility between sexes (95, 122, 245). This underscores the need to consider endocrine regulation when interpreting sex-biased immune responses in infection models.

Therefore, the subsequent analysis focused on how 5α-dihydrotestosterone (DHT) and 17β-estradiol (E2) treatments distinctly modulate gene expression patterns in naïve hMdMs and in *M. tuberculosis* infected hMdMs. HMdMs were treated with physiological to supraphysiological concentrations (10 nM–5 µM) of either E2 or DHT. HCS analysis allowed to test for multiple concentrations in parallel while for downstream analysis only 10 nM of each hormone was applied. Hormone treatment was sustained throughout macrophage differentiation and *M. tuberculosis* infection. In this study, macrophage viability and metabolism remained robust across both physiological and supraphysiological levels of DHT and E2, confirmed by LDH release and MTT reduction, demonstrating that observed functional changes were not secondary to cytotoxicity or metabolic impairment.

Notably, under the hormone treatment conditions tested in hMdMs derived from both sexes, no significant differences were detected between male- and female-derived cells in *M. tuberculosis* growth and distribution. Hormone treatment of hMdMs modestly increased both overall *M. tuberculosis* infection rates and intracellular bacterial burden at 5 dpi in both sexes, with DHT having a more pronounced effect than E2. Currently there are no studies about E2 and DHT promoting higher bacterial replication of *M. tuberculosis* in hMdMs. However, males and male animals are often more susceptible to bacterial infections, exhibiting higher bacterial loads than females, as reviewed by García-Gómez and colleagues (157). This sex bias has been linked to sex hormones affecting immune functions and pathogen control in various models. Additional evidence from castration studies in animals and investigations of GAHT in transgender individuals further support the role of sex hormones in modulating susceptibility to infections, although detailed mechanisms remain under study (95, 246).

Interestingly, instead of forming clusters in a few heavily infected hMdMs, *M. tuberculosis* showed a more even distribution across the entire macrophage culture. Consequently, the proportion of massively infected cells decreased, resulting in a more uniform bacterial load among hMdMs. The decrease in massively infected cells alongside increased overall bacterial burden suggests that hormone treatment could alter the underlying heterogeneity of the infection. This heterogeneity may result from differences in initial uptake, cell-intrinsic properties affecting bacterial replication, or paracrine signalling within the in vitro system (247). Mahamed et al., who demonstrated that bacterial replication and distribution dynamics can vary significantly within macrophage populations (184). By altering macrophage characteristics, sex hormones could interfere with the establishment of permissive subpopulations, creating a more uniform environment for bacterial growth, as pre-existing heterogeneity among human macrophages is known to affect *M.* tuberculosis growth (37, 247). Supporting this, DHT treatment shifted hMdMs polarization further away from a pro-inflammatory M1 phenotype toward an M2-like phenotype as early as 4 hpi, a finding in line with a study from Becerra-Diaz et al showing that DHT enhances M2 macrophage polarization and IL-10 production in allergic lung inflammation in mice (248).

The interplay between androgens and estrogens critically influences macrophage polarization and cytokine production, which are pivotal for shaping immune responses. Sex hormones modulate the balance between pro-inflammatory M1 and anti-inflammatory M2 macrophage phenotypes, thereby impacting inflammation and tissue repair (249-251). Given this, analysing cytokine profiles in the context of sex hormone effects is essential to understand sex-specific immune regulation. Androgen and estrogen effects on cytokine production are context-dependent (127, 252). In hMdMs, DHT and, to a lesser extent, E2 modified cytokine responses in a donor- and sex-specific manner, most notably by increasing IL-10 (particularly in female cells). The E2 induced IL-10 increase in females is consistent with Straub et al., showing E2 has a context-dependent dual role in both promoting and suppressing inflammation (253). Estrone, in the context of obesity and metabolic dysfunction, and testosterone, in monocytes, can promote IL-10 production(254). DHT also elevated IL-17A and IL-23 in females, whereas in males, DHT treatment induced IFN-α2 and decreased IL-23, highlighting the modulatory role of sex hormones but also substantial donor variability highlighting context-dependent, variable effects on different immune pathways.

5.7 The impact of sex hormones on macrophage transcriptional responses

Building on previous findings that sex hormones influence *M. tuberculosis* infection dynamics through bacterial distribution and macrophage polarization, this section explores the impact of androgen and estrogen treatments on macrophage gene expression.

A first interesting observation was that DHT had only a few effects at the transcriptomic level in naïve hMdMs, in contrast to E2, which already induced transcriptomic changes in naïve cells. In this study pathway analysis were limited due to low numbers of DEGs therefor the potential impact of those genes was analysed individually.

Many genes known to be regulated by steroid sex hormones contain hormone response elements (HREs) in their promoters, enabling direct transcriptional control. This mechanism allows steroid hormones to finely control a wide range of genes involved in processes (255). But the regulation of genes by hormones dos not always require a classical HRE because hormones can exert their effects indirectly via protein interaction and signalling network integration (256). In naïve hMdMs DHT suppressed only a few genes in total which were important for inflammatory and organizational pathways involved in growth signalling

(HBEGF), immune regulation (TRIM73), cytoskeletal architecture (PPFIA1), protein trafficking (GOLGA4), and inflammatory signalling (IL1RAP). Only HBEGF is known to be induced directly by sex steroids (257). This anti-inflammatory signature in naïve cells aligns with DHT's established role in dampening baseline immune activation (95, 127). In contrast, E2 treatment upregulated metabolic and proliferative canonical gene transcripts in naive macrophages, including epigenetic modifiers (KDM1A), cell cycle regulators (KIF15, PAK5), and RNA-binding proteins (CIRBP). This is consistent with the known role of E2 promoting macrophage proliferation through cell cycle gene upregulation (258). The transcriptomic analysis revealed that DHT and E2 exert divergent gene expression patterns on transcriptome level regardless of donor sex.

Focussing on *M. tuberculosis* infected hMdMs, DHT treatment downregulated genes involved in inflammation, tissue remodelling, and immune activation, including LIF, EPHA2, MMP1, DLL4, and CSF2 (GM-CSF). These genes play critical roles in macrophage activation, cytokine signalling, and extracellular matrix remodelling, all essential for mounting effective immune responses. These genes play critical roles in macrophage activation, cytokine signalling, and extracellular matrix remodelling, all essential for mounting effective immune responses. GM-CSF is crucial for a wide range of biological activities in innate and adaptive immunity, and it has a key role in different autoimmune and inflammatory diseases. Higher levels of GM-CSF produced by human macrophages have been directly correlated with increased life span and the ability to control *M. tuberculosis* infection (174). Reduced GM-CSF production has been observed in macrophages from active TB patients, linked to impaired bacterial control and altered macrophage metabolism (174, 259, 260). Generally, DHT promotes an anti-inflammatory M2 macrophage phenotype, which is associated with reduced production of inflammatory cytokines, including potentially GM-CSF (248). DDL4 has been shown to impede M2 macrophage differentiation through inhibition of M2-specific gene expression and apoptotic cell death (176). The genes that were upregulated upon DHT treatment in *M. tuberculosis* infected hMdMs are no typical markers of inflammation or classical macrophage activation but may reflect nuanced effects of DHT on macrophage biology under infectious stress. Studies involving individuals undergoing gender-affirming hormone therapy (GAHT) have shown systemic hormone impacts on immune function. Individuals

undergoing GAHT provide a unique opportunity to investigate the immunomodulatory function of sex steroid hormones in vivo. Brodin et al. and Lotter et al. reported that DHT induces TNF-α production (125, 261), this effect was not observed in this study but an induction of the NF-κB -pathway in male derived hMdMs upon infection. Both studies mentioned analysed monocytes from trans men undergoing GAHT, reflecting in vivo systemic hormone exposure and its broader immunological effects. The used vitro stimulation of hMdMs allowed controlled examination of direct hormone impacts on macrophage function but lacks the complex physiological context, cellular interactions, and pharmacokinetics present during GAHT in living individuals. The androgen receptor expression and responsiveness differ between monocytes and macrophages, affecting macrophage polarization and inflammatory responses depending on differentiation status and environmental context (245, 262).

E2's effects during infection were more complex, simultaneously downregulating key inflammatory and immune regulatory genes (TNFRSF18, CSF2, CCL1, IL23A) while upregulating genes involved in cytoskeletal organization, cell cycle, and metabolism. This dual modulation suggests that E2 creates a balanced immune environment that maintains metabolic activity and cellular organization while it might selectively dampen potentially harmful inflammatory responses.

Together, these findings highlight the distinct and complex regulatory effects of androgens and estrogens on macrophage gene expression during *M. tuberculosis* infection, reflecting both direct hormone action at the cellular level and broader systemic influences observed in vivo, underscoring the importance of considering hormonal milieu in TB.

5.8 Study limitations and future directions

While the present study provides important insights into the influence of biological sex on *M. tuberculosis*– macrophage interactions, several limitations related to sample size, donor variability, and experimental scope should be acknowledged to contextualize the results.

Macrophages are the primary cells infected by *M. tuberculosis* following inhalation of the pathogen. Nevertheless, lung resident macrophages mainly consist of tissue-resident AMs, deriving from fetal liver monocytes and self-renew locally, and monocyte-derived interstitial macrophages (IMs), recruited from circulating monocytes during infection and

inflammation (1, 36, 263). After inhalation of *M. tuberculosis*, the initial infection occurs predominantly in AMs in the lung. They serve as a permissive niche for bacterial growth, while subsequent recruitment of blood-derived monocytes and their differentiation into macrophages contributes to the evolving host immune response and granuloma formation. The dynamic interplay between resident and recruited macrophages influences infection outcome and pathology (35, 148, 194, 200, 264). In vitro experiments have shown that clade I mycobacterial strains, like the H37Rv, exhibit better growth in human alveolar lung cells compared to hMdMs (265). However, due to their limited availability and limited cell quantity, these cells were not suitable for explorative HCS experiments. Exploring the influence of sex and sex hormones in alveolar lung cells represents an important focus for future investigations. Therefore, although blood-derived primary macrophages like hMdMs are a valuable model reflecting aspects of human physiology, they do not fully capture the complex heterogeneity and ontogeny of lung macrophage populations that contribute to TB pathogenesis. While in vitro models offer valuable control and reproducibility, they lack the complexity of the in vivo environment. Important factors such as cell-cell interactions, tissue architecture, and systemic immune responses are not fully replicated, which can limit the physiological relevance and predictive power of the findings. Within our experimental system, only hMdMs are examined as a single cell type in an in vitro environment, meaning that the cytokines expressed by hMdMs in response to infection are initially intended to influence hMdMs function itself but primarily to activate T cell responses, which are absent in our system (58, 216). Consequently, the cells become highly influenced by their own cytokines through autocrine signalling, which likely shapes their functional phenotype differently than would occur in the complex in vivo microenvironment where paracrine interactions with multiple immune cell types modulate macrophage polarization and antimycobacterial responses (266). As a result, in vitro findings may not always translate directly to in vivo or clinical contexts (267). While limitations related to macrophage subtype differences and the reduced complexity of in vitro systems compared to the in vivo lung microenvironment are acknowledged, hMdMs remain a physiologically relevant primary cell type well-suited for high-throughput HCS approaches. Their use enables robust and scalable investigation of sex differences and the modulatory effects of sex hormones on macrophage function in TB, providing critical insights that are difficult to achieve with more complex or less scalable models.

Furthermore, while interpreting these results, one must consider that the application of DHT and E2 to the cells represents an oversimplified model of the dynamic and complex pathological and endocrinological systems observed in vivo. In vitro, 5α-dihydrotestosterone and 17β-estradiol were used as specific, potent analogues of testosterone and estradiol because they mimic the biological activity of these sex steroids while offering better stability and receptor affinity (245). Although various physiological and supraphysiological concentrations of both hormones for both sexes were employed, this experimental system has inherent limitations. Our approach does not account for menstrual cycle hormonal fluctuations, hormonal changes across the lifespan, or the baseline hormonal differences that exist between the sexes. Donor ages were carefully matched to minimize variability caused by menopause and other hormone-related changes associated with aging. These factors may significantly influence the responses of hMdMs to *M. tuberculosis* infection and could contribute to the sex-specific patterns observed in our study. For downstream cytokine profiling and transcriptomic analyses, the 10 nM condition was selected for both E2 and DHT treatments. 10 nM representing a physiological hormone concentration that has been widely used in previous hMdMs studies and allows for comparison of findings across different studies (268). However, many different hormone concentrations have been used in different studies highlighting the complexity of this field (250),(269). Studies addressing exact sex hormone concentrations specifically within the human lung tissue are limited. It is known that sex hormones such as estrogens, progesterone, and androgens are present and metabolized locally in the lung, where enzymes involved in steroid metabolism, including aromatase, are expressed (270). These hormones act through their receptors expressed in lung cells, influencing lung physiology and immune responses contextually to local levels, which can differ from systemic circulation due to local synthesis and metabolism. However, precise quantification and fluctuation of sex hormone levels in lung tissue, especially during different physiological or pathological states, remain less well characterized and require further focused research to fully understand their role in lung immune responses and diseases.

Generally substantial donor variability limited statistical significance across all hormone treatment conditions, reflecting the complex interplay of genetic, epigenetic, and environmental factors that influence individual immune responses. As demonstrated by Li

et al., inter-individual variability in cytokine responses to stimuli can be substantial due to genetic polymorphisms, previous pathogen exposures, and other host factors that modulate immune cell behaviour (271). While raw cytokine concentrations showed distinct patterns across cytokines and sex hormone treatments, normalization of cytokine levels to infected control values for each donor highlighted substantial inter-individual differences. This donor-specific normalization allowed detection of subtle, hormone-driven modulations that are otherwise obscured by overall high variability. This variability is particularly relevant in the context of TB research, as Nhamoyebonde et al. have highlighted that sex differences in TB susceptibility and disease progression involve complex interactions between hormonal, genetic, and immunological factors that vary significantly among individuals (73). Vaccination status, especially regarding BCG vaccination, is an important factor to consider as it can influence immune responses. Fortunately, BCG vaccination is not commonly administered in western parts of Germany, but the vaccination status of donors in this study is unknown and could potentially affect the results (272). For the HCS analysis, a total of 16 donors per sex were included, providing a reasonably robust sample size. However, downstream applications such as RNA sequencing involved smaller sample sizes (n=7), which, while still adequate, restrict the potential for more complex analyses, including interaction studies. The samples obtained yielded total read count of 38.4 and 79.6 million reads total per sample. Lower transcript mapping rates are explained by insufficient DNA depletion. This should be considered when interpreting the results. To address the potential DNA contamination and still obtain valid findings, a stringent threshold for the adjusted p-values (q-values), a q-value cut off of 0.01 was set for the infection comparison, while a q-value cut off of 0.05 was used for the exploratory analyses. This approach ensures that only highly significant results are considered relevant, thereby minimizing the impact of DNA contamination on our findings as much as possible. Initially, an interaction analysis (Method II, Duda et al.) was used to assess effects of sex and sex hormone treatment in both naïve and infected hMdMs (160). However, limited donor numbers reduced statistical power for detecting sex-by-infection and sex-by-treatment interactions, as these typically require larger sample sizes than main effect analyses. Comparative analyses (Method I) were therefore performed to characterize differences by sex and treatment (160).

Additionally, this study focused on snapshot analyses at defined time points post-infection, lacking longitudinal data to capture dynamic changes in macrophage responses and cytokine profiles over the course of infection.

Future studies should address these limitations by increasing donor sample sizes to enhance statistical power and to allow more detailed interaction analyses. Incorporating additional *M. tuberculosis* clinical strains with diverse virulence profiles would improve the relevance of findings to human disease. Longitudinal experimental designs capturing dynamic macrophage responses throughout different infection stages are also essential for a more comprehensive understanding. Moreover, adopting co-culture systems or organoid models integrating other immune cell types such as T cells and neutrophils would better recapitulate in vivo microenvironmental interactions and provide insight into the complex immune networks shaping TB pathogenesis. Finally, integrating functional assays alongside transcriptomic and cytokine analyses would allow correlation of molecular changes with macrophage antimicrobial activity, further elucidating sex- and hormone-dependent mechanisms in TB immunity.

Bibliography

1. Kulle A, Thanabalasuriar A, Cohen TS, Szydlowska M. Resident macrophages of the lung and liver: The guardians of our tissues. Front Immunol. 2022;13:1029085.
2. WHO. Global tuberculosis report 2024. WHO; 2024.
3. Tiemersma EW, van der Werf MJ, Borgdorff MW, Williams BG, Nagelkerke NJ. Natural history of tuberculosis: duration and fatality of untreated pulmonary tuberculosis in HIV negative patients: a systematic review. PLoS One. 2011;6(4):e17601.
4. Bagcchi S. WHO's Global Tuberculosis Report 2022. Lancet Microbe. 2023;4(1):e20.
5. Alsayed SSR, Gunosewoyo H. Tuberculosis: Pathogenesis, Current Treatment Regimens and New Drug Targets. Int J Mol Sci. 2023;24(6).
6. Hayman J. Mycobacterium ulcerans: an infection from Jurassic time? Lancet. 1984;2(8410):1015-6.
7. Barberis I, Bragazzi NL, Galluzzo L, Martini M. The history of tuberculosis: from the first historical records to the isolation of Koch's bacillus. J Prev Med Hyg. 2017;58(1):E9-E12.
8. [Die Atiologie der Tuberculose. Facsimile of the original contribution by Robert Koch in "Berliner Klinische Wochenschrift" 10 April 1882]. Fortschr Med. 1982;100(12):539.
9. Van Gelder RN. Koch's postulates and the polymerase chain reaction. Ocul Immunol Inflamm. 2002;10(4):235-8.
10. Abubakar I, Pimpin L, Ariti C, Beynon R, Mangtani P, Sterne JA, et al. Systematic review and meta-analysis of the current evidence on the duration of protection by bacillus Calmette-Guerin vaccination against tuberculosis. Health Technol Assess. 2013;17(37):1-372, v-vi.
11. Mangtani P, Nguipdop-Djomo P, Keogh RH, Sterne JAC, Abubakar I, Smith PG, et al. The duration of protection of school-aged BCG vaccination in England: a population-based case-control study. Int J Epidemiol. 2018;47(1):193-201.
12. Katelaris AL, Jackson C, Southern J, Gupta RK, Drobniewski F, Lalvani A, et al. Effectiveness of BCG Vaccination Against Mycobacterium tuberculosis Infection in Adults: A Cross-sectional Analysis of a UK-Based Cohort. J Infect Dis. 2020;221(1):146-55.
13. Ardito F, Posteraro B, Sanguinetti M, Zanetti S, Fadda G. Evaluation of BACTEC Mycobacteria Growth Indicator Tube (MGIT 960) automated system for drug susceptibility testing of Mycobacterium tuberculosis. J Clin Microbiol. 2001;39(12):4440-4.
14. Nandlal L, Perumal R, Naidoo K. Rapid Molecular Assays for the Diagnosis of Drug-Resistant Tuberculosis. Infect Drug Resist. 2022;15:4971-84.
15. Masoumi Asl HMM, Alborzi AM, Pourabbas BP, Kalani MM. QuantiFERON-TB Gold and Tuberculin Skin Test for the Diagnosis of Latent Tuberculosis Infection in Children. Iran J Med Sci. 2015;40(5):411-7.
16. Steingart KR, Schiller I, Horne DJ, Pai M, Boehme CC, Dendukuri N. Xpert(R) MTB/RIF assay for pulmonary tuberculosis and rifampicin resistance in adults. Cochrane Database Syst Rev. 2014;2014(1):CD009593.
17. Carrol ED, Clark JE, Cant AJ. Non-pulmonary tuberculosis. Paediatr Respir Rev. 2001;2(2):113-9.
18. Pai M, Behr MA, Dowdy D, Dheda K, Divangahi M, Boehme CC, et al. Tuberculosis. Nat Rev Dis Primers. 2016;2:16076.
19. Kaufmann SH, Dorhoi A. Inflammation in tuberculosis: interactions, imbalances and interventions. Curr Opin Immunol. 2013;25(4):441-9.

20. Sankar P, Mishra BB. Early innate cell interactions with Mycobacterium tuberculosis in protection and pathology of tuberculosis. Front Immunol. 2023;14:1260859.
21. Hunter RL. Pathology of post primary tuberculosis of the lung: an illustrated critical review. Tuberculosis (Edinb). 2011;91(6):497-509.
22. Helming L, Gordon S. The molecular basis of macrophage fusion. Immunobiology. 2007;212(9-10):785-93.
23. Adams DO. The structure of mononuclear phagocytes differentiating in vivo. I. Sequential fine and histologic studies of the effect of Bacillus Calmette-Guerin (BCG). Am J Pathol. 1974;76(1):17-48.
24. Ramakrishnan L. Revisiting the role of the granuloma in tuberculosis. Nat Rev Immunol. 2012;12(5):352-66.
25. Russell DG. Who puts the tubercle in tuberculosis? Nat Rev Microbiol. 2007;5(1):39-47.
26. Ulrichs T, Kaufmann SH. New insights into the function of granulomas in human tuberculosis. J Pathol. 2006;208(2):261-9.
27. Kaplan G, Post FA, Moreira AL, Wainwright H, Kreiswirth BN, Tanverdi M, et al. Mycobacterium tuberculosis growth at the cavity surface: a microenvironment with failed immunity. Infect Immun. 2003;71(12):7099-108.
28. Sasindran SJ, Torrelles JB. Mycobacterium Tuberculosis Infection and Inflammation: what is Beneficial for the Host and for the Bacterium? Front Microbiol. 2011;2:2.
29. Chandra P, Grigsby SJ, Philips JA. Immune evasion and provocation by Mycobacterium tuberculosis. Nat Rev Microbiol. 2022;20(12):750-66.
30. Geldmacher C, Ngwenyama N, Schuetz A, Petrovas C, Reither K, Heeregrave EJ, et al. Preferential infection and depletion of Mycobacterium tuberculosis-specific CD4 T cells after HIV-1 infection. J Exp Med. 2010;207(13):2869-81.
31. Veatch AV, Kaushal D. Opening Pandora's Box: Mechanisms of Mycobacterium tuberculosis Resuscitation. Trends Microbiol. 2018;26(2):145-57.
32. Mattila JT, Ojo OO, Kepka-Lenhart D, Marino S, Kim JH, Eum SY, et al. Microenvironments in tuberculous granulomas are delineated by distinct populations of macrophage subsets and expression of nitric oxide synthase and arginase isoforms. J Immunol. 2013;191(2):773-84.
33. Cronan MR. In the Thick of It: Formation of the Tuberculous Granuloma and Its Effects on Host and Therapeutic Responses. Front Immunol. 2022;13:820134.
34. Cosma CL, Sherman DR, Ramakrishnan L. The secret lives of the pathogenic mycobacteria. Annu Rev Microbiol. 2003;57:641-76.
35. Cohen SB, Gern BH, Delahaye JL, Adams KN, Plumlee CR, Winkler JK, et al. Alveolar Macrophages Provide an Early Mycobacterium tuberculosis Niche and Initiate Dissemination. Cell Host Microbe. 2018;24(3):439-46 e4.
36. Hashimoto D, Chow A, Noizat C, Teo P, Beasley MB, Leboeuf M, et al. Tissue-resident macrophages self-maintain locally throughout adult life with minimal contribution from circulating monocytes. Immunity. 2013;38(4):792-804.
37. Russell DG, Simwela NV, Mattila JT, Flynn J, Mwandumba HC, Pisu D. How macrophage heterogeneity affects tuberculosis disease and therapy. Nat Rev Immunol. 2025;25(5):370-84.
38. Malla S, Sajeevan KA, Acharya B, Chowdhury R, Saha R. Dissecting metabolic landscape of alveolar macrophage. Sci Rep. 2024;14(1):30383.

39. Lee W, VanderVen BC, Fahey RJ, Russell DG. Intracellular Mycobacterium tuberculosis exploits host-derived fatty acids to limit metabolic stress. J Biol Chem. 2013;288(10):6788-800.
40. Lee J, Boyce S, Powers J, Baer C, Sassetti CM, Behar SM. CD11cHi monocyte-derived macrophages are a major cellular compartment infected by Mycobacterium tuberculosis. PLoS Pathog. 2020;16(6):e1008621.
41. Lowe DM, Redford PS, Wilkinson RJ, O'Garra A, Martineau AR. Neutrophils in tuberculosis: friend or foe? Trends Immunol. 2012;33(1):14-25.
42. Marakalala MJ, Raju RM, Sharma K, Zhang YJ, Eugenin EA, Prideaux B, et al. Inflammatory signaling in human tuberculosis granulomas is spatially organized. Nat Med. 2016;22(5):531-8.
43. Gaffney E, Murphy D, Walsh A, Connolly S, Basdeo SA, Keane J, et al. Defining the role of neutrophils in the lung during infection: Implications for tuberculosis disease. Front Immunol. 2022;13:984293.
44. Dallenga T, Repnik U, Corleis B, Eich J, Reimer R, Griffiths GW, et al. M. tuberculosis-Induced Necrosis of Infected Neutrophils Promotes Bacterial Growth Following Phagocytosis by Macrophages. Cell Host Microbe. 2017;22(4):519-30 e3.
45. Zimmerli S, Edwards S, Ernst JD. Selective receptor blockade during phagocytosis does not alter the survival and growth of Mycobacterium tuberculosis in human macrophages. Am J Respir Cell Mol Biol. 1996;15(6):760-70.
46. Armstrong JA, Hart PD. Phagosome-lysosome interactions in cultured macrophages infected with virulent tubercle bacilli. Reversal of the usual nonfusion pattern and observations on bacterial survival. J Exp Med. 1975;142(1):1-16.
47. Cambier CJ, Falkow S, Ramakrishnan L. Host evasion and exploitation schemes of Mycobacterium tuberculosis. Cell. 2014;159(7):1497-509.
48. Jo EK. Mycobacterial interaction with innate receptors: TLRs, C-type lectins, and NLRs. Curr Opin Infect Dis. 2008;21(3):279-86.
49. Means TK, Wang S, Lien E, Yoshimura A, Golenbock DT, Fenton MJ. Human toll-like receptors mediate cellular activation by Mycobacterium tuberculosis. J Immunol. 1999;163(7):3920-7.
50. Harding CV, Boom WH. Regulation of antigen presentation by Mycobacterium tuberculosis: a role for Toll-like receptors. Nat Rev Microbiol. 2010;8(4):296-307.
51. Ishikawa E, Mori D, Yamasaki S. Recognition of Mycobacterial Lipids by Immune Receptors. Trends Immunol. 2017;38(1):66-76.
52. Songane M, Kleinnijenhuis J, Netea MG, van Crevel R. The role of autophagy in host defence against Mycobacterium tuberculosis infection. Tuberculosis (Edinb). 2012;92(5):388-96.
53. Quesniaux V, Fremond C, Jacobs M, Parida S, Nicolle D, Yeremeev V, et al. Toll-like receptor pathways in the immune responses to mycobacteria. Microbes Infect. 2004;6(10):946-59.
54. Boritsch EC, Frigui W, Cascioferro A, Malaga W, Etienne G, Laval F, et al. pks5-recombination-mediated surface remodelling in Mycobacterium tuberculosis emergence. Nat Microbiol. 2016;1:15019.
55. Chai Q, Lu Z, Liu CH. Host defense mechanisms against Mycobacterium tuberculosis. Cell Mol Life Sci. 2020;77(10):1859-78.

56. Cambier CJ, Takaki KK, Larson RP, Hernandez RE, Tobin DM, Urdahl KB, et al. Mycobacteria manipulate macrophage recruitment through coordinated use of membrane lipids. Nature. 2014;505(7482):218-22.
57. Hirsch CS, Ellner JJ, Russell DG, Rich EA. Complement receptor-mediated uptake and tumor necrosis factor-alpha-mediated growth inhibition of Mycobacterium tuberculosis by human alveolar macrophages. J Immunol. 1994;152(2):743-53.
58. Arango Duque G, Descoteaux A. Macrophage cytokines: involvement in immunity and infectious diseases. Front Immunol. 2014;5:491.
59. Zaheen A, Bloom BR. Tuberculosis in 2020 - New Approaches to a Continuing Global Health Crisis. N Engl J Med. 2020;382(14):e26.
60. Mihret A. The role of dendritic cells in Mycobacterium tuberculosis infection. Virulence. 2012;3(7):654-9.
61. Groschel MI, Sayes F, Simeone R, Majlessi L, Brosch R. ESX secretion systems: mycobacterial evolution to counter host immunity. Nat Rev Microbiol. 2016;14(11):677-91.
62. Chen Z, Wang T, Liu Z, Zhang G, Wang J, Feng S, et al. Inhibition of Autophagy by MiR-30A Induced by Mycobacteria tuberculosis as a Possible Mechanism of Immune Escape in Human Macrophages. Jpn J Infect Dis. 2015;68(5):420-4.
63. Zhai W, Wu F, Zhang Y, Fu Y, Liu Z. The Immune Escape Mechanisms of Mycobacterium Tuberculosis. Int J Mol Sci. 2019;20(2).
64. Shin DM, Jeon BY, Lee HM, Jin HS, Yuk JM, Song CH, et al. Mycobacterium tuberculosis eis regulates autophagy, inflammation, and cell death through redox-dependent signaling. PLoS Pathog. 2010;6(12):e1001230.
65. Buchmeier NA, Newton GL, Fahey RC. A mycothiol synthase mutant of Mycobacterium tuberculosis has an altered thiol-disulfide content and limited tolerance to stress. J Bacteriol. 2006;188(17):6245-52.
66. Malik ZA, Denning GM, Kusner DJ. Inhibition of Ca(2+) signaling by Mycobacterium tuberculosis is associated with reduced phagosome-lysosome fusion and increased survival within human macrophages. J Exp Med. 2000;191(2):287-302.
67. What is gender? What is sex? Canadian Institutes of Health Research webpage: Canadian Institutes of Health Research; 2023 [Available from: https://cihr-irsc.gc.ca/e/48642.html.
68. Organization WH. Gender and health [Available from: https://www.who.int/health-topics/gender#tab=tab_1.
69. Watkins RE, Plant AJ. Does smoking explain sex differences in the global tuberculosis epidemic? Epidemiol Infect. 2006;134(2):333-9.
70. Maurya V, Vijayan VK, Shah A. Smoking and tuberculosis: an association overlooked. Int J Tuberc Lung Dis. 2002;6(11):942-51.
71. Hertz D, Schneider B. Sex differences in tuberculosis. Semin Immunopathol. 2019;41(2):225-37.
72. Lansang MAD, Alejandria MM, Law I, Juban NR, Amarillo MLE, Sison OT, et al. High TB burden and low notification rates in the Philippines: The 2016 national TB prevalence survey. PLoS One. 2021;16(6):e0252240.
73. Nhamoyebonde S, Leslie A. Biological differences between the sexes and susceptibility to tuberculosis. J Infect Dis. 2014;209 Suppl 3:S100-6.
74. Narasimhan P, Wood J, Macintyre CR, Mathai D. Risk factors for tuberculosis. Pulm Med. 2013;2013:828939.
75. WHO. TUBERCULOSIS IN WOMEN. 2019.

76. Holmes CB, Hausler H, Nunn P. A review of sex differences in the epidemiology of tuberculosis. Int J Tuberc Lung Dis. 1998;2(2):96-104.
77. Loto OM, Awowole I. Tuberculosis in pregnancy: a review. J Pregnancy. 2012;2012:379271.
78. Orazulike N, Sharma JB, Sharma S, Umeora OUJ. Tuberculosis (TB) in pregnancy - A review. Eur J Obstet Gynecol Reprod Biol. 2021;259:167-77.
79. Gold SM, Willing A, Leypoldt F, Paul F, Friese MA. Sex differences in autoimmune disorders of the central nervous system. Semin Immunopathol. 2019;41(2):177-88.
80. Schwinge D, Schramm C. Sex-related factors in autoimmune liver diseases. Semin Immunopathol. 2019;41(2):165-75.
81. Lotter H, Altfeld M. Sex differences in immunity. Semin Immunopathol. 2019;41(2):133-5.
82. Ruggieri A, Anticoli S, D'Ambrosio A, Giordani L, Viora M. The influence of sex and gender on immunity, infection and vaccination. Ann Ist Super Sanita. 2016;52(2):198-204.
83. Xing E, Billi AC, Gudjonsson JE. Sex Bias and Autoimmune Diseases. J Invest Dermatol. 2022;142(3 Pt B):857-66.
84. Khan M. A plausible explanation for male dominance in typhoid ileal perforation. Clin Exp Gastroenterol. 2012;5:213-7.
85. de Martel C, Parsonnet J. Helicobacter pylori infection and gender: a meta-analysis of population-based prevalence surveys. Dig Dis Sci. 2006;51(12):2292-301.
86. Gutierrez F, Masia M, Mirete C, Soldan B, Rodriguez JC, Padilla S, et al. The influence of age and gender on the population-based incidence of community-acquired pneumonia caused by different microbial pathogens. J Infect. 2006;53(3):166-74.
87. Schroder J, Kahlke V, Staubach KH, Zabel P, Stuber F. Gender differences in human sepsis. Arch Surg. 1998;133(11):1200-5.
88. Leone M, Honstettre A, Lepidi H, Capo C, Bayard F, Raoult D, et al. Effect of sex on Coxiella burnetii infection: protective role of 17beta-estradiol. J Infect Dis. 2004;189(2):339-45.
89. Oliver JD. Wound infections caused by Vibrio vulnificus and other marine bacteria. Epidemiol Infect. 2005;133(3):383-91.
90. Fabbian F, De Giorgi A, Lopez-Soto PJ, Pala M, Tiseo R, Cultrera R, et al. Is female gender as harmful as bacteria? analysis of hospital admissions for urinary tract infections in elderly patients. J Womens Health (Larchmt). 2015;24(7):587-92.
91. Jarefors S, Bennet L, You E, Forsberg P, Ekerfelt C, Berglund J, et al. Lyme borreliosis reinfection: might it be explained by a gender difference in immune response? Immunology. 2006;118(2):224-32.
92. Hafner LM, Cunningham K, Beagley KW. Ovarian steroid hormones: effects on immune responses and Chlamydia trachomatis infections of the female genital tract. Mucosal Immunol. 2013;6(5):859-75.
93. Pasche B, Kalaydjiev S, Franz TJ, Kremmer E, Gailus-Durner V, Fuchs H, et al. Sex-dependent susceptibility to Listeria monocytogenes infection is mediated by differential interleukin-10 production. Infect Immun. 2005;73(9):5952-60.
94. Vazquez-Martinez ER, Garcia-Gomez E, Camacho-Arroyo I, Gonzalez-Pedrajo B. Sexual dimorphism in bacterial infections. Biol Sex Differ. 2018;9(1):27.
95. Klein SL, Flanagan KL. Sex differences in immune responses. Nat Rev Immunol. 2016;16(10):626-38.

96. Patin E, Hasan M, Bergstedt J, Rouilly V, Libri V, Urrutia A, et al. Natural variation in the parameters of innate immune cells is preferentially driven by genetic factors. Nat Immunol. 2018;19(3):302-14.
97. Abdullah M, Chai PS, Chong MY, Tohit ER, Ramasamy R, Pei CP, et al. Gender effect on in vitro lymphocyte subset levels of healthy individuals. Cell Immunol. 2012;272(2):214-9.
98. Wikby A, Mansson IA, Johansson B, Strindhall J, Nilsson SE. The immune risk profile is associated with age and gender: findings from three Swedish population studies of individuals 20-100 years of age. Biogerontology. 2008;9(5):299-308.
99. Forsyth KS, Jiwrajka N, Lovell CD, Toothacre NE, Anguera MC. The conneXion between sex and immune responses. Nat Rev Immunol. 2024;24(7):487-502.
100. Khan SR, van der Burgh AC, Peeters RP, van Hagen PM, Dalm V, Chaker L. Determinants of Serum Immunoglobulin Levels: A Systematic Review and Meta-Analysis. Front Immunol. 2021;12:664526.
101. Melzer S, Zachariae S, Bocsi J, Engel C, Loffler M, Tarnok A. Reference intervals for leukocyte subsets in adults: Results from a population-based study using 10-color flow cytometry. Cytometry B Clin Cytom. 2015;88(4):270-81.
102. Lyon MF. Gene action in the X-chromosome of the mouse (Mus musculus L.). Nature. 1961;190:372-3.
103. Brown CJ, Ballabio A, Rupert JL, Lafreniere RG, Grompe M, Tonlorenzi R, et al. A gene from the region of the human X inactivation centre is expressed exclusively from the inactive X chromosome. Nature. 1991;349(6304):38-44.
104. Heard E, Clerc P, Avner P. X-chromosome inactivation in mammals. Annu Rev Genet. 1997;31:571-610.
105. Fish EN. The X-files in immunity: sex-based differences predispose immune responses. Nat Rev Immunol. 2008;8(9):737-44.
106. Youness A, Miquel CH, Guery JC. Escape from X Chromosome Inactivation and the Female Predominance in Autoimmune Diseases. Int J Mol Sci. 2021;22(3).
107. Meester I, Manilla-Munoz E, Leon-Cachon RBR, Paniagua-Frausto GA, Carrion-Alvarez D, Ruiz-Rodriguez CO, et al. SeXY chromosomes and the immune system: reflections after a comparative study. Biol Sex Differ. 2020;11(1):3.
108. Wilson MA. The Y chromosome and its impact on health and disease. Hum Mol Genet. 2021;30(R2):R296-R300.
109. Randall VA. Role of 5 alpha-reductase in health and disease. Baillieres Clin Endocrinol Metab. 1994;8(2):405-31.
110. Gubbels Bupp MR, Jorgensen TN. Androgen-Induced Immunosuppression. Front Immunol. 2018;9:794.
111. Simpson ER. Sources of estrogen and their importance. J Steroid Biochem Mol Biol. 2003;86(3-5):225-30.
112. Cornejo Ulloa PE, Krom BP, Schoonmade LJ, van der Veen MH. Sex steroid hormones: an overlooked yet fundamental factor in oral homeostasis in humans. Front Endocrinol (Lausanne). 2024;15:1400640.
113. Ozanne DM, Brady ME, Cook S, Gaughan L, Neal DE, Robson CN. Androgen receptor nuclear translocation is facilitated by the f-actin cross-linking protein filamin. Mol Endocrinol. 2000;14(10):1618-26.
114. Lonergan PE, Tindall DJ. Androgen receptor signaling in prostate cancer development and progression. J Carcinog. 2011;10:20.

115. Oliva M, Munoz-Aguirre M, Kim-Hellmuth S, Wucher V, Gewirtz ADH, Cotter DJ, et al. The impact of sex on gene expression across human tissues. Science. 2020;369(6509).
116. Harding AT, Heaton NS. The Impact of Estrogens and Their Receptors on Immunity and Inflammation during Infection. Cancers (Basel). 2022;14(4).
117. Gupta M, Srikrishna G, Klein SL, Bishai WR. Genetic and hormonal mechanisms underlying sex-specific immune responses in tuberculosis. Trends Immunol. 2022;43(8):640-56.
118. Fuentes N, Silveyra P. Estrogen receptor signaling mechanisms. Adv Protein Chem Struct Biol. 2019;116:135-70.
119. Koszegi Z, Cheong RY. Targeting the non-classical estrogen pathway in neurodegenerative diseases and brain injury disorders. Front Endocrinol (Lausanne). 2022;13:999236.
120. Karpuzoglu E, Ahmed SA. Estrogen regulation of nitric oxide and inducible nitric oxide synthase (iNOS) in immune cells: implications for immunity, autoimmune diseases, and apoptosis. Nitric Oxide. 2006;15(3):177-86.
121. Liang M, Ekblad E, Lydrup ML, Nilsson BO. Combined lack of estrogen receptors alpha and beta affects vascular iNOS protein expression. Cell Tissue Res. 2003;313(1):63-70.
122. Kovats S. Estrogen receptors regulate innate immune cells and signaling pathways. Cell Immunol. 2015;294(2):63-9.
123. D'Agostino P, Milano S, Barbera C, Di Bella G, La Rosa M, Ferlazzo V, et al. Sex hormones modulate inflammatory mediators produced by macrophages. Ann N Y Acad Sci. 1999;876:426-9.
124. Liva SM, Voskuhl RR. Testosterone acts directly on CD4+ T lymphocytes to increase IL-10 production. J Immunol. 2001;167(4):2060-7.
125. Lakshmikanth T, Consiglio C, Sardh F, Forlin R, Wang J, Tan Z, et al. Immune system adaptation during gender-affirming testosterone treatment. Nature. 2024;633(8028):155-64.
126. Kwon H, Schafer JM, Song NJ, Kaneko S, Li A, Xiao T, et al. Androgen conspires with the CD8(+) T cell exhaustion program and contributes to sex bias in cancer. Sci Immunol. 2022;7(73):eabq2630.
127. Trigunaite A, Dimo J, Jorgensen TN. Suppressive effects of androgens on the immune system. Cell Immunol. 2015;294(2):87-94.
128. Dragin N, Bismuth J, Cizeron-Clairac G, Biferi MG, Berthault C, Serraf A, et al. Estrogen-mediated downregulation of AIRE influences sexual dimorphism in autoimmune diseases. J Clin Invest. 2016;126(4):1525-37.
129. Tyagi AM, Srivastava K, Mansoori MN, Trivedi R, Chattopadhyay N, Singh D. Estrogen deficiency induces the differentiation of IL-17 secreting Th17 cells: a new candidate in the pathogenesis of osteoporosis. PLoS One. 2012;7(9):e44552.
130. Yalcinkaya A, Yalcinkaya R, Sardh F, Landegren N. Immune dynamics throughout life in relation to sex hormones and perspectives gained from gender-affirming hormone therapy. Front Immunol. 2024;15:1501364.
131. Patel H, Arruarana V, Yao L, Cui X, Ray E. Effects of hormones and hormone therapy on breast tissue in transgender patients: a concise review. Endocrine. 2020;68(1):6-15.
132. Jackson SS, Nambiar KZ, O'Callaghan S, Berner AM. Understanding the role of sex hormones in cancer for the transgender community. Trends Cancer. 2022;8(4):273-5.
133. Brundin PMA, Landgren BM, Fjallstrom P, Shamekh MM, Gustafsson JA, Johansson AF, et al. Expression of Sex Hormone Receptor and Immune Response Genes in Peripheral

Blood Mononuclear Cells During the Menstrual Cycle. Front Endocrinol (Lausanne). 2021;12:721813.
134. Izzo RA, Cicardo VH. Gonads and experimental tuberculosis. Nature. 1947;159(4057):155.
135. Tsuyuguchi K, Suzuki K, Matsumoto H, Tanaka E, Amitani R, Kuze F. Effect of oestrogen on Mycobacterium avium complex pulmonary infection in mice. Clin Exp Immunol. 2001;123(3):428-34.
136. Dibbern J, Eggers L, Schneider BE. Author Correction: Sex differences in the C57BL/6 model of Mycobacterium tuberculosis infection. Sci Rep. 2018;8(1):6354.
137. Bini EI, Mata Espinosa D, Marquina Castillo B, Barrios Payan J, Colucci D, Cruz AF, et al. The influence of sex steroid hormones in the immunopathology of experimental pulmonary tuberculosis. PLoS One. 2014;9(4):e93831.
138. Braverman J, Stanley SA. Nitric Oxide Modulates Macrophage Responses to Mycobacterium tuberculosis Infection through Activation of HIF-1alpha and Repression of NF-kappaB. J Immunol. 2017;199(5):1805-16.
139. Tang J, Sun M, Shi G, Xu Y, Han Y, Li X, et al. Toll-Like Receptor 8 Agonist Strengthens the Protective Efficacy of ESAT-6 Immunization to Mycobacterium tuberculosis Infection. Front Immunol. 2017;8:1972.
140. Mogues T, Goodrich ME, Ryan L, LaCourse R, North RJ. The relative importance of T cell subsets in immunity and immunopathology of airborne Mycobacterium tuberculosis infection in mice. J Exp Med. 2001;193(3):271-80.
141. Klein SL. Immune cells have sex and so should journal articles. Endocrinology. 2012;153(6):2544-50.
142. Hertz D, Dibbern J, Eggers L, von Borstel L, Schneider BE. Increased male susceptibility to Mycobacterium tuberculosis infection is associated with smaller B cell follicles in the lungs. Sci Rep. 2020;10(1):5142.
143. Dutta NK, Schneider BE. Are There Sex-Specific Differences in Response to Adjunctive Host-Directed Therapies for Tuberculosis? Front Immunol. 2020;11:1465.
144. Bea A. Sex-specific factors affecting intracellular

infection of human primary macrophages by

visceral Leishmania spp.: Univeristy Hamburg; 2024.
145. Health Product Policy and Standards (HPS) NaSfBPN. General Requirements for he sterility of biological substances. In: WHO, editor. WHO Technical Resport Series No 5301973. p. 22.
146. WHO. WHO operational handbook on tuberculosis. 2025.
147. Fehling H, Niss H, Bea A, Kottmayr N, Brinker C, Hoenow S, et al. High Content Analysis of Macrophage-Targeting EhPIb-Compounds against Cutaneous and Visceral Leishmania Species. Microorganisms. 2021;9(2).
148. Ahmad F, Rani A, Alam A, Zarin S, Pandey S, Singh H, et al. Macrophage: A Cell With Many Faces and Functions in Tuberculosis. Front Immunol. 2022;13:747799.
149. Dinarello CA. Overview of the IL-1 family in innate inflammation and acquired immunity. Immunol Rev. 2018;281(1):8-27.
150. Parameswaran N, Patial S. Tumor necrosis factor-alpha signaling in macrophages. Crit Rev Eukaryot Gene Expr. 2010;20(2):87-103.
151. Siebeler R, de Winther MPJ, Hoeksema MA. The regulatory landscape of macrophage interferon signaling in inflammation. J Allergy Clin Immunol. 2023;152(2):326-37.

152. Tanaka T, Narazaki M, Kishimoto T. IL-6 in inflammation, immunity, and disease. Cold Spring Harb Perspect Biol. 2014;6(10):a016295.
153. Saraiva M, O'Garra A. The regulation of IL-10 production by immune cells. Nat Rev Immunol. 2010;10(3):170-81.
154. Meniailo ME, Malashchenko VV, Shmarov VA, Gazatova ND, Melashchenko OB, Goncharov AG, et al. Interleukin-8 favors pro-inflammatory activity of human monocytes/macrophages. Int Immunopharmacol. 2018;56:217-21.
155. Verreck FA, de Boer T, Langenberg DM, Hoeve MA, Kramer M, Vaisberg E, et al. Human IL-23-producing type 1 macrophages promote but IL-10-producing type 2 macrophages subvert immunity to (myco)bacteria. Proc Natl Acad Sci U S A. 2004;101(13):4560-5.
156. Garcia-Dominguez M. The Role of IL-23 in the Development of Inflammatory Diseases. Biology (Basel). 2025;14(4).
157. Garcia-Gomez E, Gonzalez-Pedrajo B, Camacho-Arroyo I. Role of sex steroid hormones in bacterial-host interactions. Biomed Res Int. 2013;2013:928290.
158. Mantovani A, Sica A, Sozzani S, Allavena P, Vecchi A, Locati M. The chemokine system in diverse forms of macrophage activation and polarization. Trends Immunol. 2004;25(12):677-86.
159. Calippe B, Douin-Echinard V, Delpy L, Laffargue M, Lelu K, Krust A, et al. 17Beta-estradiol promotes TLR4-triggered proinflammatory mediator production through direct estrogen receptor alpha signaling in macrophages in vivo. J Immunol. 2010;185(2):1169-76.
160. Duda JC, Drenda C, Kastel H, Rahnenfuhrer J, Kappenberg F. Benefit of using interaction effects for the analysis of high-dimensional time-response or dose-response data for two-group comparisons. Sci Rep. 2023;13(1):20804.
161. Dao DT, Anez-Bustillos L, Adam RM, Puder M, Bielenberg DR. Heparin-Binding Epidermal Growth Factor-Like Growth Factor as a Critical Mediator of Tissue Repair and Regeneration. Am J Pathol. 2018;188(11):2446-56.
162. Yang W, Gu Z, Zhang H, Hu H. To TRIM the Immunity: From Innate to Adaptive Immunity. Front Immunol. 2020;11:02157.
163. Gao Y, Guan L, Jia R, Xiao W, Han Y, Li Y, et al. High expression of PPFIA1 in human esophageal squamous cell carcinoma correlates with tumor metastasis and poor prognosis. BMC Cancer. 2023;23(1):417.
164. Guo S, Chunyu L, Ouyang S, Wang X, Liao A, Yuan S. GOLGA4, A Golgi matrix protein, is dispensable for spermatogenesis and male fertility in mice. Biochem Biophys Res Commun. 2020;529(3):642-6.
165. Zhang Y, Chen X, Wang H, Gordon-Mitchell S, Sahu S, Bhagat TD, et al. Correction: Innate immune mediator, Interleukin-1 receptor accessory protein (IL1RAP), is expressed and pro-tumorigenic in pancreatic cancer. J Hematol Oncol. 2022;15(1):100.
166. Kang MK, Mehrazarin S, Park NH, Wang CY. Epigenetic gene regulation by histone demethylases: emerging role in oncogenesis and inflammation. Oral Dis. 2017;23(6):709-20.
167. Zhu X, Guan R, Zou Y, Li M, Chen J, Zhang J, et al. Cold-inducible RNA binding protein alleviates iron overload-induced neural ferroptosis under perinatal hypoxia insult. Cell Death Differ. 2024;31(4):524-39.
168. Wang Q, Taschner M, Ganzinger KA, Kelley C, Villasenor A, Heymann M, et al. Membrane association and remodeling by intraflagellar transport protein IFT172. Nat Commun. 2018;9(1):4684.

169. Jonker CTH, Galmes R, Veenendaal T, Ten Brink C, van der Welle REN, Liv N, et al. Author Correction: Vps3 and Vps8 control integrin trafficking from early to recycling endosomes and regulate integrin-dependent functions. Nat Commun. 2021;12(1):5828.
170. Liu S, Zhang Z, Wang Y, Zhang Y, Min J, Li X, et al. The chemokine CCL1 facilitates pulmonary fibrosis by promoting macrophage migration and M2 polarization. Int Immunopharmacol. 2023;120:110343.
171. Schroder WA, Hirata TD, Le TT, Gardner J, Boyle GM, Ellis J, et al. SerpinB2 inhibits migration and promotes a resolution phase signature in large peritoneal macrophages. Sci Rep. 2019;9(1):12421.
172. Tokunaga R, Zhang W, Naseem M, Puccini A, Berger MD, Soni S, et al. CXCL9, CXCL10, CXCL11/CXCR3 axis for immune activation - A target for novel cancer therapy. Cancer Treat Rev. 2018;63:40-7.
173. Parasa VR, Muvva JR, Rose JF, Braian C, Brighenti S, Lerm M. Inhibition of Tissue Matrix Metalloproteinases Interferes with Mycobacterium tuberculosis-Induced Granuloma Formation and Reduces Bacterial Load in a Human Lung Tissue Model. Front Microbiol. 2017;8:2370.
174. Mishra A, Singh VK, Actor JK, Hunter RL, Jagannath C, Subbian S, et al. GM-CSF Dependent Differential Control of Mycobacterium tuberculosis Infection in Human and Mouse Macrophages: Is Macrophage Source of GM-CSF Critical to Tuberculosis Immunity? Front Immunol. 2020;11:1599.
175. Wang J, Chang CY, Yang X, Zhou F, Liu J, Feng Z, et al. Leukemia inhibitory factor, a double-edged sword with therapeutic implications in human diseases. Mol Ther. 2023;31(2):331-43.
176. Pagie S, Gerard N, Charreau B. Notch signaling triggered via the ligand DLL4 impedes M2 macrophage differentiation and promotes their apoptosis. Cell Commun Signal. 2018;16(1):4.
177. Tian J, Zhang B, Rui K, Wang S. The Role of GITR/GITRL Interaction in Autoimmune Diseases. Front Immunol. 2020;11:588682.
178. Dougan M, Dranoff G, Dougan SK. GM-CSF, IL-3, and IL-5 Family of Cytokines: Regulators of Inflammation. Immunity. 2019;50(4):796-811.
179. Horton KC, MacPherson P, Houben RM, White RG, Corbett EL. Sex Differences in Tuberculosis Burden and Notifications in Low- and Middle-Income Countries: A Systematic Review and Meta-analysis. PLoS Med. 2016;13(9):e1002119.
180. Diwan VK, Thorson A. Sex, gender, and tuberculosis. Lancet. 1999;353(9157):1000-1.
181. Humayun M, Chirenda J, Ye W, Mukeredzi I, Mujuru HA, Yang Z. Effect of Gender on Clinical Presentation of Tuberculosis (TB) and Age-Specific Risk of TB, and TB-Human Immunodeficiency Virus Coinfection. Open Forum Infect Dis. 2022;9(10):ofac512.
182. Tazoll SC. Mycobacterium tuberculosis infection of human macrophages: effects on cellular metabolism and lipid droplet composition: Lübeck; 2022.
183. Aylan B, Botella L, Gutierrez MG, Santucci P. High content quantitative imaging of Mycobacterium tuberculosis responses to acidic microenvironments within human macrophages. FEBS Open Bio. 2023;13(7):1204-17.
184. Mahamed D, Boulle M, Ganga Y, Mc Arthur C, Skroch S, Oom L, et al. Intracellular growth of Mycobacterium tuberculosis after macrophage cell death leads to serial killing of host cells. Elife. 2017;6.

185. Quigley J, Hughitt VK, Velikovsky CA, Mariuzza RA, El-Sayed NM, Briken V. The Cell Wall Lipid PDIM Contributes to Phagosomal Escape and Host Cell Exit of Mycobacterium tuberculosis. mBio. 2017;8(2).
186. Blanc L, Gilleron M, Prandi J, Song OR, Jang MS, Gicquel B, et al. Mycobacterium tuberculosis inhibits human innate immune responses via the production of TLR2 antagonist glycolipids. Proc Natl Acad Sci U S A. 2017;114(42):11205-10.
187. Khan A, Zhang K, Singh VK, Mishra A, Kachroo P, Bing T, et al. Human M1 macrophages express unique innate immune response genes after mycobacterial infection to defend against tuberculosis. Commun Biol. 2022;5(1):480.
188. Benoit M, Desnues B, Mege JL. Macrophage polarization in bacterial infections. J Immunol. 2008;181(6):3733-9.
189. Huang Z, Luo Q, Guo Y, Chen J, Xiong G, Peng Y, et al. Mycobacterium tuberculosis-Induced Polarization of Human Macrophage Orchestrates the Formation and Development of Tuberculous Granulomas In Vitro. PLoS One. 2015;10(6):e0129744.
190. Mege JL, Mehraj V, Capo C. Macrophage polarization and bacterial infections. Curr Opin Infect Dis. 2011;24(3):230-4.
191. Labonte AC, Tosello-Trampont AC, Hahn YS. The role of macrophage polarization in infectious and inflammatory diseases. Mol Cells. 2014;37(4):275-85.
192. Lugo-Villarino G, Verollet C, Maridonneau-Parini I, Neyrolles O. Macrophage polarization: convergence point targeted by mycobacterium tuberculosis and HIV. Front Immunol. 2011;2:43.
193. Mills CD, Kincaid K, Alt JM, Heilman MJ, Hill AM. M-1/M-2 macrophages and the Th1/Th2 paradigm. J Immunol. 2000;164(12):6166-73.
194. Berrington WR, Hawn TR. Mycobacterium tuberculosis, macrophages, and the innate immune response: does common variation matter? Immunol Rev. 2007;219:167-86.
195. Biswas SK, Chittezhath M, Shalova IN, Lim JY. Macrophage polarization and plasticity in health and disease. Immunol Res. 2012;53(1-3):11-24.
196. Huang CC, Nguyen D, Fernandez J, Yun KY, Fry KE, Bradley DW, et al. Molecular cloning and sequencing of the Mexico isolate of hepatitis E virus (HEV). Virology. 1992;191(2):550-8.
197. Bea A, Fehling H, Hausmann F, Habib FM, Lutkemeyer M, Buer L, et al. Transcriptome profiling of L. infantum-infected human macrophages reveals sex-specific type I interferon induction. PLoS Pathog. 2025;21(8):e1013427.
198. Yang Z, Huang YC, Koziel H, de Crom R, Ruetten H, Wohlfart P, et al. Female resistance to pneumonia identifies lung macrophage nitric oxide synthase-3 as a therapeutic target. Elife. 2014;3.
199. Prabowo SA, Smith SG, Seifert K, Fletcher HA. Impact of individual-level factors on Ex vivo mycobacterial growth inhibition: Associations of immune cell phenotype, cytomegalovirus-specific response and sex with immunity following BCG vaccination in humans. Tuberculosis (Edinb). 2019;119:101876.
200. Lerner TR, Borel S, Gutierrez MG. The innate immune response in human tuberculosis. Cell Microbiol. 2015;17(9):1277-85.
201. Yan L, Wang J, Cai X, Liou YC, Shen HM, Hao J, et al. Macrophage plasticity: signaling pathways, tissue repair, and regeneration. MedComm (2020). 2024;5(8):e658.
202. Tiwari D, Martineau AR. Inflammation-mediated tissue damage in pulmonary tuberculosis and host-directed therapeutic strategies. Semin Immunol. 2023;65:101672.

203. Ashenafi S, Loreti MG, Bekele A, Aseffa G, Amogne W, Kassa E, et al. Inflammatory immune profiles associated with disease severity in pulmonary tuberculosis patients with moderate to severe clinical TB or anemia. Front Immunol. 2023;14:1296501.
204. Tobin DM, Roca FJ, Oh SF, McFarland R, Vickery TW, Ray JP, et al. Host genotype-specific therapies can optimize the inflammatory response to mycobacterial infections. Cell. 2012;148(3):434-46.
205. Silva D, Silva MVD, Barros CCO, Alexandre PBD, Timoteo RP, Catarino JS, et al. TNF-alpha blockade impairs in vitro tuberculous granuloma formation and down modulate Th1, Th17 and Treg cytokines. PLoS One. 2018;13(3):e0194430.
206. Yuk JM, Kim JK, Kim IS, Jo EK. TNF in Human Tuberculosis: A Double-Edged Sword. Immune Netw. 2024;24(1):e4.
207. Temple SE, Pham K, Glendenning P, Phillips M, Waterer GW. Endotoxin induced TNF and IL-10 mRNA production is higher in male than female donors: correlation with elevated expression of TLR4. Cell Immunol. 2008;251(2):69-71.
208. Okeke C, Okonkwo R, Ibeh N, Chukwuma O, Okeke C. Assessment of gender differences in some inflammatory cytokines of tuberculosis patients before and during treatment. Afr Health Sci. 2023;23(3):336-42.
209. Satoskar A, Alexander J. Sex-determined susceptibility and differential IFN-gamma and TNF-alpha mRNA expression in DBA/2 mice infected with Leishmania mexicana. Immunology. 1995;84(1):1-4.
210. Khader SA, Cooper AM. IL-23 and IL-17 in tuberculosis. Cytokine. 2008;41(2):79-83.
211. Fuseini H, Cephus JY, Wu P, Davis JB, Contreras DC, Gandhi VD, et al. ERalpha Signaling Increased IL-17A Production in Th17 Cells by Upregulating IL-23R Expression, Mitochondrial Respiration, and Proliferation. Front Immunol. 2019;10:2740.
212. Moreira-Teixeira L, Mayer-Barber K, Sher A, O'Garra A. Type I interferons in tuberculosis: Foe and occasionally friend. J Exp Med. 2018;215(5):1273-85.
213. Nair S, Huynh JP, Lampropoulou V, Loginicheva E, Esaulova E, Gounder AP, et al. Irg1 expression in myeloid cells prevents immunopathology during M. tuberculosis infection. J Exp Med. 2018;215(4):1035-45.
214. Howard NC, Khader SA. Immunometabolism during Mycobacterium tuberculosis Infection. Trends Microbiol. 2020;28(10):832-50.
215. Zhou X, Yang J, Zhang Z, Zhang L, Zhu B, Lie L, et al. Different Signaling Pathways Define Different Interferon-Stimulated Gene Expression during Mycobacteria Infection in Macrophages. Int J Mol Sci. 2019;20(3).
216. Domingo-Gonzalez R, Prince O, Cooper A, Khader SA. Cytokines and Chemokines in Mycobacterium tuberculosis Infection. Microbiol Spectr. 2016;4(5).
217. Deymier S, Louvat C, Fiorini F, Cimarelli A. ISG20: an enigmatic antiviral RNase targeting multiple viruses. FEBS Open Bio. 2022;12(6):1096-111.
218. Truong T, Martin K, Salemi M, Ray A, Phinney BS, Penn BH. The balance between antiviral and antibacterial responses during M. tuberculosis infection is regulated by the ubiquitin ligase CBL. bioRxiv. 2024.
219. Berry MP, Graham CM, McNab FW, Xu Z, Bloch SA, Oni T, et al. An interferon-inducible neutrophil-driven blood transcriptional signature in human tuberculosis. Nature. 2010;466(7309):973-7.
220. Maertzdorf J, Ota M, Repsilber D, Mollenkopf HJ, Weiner J, Hill PC, et al. Functional correlations of pathogenesis-driven gene expression signatures in tuberculosis. PLoS One. 2011;6(10):e26938.

221. Resztak JA, Choe J, Nirmalan S, Wei J, Bruinsma J, Houpt R, et al. Analysis of transcriptional changes in the immune system associated with pubertal development in a longitudinal cohort of children with asthma. Nat Commun. 2023;14(1):230.
222. Nowak TJ, Muehlenbein MP. Toward understanding sexual immune dimorphism in humans. Front Immunol. 2025;16:1570565.
223. Kotov DI, Lee OV, Fattinger SA, Langner CA, Guillen JV, Peters JM, et al. Early cellular mechanisms of type I interferon-driven susceptibility to tuberculosis. Cell. 2023;186(25):5536-53 e22.
224. Pujantell M, Altfeld M. Consequences of sex differences in Type I IFN responses for the regulation of antiviral immunity. Front Immunol. 2022;13:986840.
225. Pujantell M, Skenteris NT, Claussen JM, Grunhagel B, Thiele RJ, Altfeld M. Sex-dependent differences in type I IFN-induced natural killer cell activation. Front Immunol. 2023;14:1277967.
226. Gupta S, Nakabo S, Blanco LP, O'Neil LJ, Wigerblad G, Goel RR, et al. Sex differences in neutrophil biology modulate response to type I interferons and immunometabolism. Proc Natl Acad Sci U S A. 2020;117(28):16481-91.
227. O'Garra A, Redford PS, McNab FW, Bloom CI, Wilkinson RJ, Berry MP. The immune response in tuberculosis. Annu Rev Immunol. 2013;31:475-527.
228. Xu J, Zhou Y, Yang Y, Lv C, Liu X, Wang Y. Involvement of ABC-transporters and acyltransferase 1 in intracellular cholesterol-mediated autophagy in bovine alveolar macrophages in response to the Bacillus Calmette-Guerin (BCG) infection. BMC Immunol. 2020;21(1):26.
229. Weinberg ED. Nutritional immunity. Host's attempt to withold iron from microbial invaders. JAMA. 1975;231(1):39-41.
230. Mahajan S, Dkhar HK, Chandra V, Dave S, Nanduri R, Janmeja AK, et al. Mycobacterium tuberculosis modulates macrophage lipid-sensing nuclear receptors PPARgamma and TR4 for survival. J Immunol. 2012;188(11):5593-603.
231. Ye Y, Liu J, Guo Y, Gao Y, Rao J, Su R, et al. PPARgamma Ameliorates Mycobacterium tuberculosis H37Ra-Induced Foamy Macrophage Formation via the ABCG1-Dependent Cholesterol Efflux Pathway in THP-1 Macrophages. Front Microbiol. 2022;13:829870.
232. Zhang Y, Zhang Y, Sun K, Meng Z, Chen L. The SLC transporter in nutrient and metabolic sensing, regulation, and drug development. J Mol Cell Biol. 2019;11(1):1-13.
233. Sheldon JR, Skaar EP. Metals as phagocyte antimicrobial effectors. Curr Opin Immunol. 2019;60:1-9.
234. Neyrolles O, Mintz E, Catty P. Zinc and copper toxicity in host defense against pathogens: Mycobacterium tuberculosis as a model example of an emerging paradigm. Front Cell Infect Microbiol. 2013;3:89.
235. Reeme AE, Miller HE, Robinson RT. IL12B expression is sustained by a heterogenous population of myeloid lineages during tuberculosis. Tuberculosis (Edinb). 2013;93(3):343-56.
236. Ahsan F, Moura-Alves P, Guhlich-Bornhof U, Klemm M, Kaufmann SH, Maertzdorf J. Role of Interleukin 36gamma in Host Defense Against Tuberculosis. J Infect Dis. 2016;214(3):464-74.
237. Gabay C, Towne JE. Regulation and function of interleukin-36 cytokines in homeostasis and pathological conditions. J Leukoc Biol. 2015;97(4):645-52.

238. Dorhoi A, Yeremeev V, Nouailles G, Weiner J, 3rd, Jorg S, Heinemann E, et al. Type I IFN signaling triggers immunopathology in tuberculosis-susceptible mice by modulating lung phagocyte dynamics. Eur J Immunol. 2014;44(8):2380-93.
239. Brace PT, Tezera LB, Bielecka MK, Mellows T, Garay D, Tian S, et al. Mycobacterium tuberculosis subverts negative regulatory pathways in human macrophages to drive immunopathology. PLoS Pathog. 2017;13(6):e1006367.
240. Sathyamoorthy T, Sandhu G, Tezera LB, Thomas R, Singhania A, Woelk CH, et al. Gender-dependent differences in plasma matrix metalloproteinase-8 elevated in pulmonary tuberculosis. PLoS One. 2015;10(1):e0117605.
241. Rio P, Caldarelli M, Miccoli E, Guazzarotti G, Gasbarrini A, Gambassi G, et al. Sex Differences in Immune Responses to Infectious Diseases: The Role of Genetics, Hormones, and Aging. Diseases. 2025;13(6).
242. vom Steeg LG, Klein SL. SeXX Matters in Infectious Disease Pathogenesis. PLoS Pathog. 2016;12(2):e1005374.
243. Migeon BR. The role of X inactivation and cellular mosaicism in women's health and sex-specific diseases. JAMA. 2006;295(12):1428-33.
244. Cunningham CM, Li M, Ruffenach G, Doshi M, Aryan L, Hong J, et al. Y-Chromosome Gene, Uty, Protects Against Pulmonary Hypertension by Reducing Proinflammatory Chemokines. Am J Respir Crit Care Med. 2022;206(2):186-96.
245. Becerra-Diaz M, Song M, Heller N. Androgen and Androgen Receptors as Regulators of Monocyte and Macrophage Biology in the Healthy and Diseased Lung. Front Immunol. 2020;11:1698.
246. Lakshmikanth T, Consiglio C, Sardh F, Forlin R, Wang J, Tan Z, et al. Immune system adaptation during gender-affirming testosterone treatment. Nature. 2024;633(8028):155-64.
247. Khan A, Singh VK, Hunter RL, Jagannath C. Macrophage heterogeneity and plasticity in tuberculosis. J Leukoc Biol. 2019;106(2):275-82.
248. Becerra-Diaz M, Strickland AB, Keselman A, Heller NM. Androgen and Androgen Receptor as Enhancers of M2 Macrophage Polarization in Allergic Lung Inflammation. J Immunol. 2018;201(10):2923-33.
249. Shu Z, Zhang G, Zhu X, Xiong W. Estrogen receptor alpha mediated M1/M2 macrophages polarization plays a critical role in NASH of female mice. Biochem Biophys Res Commun. 2022;596:63-70.
250. Enright S, Werstuck GH. Investigating the Effects of Sex Hormones on Macrophage Polarization. Int J Mol Sci. 2024;25(2).
251. Belboul A, Ashworth J, Fadel A, McLoughlin J, Mahmoud A, El Mohtadi M. Estrogen induces the alternative activation of macrophages through binding to estrogen receptor-alpha. Exp Mol Pathol. 2025;143:104971.
252. Shepherd R, Cheung AS, Pang K, Saffery R, Novakovic B. Sexual Dimorphism in Innate Immunity: The Role of Sex Hormones and Epigenetics. Front Immunol. 2020;11:604000.
253. Straub RH. The complex role of estrogens in inflammation. Endocr Rev. 2007;28(5):521-74.
254. Subramanian N, Tavira B, Hofwimmer K, Gutsmann B, Massier L, Abildgaard J, et al. Sex-specific regulation of IL-10 production in human adipose tissue in obesity. Front Endocrinol (Lausanne). 2022;13:996954.
255. Lisse TS, Hewison M, Adams JS. Hormone response element binding proteins: novel regulators of vitamin D and estrogen signaling. Steroids. 2011;76(4):331-9.

256. Truss M, Chalepakis G, Pina B, Barettino D, Bruggemeier U, Kalff M, et al. Transcriptional control by steroid hormones. J Steroid Biochem Mol Biol. 1992;41(3-8):241-8.
257. Armant DR, Kilburn BA, Petkova A, Edwin SS, Duniec-Dmuchowski ZM, Edwards HJ, et al. Human trophoblast survival at low oxygen concentrations requires metalloproteinase-mediated shedding of heparin-binding EGF-like growth factor. Development. 2006;133(4):751-9.
258. Batty MJ, Chabrier G, Sheridan A, Gage MC. Metabolic Hormones Modulate Macrophage Inflammatory Responses. Cancers (Basel). 2021;13(18).
259. Rothchild AC, Stowell B, Goyal G, Nunes-Alves C, Yang Q, Papavinasasundaram K, et al. Role of Granulocyte-Macrophage Colony-Stimulating Factor Production by T Cells during Mycobacterium tuberculosis Infection. mBio. 2017;8(5).
260. Bryson BD, Rosebrock TR, Tafesse FG, Itoh CY, Nibasumba A, Babunovic GH, et al. Heterogeneous GM-CSF signaling in macrophages is associated with control of Mycobacterium tuberculosis. Nat Commun. 2019;10(1):2329.
261. Sellau J, Groneberg M, Fehling H, Thye T, Hoenow S, Marggraff C, et al. Androgens predispose males to monocyte-mediated immunopathology by inducing the expression of leukocyte recruitment factor CXCL1. Nat Commun. 2020;11(1):3459.
262. Yang J, Zhang L, Yu C, Yang XF, Wang H. Monocyte and macrophage differentiation: circulation inflammatory monocyte as biomarker for inflammatory diseases. Biomark Res. 2014;2(1):1.
263. Guilliams M, De Kleer I, Henri S, Post S, Vanhoutte L, De Prijck S, et al. Alveolar macrophages develop from fetal monocytes that differentiate into long-lived cells in the first week of life via GM-CSF. J Exp Med. 2013;210(10):1977-92.
264. de Martino M, Galli L, Chiappini E. Reflections on the immunology of tuberculosis: will we ever unravel the skein? BMC Infect Dis. 2014;14 Suppl 1:S1.
265. Reiling N, Homolka S, Walter K, Brandenburg J, Niwinski L, Ernst M, et al. Clade-specific virulence patterns of Mycobacterium tuberculosis complex strains in human primary macrophages and aerogenically infected mice. mBio. 2013;4(4).
266. Banks DA, Ahlbrand SE, Hughitt VK, Shah S, Mayer-Barber KD, Vogel SN, et al. Mycobacterium tuberculosis Inhibits Autocrine Type I IFN Signaling to Increase Intracellular Survival. J Immunol. 2019;202(8):2348-59.
267. Zhao C. Cell culture: in vitro model system and a promising path to in vivo applications. J Histotechnol. 2023;46(1):1-4.
268. Corcoran MP, Lichtenstein AH, Meydani M, Dillard A, Schaefer EJ, Lamon-Fava S. The effect of 17beta-estradiol on cholesterol content in human macrophages is influenced by the lipoprotein milieu. J Mol Endocrinol. 2011;47(1):109-17.
269. Lou Y, Fu Z, Tian Y, Hu M, Wang Q, Zhou Y, et al. Estrogen-sensitive activation of SGK1 induces M2 macrophages with anti-inflammatory properties and a Th2 response at the maternal-fetal interface. Reprod Biol Endocrinol. 2023;21(1):50.
270. Pelizzo G, Calcaterra V, Baldassarre P, Marinaro M, Taranto S, Ceresola M, et al. The impact of hormones on lung development and function: an overlooked aspect to consider from early childhood. Front Endocrinol (Lausanne). 2024;15:1425149.
271. Li Y, Oosting M, Deelen P, Ricano-Ponce I, Smeekens S, Jaeger M, et al. Corrigendum: Inter-individual variability and genetic influences on cytokine responses to bacteria and fungi. Nat Med. 2016;22(10):1192.

272. Hauer J, Fischer U, Auer F, Borkhardt A. Regional BCG vaccination policy in former East- and West Germany may impact on both severity of SARS-CoV-2 and incidence of childhood leukemia. Leukemia. 2020;34(8):2217-9.

Supplementary data

Analysis Building block	Parameters	Objective
Define Output		
Input Image	Channel: DAPI, dsRed, GFP (depending on experimental set-up and staining) Flatfield correction: None Stack processing: Maximum projection	Merging of images from different fluoresce channels and stacks
Find Objects		
Find Nuclei	Channel: DAPI ROI= None Method: B Common threshold: 0.02 Area: >40 µM^2 Splitting coefficient: 19.9 Individual threshold: 0.14 Contrast: > -0.71 **Output population:** Macrophages	Image segmentation: Determination of nuclei in host cells
Find Cytoplasm	Channel: dsRed Nuclei: Macrophages Method: An Individual threshold: 0.06 **Output region:** Cell, Cytoplasm, Membrane	Image segmentation: Defining single cells by determination of host cell cytoplasm

Find Spots	Channel: dsRed ROI: Macrophages Cell Method: B Detection Sensitivity: 0.11 Splitting Sensitivity: 0.844 **Output population:** Spots	Identification of intracellular spots within defined macrophages
Calculate Object properties		
Calculate Intensity properties	Channel: DAPI Population: Macrophages Region: Nucleus Method: Standard Calculate: Mean Property Prefix: Intensity Nucleus DAPI **Output Property**: Intensity Nucleus DAPI Mean Channel: dsRed Population: Macrophages Region: Cytoplasm Method: Standard Calculate: Mean Property Prefix: Intensity Cytoplasm dsRed **Output Property**: Intensity Cytoplasm dsRed Mean	Quantification of properties inside defined regions. Removal of border objects

Analysis Building block	Parameters	Objective
	Population: Spots Region: Spot Method: Standard Calculate: Mean Property Prefix: Intensity Spot DAPI Output Property: Intensity Spot DAPI Mean Channel: dsRed Population: Spots Region: Spot Method: Standard Calculate: Mean Property Prefix: Intensity Spot dsRed **Output Property**: Intensity Spot dsRed Mean	
Calculate morphology properties	Channel: dsRed Population: Macrophages Region: Cytoplasm Method: Standard Calculate: Area[µm], Roundness, Width[µm], Length[µm], Ration Width to Length Property prefix: M1 Cytoplasm **Output Property**: Standard Channel: dsRed Population: Macrophages Region: Cytoplasm Method: Standard (deprecated)	Quantification of properties inside defined regions. Removal of border objects

	Calculate: Area[µm], Roundness, Width[µm], Length[µm], Ration Width to Length Property prefix: M2 Cytoplasm **Output Property**: Standard Channel: dsRed Population: Spots Region: Spot Method: Standard (deprecated) Calculate: Area[µm], Roundness Property prefix: Spot **Output Property:** Standard	
Calculate properties	Population: Spots Method: By Formula Formula: A/B Variable A: Intensity Spot dsRed Mean Variable B: Intensity Spot DAPI Mean **Output Property:** dsRed / DAPI Ratio	Calculation of properties of intracellular bacteria
Analysis Building block	**Parameters**	**Objective**
Select a Population of Objects		
Select population I (interesting spots)	Population: Spots Method: Filter By Properties Parameter: Spot Roudness f 1.2 Spot Area [px2] 15 f X f 900	Identification of population: Discrimination of

	Spot Roundness > 0.25 Relative Spot intensity > 0.4 Spot Contrast > 0.1 Region intensity >150 Corrected Spot intensity = Staining-dependent, must be adapted Output Population: interesting spots	interesting spots from total spots
Select population II (Mycobacteria)	Population: interesting spots Method: Linear classifier Number of classes = 2 Parameter: ○ Spot Roudness ○ Spot Area [px2] ○ Spot Contrast ○ Relative Spot intensity ○ Region intensity ○ Spot to Region intensity ○ Spot Background intensity ○ Corrected Spot intensity ○ Uncorrected Spot intensity Intensity Spot dsRed Mean Intensity ○ Spot DAPI Mean **Output Population A**: Mtb selected selected **Output Population B:** false-positive Population: interesting spots Method: Filter by property Parameter: ○ Regression A-B < -3 **Output Population**: Mtb	Identification of population: Discrimination of mycobacteria from unspecific intracellular spots (as GMO was used not really needed)
Calculate properties	Population: Macrophages Method: By related population	

	Related population: Mtb Parameter: ○ Number of Mtb ○ Mean of Spot Area [px2] ○ Mean of Spot Roundness ○ Mean of Spot Contrast ○ Mean of Relative Spot intensity ○ Mean of Region intensity ○ Mean of Spot to Region intensity	
Analysis Building block	**Parameters**	**Objective**
	○ Mean of Spot Background intensity Mean of Corrected Spot intensity ○ Mean of Uncorrected Spot intensity Mean of Intensity Spot dsRed Mean Mean of Intensity Spot DAPI Mean Mean of dsRed/DAPI Ratio ○ Mean of Regression A-B Mean of Mtb selected ○ Mean of false-positive Property Suffix: per Cell **Output Properties**: By related Population	
Select population III (infected macrophages)	Population: Macrophages Method: Filter by Property Parameter: ○ Number of Mtb per cell > 0 **Output Population:** infected macrophages Population: Macrophages Method: Filter by Property	Identification of population: Discrimination of infected from uninfected macrophages

	Parameter: Number of Mtb per cell > 0 Output Population: infected macrophages Population: Macrophages Method: Filter by Property Parameter: ○ Number of Mtb per cell > 3 **Output Population:** massive infected macrophages	
Select population IV (M1-like polarised macrophages)	Population: Macrophages Method: Filter by Property Parameter: ○ -M1 Cytoplasm Roundness 0.38 f X f 0.62 ○ -M1 Cytoplasm Length f 55 ○ -M1 Cytoplasm Width f 25 M1 -Cytoplasm Ratio Width to Length 0.3 f X f 0.579 **Output Population:** M1 macrophages Population: M1 macrophages Method: Filter by Property Parameter: ○ Number of Mtb per cell **Output Population:** infected M1 macrophages	
Analysis Building block	**Parameters**	**Objective**

Select population V (M2-like polarised macrophages)	Population: Macrophages Method: Filter by Property Parameter: ○ -M2 Cytoplasm Roundness 0.15 f X f 0.51 ○ -M2 Cytoplasm Length g 48 ○ -M2 Cytoplasm Width f 40 ○ -M2 Cytoplasm Ratio Width to Length 0.0 g X f 0.37 **Output Population:** M2 macrophages Population: M2 macrophages Method: Filter by Property Parameter: ○ Number of Mtb per cell **Output Population:** infected M2 macrophages	
Calculate Collected Readout Values		
Define Results	Method: List of Outputs Populations: ○ Macrophages ○ M1 macrophages ○ M2 macrophages ○ Total Mtb ○ Mean of Mtb per cell ○ infected macrophages ○ double infected macrophages ○ massive infected macrophages infected M1 macrophages ○ infected M2 macrophages ○ Method: Formula ○ Output: a/b ○ Variable a: Mtb ○ Variable b: macrophages	

	○ Output Name: Mtb per macrophages Method: Formula ○ Output: a/b ○ Variable a: Mtb ○ Variable b: infected macrophages Output Name: Mtb per infected macrophages ○ Method: Formula ○ Output: a/b*100 ○ Variable a: infected macrophages Variable b: macrophages **Output Name**: percent infected macrophages	

Acknowledgments

I would like to dedicate this work to my grandfather and father, who always had an open ear and supported me not only with professional advice but also with unwavering encouragement. Both have profoundly influenced my life in countless positive ways. I am also deeply grateful to the rest of my family, especially my mother, whose constant encouragement, understanding, and support have been invaluable throughout my research journey. I am deeply grateful to my husband Chris, who left his hometown to join me on this journey and endured every high and low along the way with unwavering patience and support, never once questioning his choices and always offering me strength and comfort when I needed it most.

My sincere gratitude goes to Dr. Bianca Schneider, my supervisor, without whom this work would not have been possible. She consistently supported me with valuable advice and guidance, allowing me the freedom to pursue and implement my own ideas. Her trust and encouragement helped me develop the confidence to work independently, for which I am deeply grateful. I look forward to continuing our collaboration on many exciting research projects in the future.

I would like to sincerely thank PD Norbert Reiling for stepping in as the first examiner and providing invaluable guidance and input throughout my entire thesis. Many thanks also to Prof. Dennis Nurjadi for his support as the second supervisor, and to Prof. Stefan Taube for his role as chairperson of my examination committee.

Many thanks to the group at BNITM around Prof. Hanna Lotter, especially to Prof. Hanna Lotter, Dr. Helena Fehling and Dr. Annika Bea, who introduced me thoroughly to everything related to the HCS system. I am also deeply grateful to the Flow Facility, particularly Dr. Jochen Behrends and Martina Hein, as well as the microscopy unit at the LIV, for their invaluable assistance and technical support throughout the project. Special thanks to my colleagues in the host-pathogen interaction group, particularly Jaqueline and Lars; and especially Linda—when colleagues become friends, everything becomes possible. I loved working within our little BSL3 bubble.

Finally, I thank Urmel and Stuti, my dog and horse, who have taken care of my mental well-being throughout this journey. Chapter closed!

Publication List

"Transcriptome profiling of L. infantum-infected human macrophages reveals sex-specific type I interferon induction" in PLOSPathogen, 12.08.2025

Annika Bea, Helena Fehling, Fabian Hausmann, Fahten Margot Habib, Melanie Lütkemeyer, **Lara Buer**, Carola Schäfer, Charlotte Sophie Hansen, Barbara Honecker, Stefan Bonn, Bianca Elisabeth Schneider, Joachim Clos, Hanna Lotter

Conference Presentations (highlights)

- DGfI Rothenfels Symposium, Burg Rothenfels, Germany. 27.04.2022 to 29.04.2022

Oral presentation

- DGfI Rothenfels Symposium, Burg Rothenfels, Germany. 22.03.2023 to 24.03.2023

Oral presentation

- DGfI Rothenfels Symposium, Burg Rothenfels, Germany. 04.03.2024 to 06.03.2024

Oral presentation

- DGfI Rothenfels Symposium, Burg Rothenfels, Germany. 24.03.2025 to 26.03.2025

Oral presentation

- DGfI Autumn School, Merseburg-Halle. 09.10.2022 to 14.10.2022

Poster presentation

- DGfI-SFI Joint Meeting 2023, Strasbourg, France. 26.09.2023 to 29.09.2023

Poster presentation

- Sex Differences in the Immune System, Dublin, Ireland. 12.06.2023 to 14.06.2023

Poster presentation

- 18th International Congress of Immunology, Cape Town, South Africa. 27.11.2023 to 02.12.2023

Poster presentation

Erklärung

Hiermit versichere ich, dass ich die vorliegende Arbeit selbstständig verfasst und keine anderen als die angegebenen Hilfsmittel benutzt habe. Weder vorher noch gleichzeitig habe ich andernorts einen Zulassungsantrag gestellt oder diese Dissertation vorgelegt. Ich habe mich bisher noch keinem Promotionsverfahren unterzogen.

Bargteheide, 22.09.2025 _____

Lara Buer